Novel, Simple and Efficient Cardiomyocyte Differentiation Protocol for iPSCs and the Effects on Cardiomyocyte Differentiation exerted by ECM-bound Growth Factors in a PEG Hydrogel

Thesis submitted in partial fulfillment of the requirements for the degree of Master of Science in Engineering at the University of Applied Sciences Technikum Wien - Degree Program MTE

By: Pablo Hofbauer, BSc

Student Number: 1310692004

Supervisor 1: Wolfgang Holnthoner, PhD

Supervisor 2: Brenda Ogle, PhD

Minneapolis, Minnesota, U. S. A., October 28, 2015

FACHHOCHSCHULE
TECHNIKUM WIEN

Declaration

”I confirm that this thesis is entirely my own work. All sources and quotations have been fully acknowledged in the appropriate places with adequate footnotes and citations. Quotations have been properly acknowledged and marked with appropriate punctuation. The works consulted are listed in the bibliography. This paper has not been submitted to another examination panel in the same or a similar form, and has not been published. I declare that the present paper is identical to the version uploaded.”

Vienna, 28.10.2015

Place, Date

Signature

Kurzfassung

Herz-Kreislauf-Erkrankungen machen etwa 30% aller Tode in der westlichen Welt aus und sind damit die häufigste Todesursache. Da das Herz nur ein sehr begrenztes Regenerationsvermögen hat, ist das Ersetzen oder die Regeneration von Herzgewebe eines der wichtigsten Forschungsziele.

In dieser Arbeit wurde ein neues Kardiomyozyten Differenzierungsprotokoll entwickelt, das aus einer simplen sich ändernden spezifischen Frequenz und Menge des Mediumwechsels besteht. Außerdem wurden die Wachstumsfaktoren BMP4 und bFGF nicht kovalent an die extrazelluläre Matrix Proteine Kollagen I und Fibronektin gebunden und zusammen mit iPS Zellen in PEG Hydrogelen eingeschlossen.

Das neu entwickelte Protokoll führte zu einer signifikanten Nummer an schlagenden Regionen, die positiv für cTnT waren und deren Quantifizierung eine signifikant größere cTnT positive Fläche, verglichen mit standard „Embryoid Bodies“ (EB)-basierten Differenzierungsprotokollen, enthüllte. Zudem zeigte die Quantifizierung von aktivem β-Catenin, dass der Wnt Signalweg zuerst aktiviert und anschließend deaktiviert wird. Dieser beobachtete Mechanismus könnte die Grundlage für die Kardiomyozyten Differenzierung sein. EB-basierte Protokolle und die Tatsache, dass andere pluripotente Stammzellen nicht annähernde Ergebnisse lieferten heben die Heterogenität in der Differenzierung der Protokolle und Zelllinien heraus. Weiters wurden iPS Zellen in PEG Hydrogelen zusammen mit EZM-gebundenen Wachstumsfaktoren eingeschlossen und demonstrierten nicht nur Viabilität, sondern auch erhöhte cTnT positive Fläche.

Zusammenfassend wurde ein neues Kardiomyozyten-Differenzierungsprotokoll entwickelt, das vor allem sehr einfach ist und zumindest partiell durch die Manipulierung des Wnt Signalwegs wirkt. Die beobachtete erhöhte Kardiomyozyten Differenzierung in PEG Hydrogelen, die EZM-gebundene Wachstumsfaktoren beinhalteten, führt mich zu der Vision, dass solche Kombinationen aus Gerüst, Zellen und Wachstumsfaktoren in Zukunft als Therapie eingesetzt werden könnten. Diese Kombinationen könnten nicht nur Stammzellen zur Zielregion bringen, sondern gleichzeitig auch die Differenzierung vorantreiben.

Schlagwörter: Pluripotente Stammzellen, Kardiomyozyten Differenzierung, Simples Differenzierungsprotokoll, Wnt Signalweg, Extrazelluläre Matrix, EZM-gebundene Wachstumsfaktoren, PEG Hydrogele

Abstract

Cardiovascular diseases account for approximately 30% of deaths in developed countries, making it the leading cause of death. Because the heart's ability to regenerate is very limited, replacing or regenerating lost or damaged cardiac cells has become a crucial target of research.

Here, a novel cardiomyocyte differentiation protocol for iPS cells, based on the timely exchange of a specific amount of medium, was developed. Moreover, growth factors BMP4 and bFGF were non-covalently bound to the ECM-molecules collagen I and fibronectin, and entrapped together with iPS cells in a PEG hydrogel cross-linked by native chemical ligation.

The newly developed protocol led to the emergence of a significant number of beating areas that stained positive for cTnT and quantification revealed a significantly increased cardiomyocyte-covered area compared to standard EB-based protocols. Furthermore, active β-Catenin staining revealed sequential Wnt activation and inhibition as a probable mechanism of action of the newly developed protocol. EB-based protocols and the fact that other pluripotent stem cells failed to produce similar numbers of cardiomyocytes clearly highlights the existing heterogeneity of pluripotent stem cells and differentiation protocols in regard to cardiomyocyte differentiation efficiency. In addition, iPS cells were encapsulated in PEG hydrogels together with ECM-bound growth factors and not only demonstrated viability in the hydrogels but also increased cardiomyocyte-covered area based on cTnT expression.

In conclusion, I was able to develop a novel protocol that excels through its simplicity and I determined that it is at least partially mediated by the activation and inhibition of Wnt signaling. The observed improved cardiomyocyte differentiation through incorporation of growth factors leads me to envision a set-up that employs similar combinations of scaffold, factors and cells to serve as an effective means to not only deliver stem cells or associated progeny to damaged cardiac tissue but also spur cardiomyocyte differentiation of transplanted cells.

Keywords: Pluripotent Stem Cells, Cardiomyocyte Differentiation, Simple Differentiation Protocol, Wnt Signaling, Extracellular Matrix, ECM-bound Growth Factors, PEG Hydrogels

Acknowledgements

Herein, I would like to express my gratitude to the many people who made this work possible.

First and foremost, I'd like to extend my deepest gratitude to Gloria and Bill Thielen, who welcomed me into their home and who have become like a second family to me. None of this work would have been possible without you. I would also like to thank Barb and Mike Holmin, who have also been amazingly kind to me.

Secondly, I am grateful to my supervisors Brenda Ogle and Philip Jung, who granted me the opportunity to work at the University of Minnesota and who helped and guided me along the way.

I would also like to thank all of the wonderful people who made my stay in Minnesota as great as it was. Thank you to Eric, Sara, Garret, Alex, Kelly, Cady, and my colleagues Philip, Molly, Brian, Claire, Julia, and Tanner.

And last but not least, I would also like to thank Wolfgang Holnthoner. It was with his help that I initiated this endeavor and he, together with Sabrina Rohringer, helped and guided me as I took my first steps as a scientist.

Finally, I would also like to thank the Austrian Marshall Plan Foundation for granting me a scholarship for my stay in the United States.

Contents

1 Introduction **6**
1.1 Induced Pluripotent Stem Cells (iPS cells) . . . 6
1.1.1 Current Application of iPS cells . . . 8
1.2 Induction of Cardiac Differentiation . . . 9
1.2.1 The Wnt Signaling Pathway . . . 12
1.3 The Extracellular Matrix (ECM) and the ECM of the Heart . . . 13
1.3.1 Collagen . . . 13
1.3.2 Laminin . . . 14
1.3.3 Fibronectin . . . 14
1.3.4 The ECM of the Heart . . . 14
1.3.5 The Glycosaminoglycan Heparin . . . 15
1.4 Polyethylene Glycol (PEG) Hydrogels and Native Chemical Ligation (NCL) . . . 16
1.4.1 Polyethylene Glycol (PEG) Hydrogels . . . 16
1.4.2 Native Chemical Ligation (NCL) . . . 16

2 Methods **19**
2.1 Cell Culture . . . 19
2.1.1 Murine Induced Pluripotent Stem Cells (miPS cells) . . . 19
2.1.2 Murine Embryonic Stem Cells (mESCs) . . . 19
2.2 Cardiac Differentiation Protocols . . . 20
2.2.1 Newly Developed “Simple but Efficient Cardiomyocyte Differentiation” (SECD)-Protocol . . . 20
2.2.2 3D Differentiation Protocols . . . 20
2.3 Poly Ethylene Glycol (PEG) Hydrogel Formation . . . 21
2.3.1 Chemicals . . . 21
2.3.2 Synthesis of 4-Armed PEG Terminated with Either Thioester or Cysteine Groups . . . 21
2.3.3 Hydrogel Formation to Encapsulate Cells and ECM . . . 23
2.4 Characterization of miPS Cells and miPS Cell-Derived Cardiomyocytes . . . 24
2.4.1 Immunofluorescence . . . 24
2.4.2 Pluripotency . . . 25
2.4.3 Cardiac Differentiation - cTnT Staining . . . 25
2.4.4 Cardiac Differentiation – Wnt Activation (β-Catenin Staining) . . . 25
2.5 Growth Factor and Heparin Binding Assays . . . 26
2.5.1 Collagen Binding and Fibronectin Binding . . . 26
2.5.2 Enzyme-linked Immunosorbent Assay (ELISA) . . . 27
2.5.3 Dimethyl Methylene Blue Assay (DMMB) . . . 28
2.5.4 Statistics . . . 28

3 Results **29**
3.1 Oct3/4 Staining Confirms Pluripotent Status of miPS Cells . . . 29
3.2 Use of SECD-Protocol Leads to Significant Cardiomyocyte Generation from miPS Cells (2D) . . . 29
3.3 Quantification of Wnt-Signaling During Cardiac Differentiation with the SECD-Protocol Reveals an Initial Increase and Subsequent Drop in Active β-Catenin 35

3.4 Directed Differentiation into Cardiomyocytes Utilizing Standard EB-based Protocols Showed Contrasting Results (3D) 38
3.5 Successful PEG-Hydrogel Formation Encapsulates Cells and ECM Molecules and miPS Cells Remain Viable in PEG Hydrogel Culture 44
3.6 Growth Factors and Heparin Showed an Inherent Ability to Non-Covalently Bind to ECM Molecules 46
3.7 Attaching Growth Factors Non-Covalently to ECM Molecules Encapsulated in PEG Hydrogels Enhances the cTnT Expression of miPS Cells Undergoing Cardiac Differentiation 48

4 Discussion **52**

List of Figures **59**

List of Tables **59**

List of Abbreviations **60**

References **61**

1 Introduction

Cardiovascular diseases (CVD) are the leading cause of death in the developed countries accounting for approximately 30% ($\approx$ 800,000 cases/year) of all deaths per year in the United States alone [1]. A primary contributor to CVD is myocardial infarction, which causes the death of approximately 1 billion cardiomyocytes (CMs) in a relatively short period of time [2]. Unfortunately, the adult heart has generally displayed a very limited capacity to fully regenerate the lost myocardium, which has prompted researchers around the globe to address this challenge and has made replacing lost CMs the primary target of research. Some of the possible treatments identified are heart transplantations, which are limited by the number of donors, treatment with autologous stem cells, already in use in clinical trials, and the use of CMs derived from pluripotent stem cells (PSCs). CM derived from PSCs hold great promise in cardiac regeneration research as they can be employed as patient-specific tools for e.g. drug screening, toxicity testing, disease modeling and transplantation. Moreover, a further advantage of using CMs derived from PSCs is the fact that they can also be obtained in large quantities and from a single clonal source due to the nature of these PSCs [2, 3, 4].

Characteristics, efforts and approaches to differentiate PSCs, specifically induced pluripotent stem cells (iPS cells), as well as some of the known underlying mechanisms of cardiac differentiation will be provided in the following pages to give an introduction to this thesis' work. Moreover, background information on extracellular matrix (ECM) molecules, their involvement in the heart and polyethylene glycol (PEG)-hydrogels will be given.

1.1 Induced Pluripotent Stem Cells (iPS cells)

Cellular reprogramming is a process that occurs naturally during the early developmental stages. Fertilized oocytes, for example, delete almost all epigenetic information by de-methylation [5] before blastocyst formation and reconstruct it during differentiation. Therefore, researchers had been trying to reprogram cells themselves and in 2006, Shinya Yamanaka and colleagues were able to artificially induce reprogramming of somatic cells into an early developmental stage [6]. These so called induced Pluripotent Stem Cells (iPS cells) are cells that are reprogrammed to an early pluripotent stage by the forced expression of several transcription factors. The method is based on the fact that the forced expression of these factors induces embryonic stem cell (ESC)-like transcription networks in somatic cells, thereby reprogramming them into a pluripotent state. The four canonical factors are Oct3/4, Sox2, Klf4 and c-Myc. The expression of these four factors is capable of producing iPS cells from somatic cells of humans, mice, rats, monkeys and dogs. However, some factors can be replaced or left out all together, which leads to changes in the reprogramming efficiency. For instance, Sox2 can be replaced with Sox1, Sox3, Sox7, Sox15, Sox 17 or Sox 18 and Klf4 can be replaced with Klf2. Scientists were also able to achieve reprogramming using different combinations of classical and non-classical factors such as Oct3/4, Sox2, Nanog and Lin28. Lin28 acts as a negative regulator of the Let7 micro RNAs (miRNA), which improves pluripotency induction. Furthermore, cells that already express some of the necessary transcription factors do not need to be reprogrammed by the full transcription factor cocktail. For instance, neural precursor cells that express endogenous Sox2, Klf4 and c-Myc can be reprogrammed by the addition of only Oct3/4 [7].

The way these factors exert their reprogramming capabilities are numerous and not fully elucidated yet but Nanog, for instance, makes a transcriptional circuit with Oct3/4, Sox2 and Klf4 and is one of the most important factors for stabilizing pluripotency. Oct3/4, Sox2 and Nanog have been reported to bind and increase the expression of ES cell-specific genes like STAT3 and ZIC3 as well as decreasing the expression of developmental regulator genes. The exact function of the last of the classical factors, c-Myc, is not entirely clear, but c-Myc generally functions as an up-regulator of proliferation and suppressor of senescence. Considering that it is thought that the efficiency of iPS cell induction is also dependent on stochastic events of cell proliferation, such as the DNA methylation status, it is not surprising that c-Myc enhances iPS cell induction. Moreover, c-Myc is known to bind to over 4,000 sites on the genome and is therefore thought to loosen up heterochromatin and should thus increase the access of transcription factors such as Oct3/4, Sox2 and Klf4. Increasing proliferation and suppressing senescence by e.g. targeting the p53 and p21 pathways can significantly strengthen pluripotency induction efficiency. Nevertheless, suppressing the p53 and p21 pathways or using c-Myc in the transcription cocktail increases genomic instability and should only be employed temporarily, if at all [7].

In addition to the transcription factors, there are other factors that influence cellular reprogramming such as the method used to introduce the transcriptions factors into the cells, the culture conditions, and the modification of cellular signaling. For instance, iPS cells were first created by introduction of the four transcription factors by retroviral vectors [6] and the retroviral promoter gradually becomes inactivated via DNA methylation as the reprogramming takes place. This method of automatic silencing is thought to effectively reprogram somatic cells, but leaves foreign DNA sequences in the genome that could eventually lead to complications. Interestingly, progress has recently been made in reprogramming somatic cells using non-integrating vectors such as the Sendai virus (SeV), which is an RNA-virus that is neither pathogenic to humans nor does it integrate into the genome [8]. Moreover, its RNA can be mutated to become temperature sensitive to allow for efficient removal after reprogramming [8, 9]. However, the original efficiency remained low and has only recently been significantly increased to yield a non-integrating, relatively efficient, temperature sensitive and easy to eliminate SeV-vector [10].

Nevertheless, and as stated previously, use of c-Myc increases genomic instability and could lead to e.g. tumor formation due to changes in the genome. Due to the abnormalities that could arise through its use, a significant amount of research has been conducted to find a way to eliminate c-Myc from the transcription factor cocktail while maintaining reprogramming efficiency. For example, using a combination of the GSK3-β inhibitor CHIR99021 and Parnate (an inhibitor of lysine-specific demethylase 1) can generate iPS cells from human keratinocytes using only two factors (Oct3/4 and Klf4) [11]. Using CHIR99021 in combination with Oct3/4 and Klf4 was also reported to generate iPS cells [11]. Other factors were also found to influence reprogramming efficiency such as the addition of Vitamin C, which is thought to alleviate cell senescence, and O_2 tension. The reprogramming efficiency from fibroblasts may increase by up to four times if reprogramming takes place under hypoxic conditions (5% O_2) [12]. The addition of the histone deacetylase inhibitor Valproic Acid is also known to increase the reprogramming efficiency and allows the

generation of iPS cells with only Oct4 and Sox2 [7]. All these additional factors likely do not fully substitute or cover all the functions of the replaced transcription factors but rather enhance the reprogramming efficiency as a whole [7].

Furthermore, induction of iPS cells necessitates the formation of an ES-like transcription circuit in somatic cells yet despite the similarities in gene expression between ES cells and iPS cells, iPS cells have epigenetic differences. These differences may predispose them into the lineage they were derived from and thus it is important to keep the origin of the iPS cells in mind [7].

1.1.1 Current Application of iPS cells

Current applications of iPS cells in medicine include the use of iPS cells for differentiation, for drug screening and understanding complicated diseases, and for generating iPS cell banks.

The arguably main advantage of iPS cells is their pluripotent differentiation potential coupled with their way of generation that allows for patient-specific therapies as well as the generation of pluripotent stem cells free of ethical concerns. Their pluripotency and their ability to generate cells from the three germ layers makes them a promising tool for a wide variety of cell therapy applications and they have been differentiated into neural cells, cardiomyocytes, adipocytes, hematopoietic progenitor cells and blood cells among others [7, 13].

iPS cells are especially promising for understanding disease ontologies as they share the same gene expression as the patient. These disease-specific cells are therefore an ideal candidate to study the disease as well as the positive and negative effects of drug candidates before proceeding with animal and clinical trials. iPS cells derived from patients with different diseases have been established already and the list includes heart conditions like long QT syndrome, muscular dystrophies, such as Duchenne muscular dystrophy, as well as amyotrophic lateral sclerosis (ALS) and immunodeficiencies [7].

iPS cell banking has been proposed as a solution to tailor-made iPS cell therapy as the cost for such a therapy would be very high. Cell banking on the other hand would lead to a high number of cell lines with different human leukocyte antigens (HLA), the main molecules responsible for transplant rejection, and would thus increase the probability of finding an HLA matched cell line for each patient. As a matter of fact, calculated estimations for the necessary size for a stem cell bank have been done for Japan and the UK. They have come to the conclusion that the random establishment of 170 iPS cell lines would provide donor lines for $\geq$80% of patients with one mismatch at one of three HLA loci in Japan [14]. A similar cell bank of 150 cell lines could provide an acceptable or better match for 84.9% of the UK population [7, 15].

1.2 Induction of Cardiac Differentiation

The idea that pluripotent stem cells can be differentiated to cardiomyocytes originated when Doetschman *et al.* [16] found that culturing murine embryonic stem cells (mESCs) in suspension led to the formation of embryoid bodies (EBs) and to differentiated tissues of all germ layers within the EBs, including spontaneously beating cardiomyocytes. It was also discovered that human pluripotent stem cells (hPSC) formed EBs with contracting cardiomyocytes that expressed typical cardiac markers such as α- and β-myosin heavy chain (α- and β-MHC), cardiac troponin I and T (cTnI, cTnT), myosin light chain (Mlc)-2a and 2v, atrial natriuretic factor, α-actinin, and the transcription factors Nkx2.5 and GATA4. Furthermore, these cardiomyocytes showed spontaneous electrical activity and intracellular calcium transients [17].

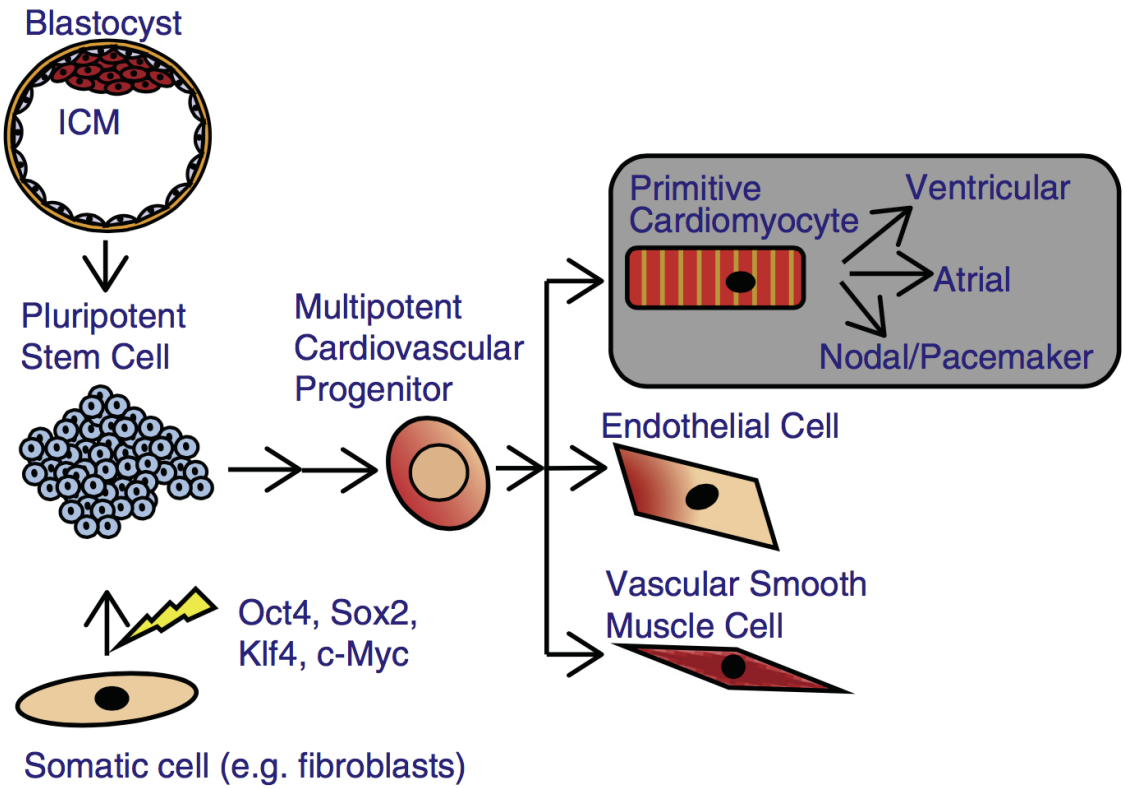

Figure 1: The differentiation path from pluripotent stem cell to cardiovascular cell, including differentiation into cardiomyocytes. Pluripotent stem cells can be harvested from the inner cell mass (ICM) of a blastocyst or obtained by reprogramming of somatic cells with the Yamanaka factors. Cells first undergo specification into a multipotent cardiovascular progenitor cell and can then further differentiate into cardiomyocytes (and even differentiate further into ventricular, atrial and nodal cardiomyocytes, endothelial cells and smooth muscle cells). Image adapted from Hartman *et al.* [17]

In recent years, researchers have developed a multitude of defined protocols to culture and differentiate pluripotent stem cells into cardiomyocytes. They all follow the premise that pluripotent cells have to be guided to differentiate into a mesodermal fate first before

inducing cardiac differentiation. In fact, pluripotent stem cells have to be differentiated into an early mesoderm followed by further specification into cardiac mesoderm, cardiac progenitor cells and finally cardiomyocytes. One way to determine the stages of differentiation is the expression of stage specific markers. Brachyury, for example, is a typical marker for early mesoderm and Mesp-1, Isl1 and Flk1 are typical markers for cardiac mesoderm. Interestingly, Mesp-1 has been shown to activate the expression of Dkk-1 suggesting that it might promote cardiac differentiation by inhibiting Wnt signaling through Dkk-1 [18]. Cardiac progenitors usually express the cardiac transcription factors Nkx2.5, TBX5/20, which has been linked to BMP4 signaling [19], Gata-4, Mef2c and Hand1/2. The terminally differentiated cardiomyocytes typically express the markers cTnT, α-actinin, MHC and MLC2a/v among others [4].

Overall, various signaling pathways and molecules have been implicated in the cardiac differentiation of pluripotent cells but the most prominent ones include Wnt, bone morphogenetic protein (BMP) and fibroblast growth factor (FGF) signaling pathways. Additionally, it has been established that timing the stimuli, such as the controlled and sequential Wnt activation and inhibition, plays a pivotal role in successfully differentiating pluripotent cells into cardiomyocytes. For instance, Taha *et al.* [20] showed that BMP4 can also be detrimental to the differentiation process if added continuously throughout the culture period. Generally, Wnt activation (e.g. with Wnt3a or the small molecule and GSK3β inhibitor CHIR99021) or stimulation with Activin A has been known to induce mesoderm. In order to differentiate mesodermal cells into cardiac cells, protocols have to follow up by inhibiting Wnt with either proteins (e.g. Dkk-1) or small chemicals (e.g. KY02111, XAV939) [3, 21, 22, 23]. Additional growth factors and molecules such as bFGF and vascular endothelial growth factor (VEGF) have also been used to supplement cardiac differentiation protocols to increase efficiency and in case of VEGF, even add vascular endothelial cells [24]. Another common factor that can influence the quality and efficiency of differentiation is the chosen medium, and protocols have mainly used Iscove's Modified Dulbecco's Media (IMDM), Roswell Park Memorial Institute Medium (RPMI), Glasgow Minimum Essential Medium (GMEM), Dulbecco's Modified Eagle's medium (DMEM) and mTeSR™1. Furthermore, some protocols have also employed some media with proprietary formulations such as Gibco's StemPro-34, originally intended for the culture of hematopoietic cells [25]. However, basal media are usually supplemented with serum or serum replacements. For instance, B27 supplement is often used with and without Insulin and Matrigel or Synthemax™ coated surfaces are additional modifications of some protocols. Interestingly, some research groups report that serum starvation can lead to higher cardiomyocyte yields derived from human iPS cells [26]. Moreover, other reports even state that ascorbic acid can further increase the efficacy of differentiation. The general ideas of cardiomyocyte differentiation from pluripotent stem cells are depicted in Figure 2 and several of the protocols are detailed in Figure 3 [3, 4, 17, 26, 27, 28, 29].

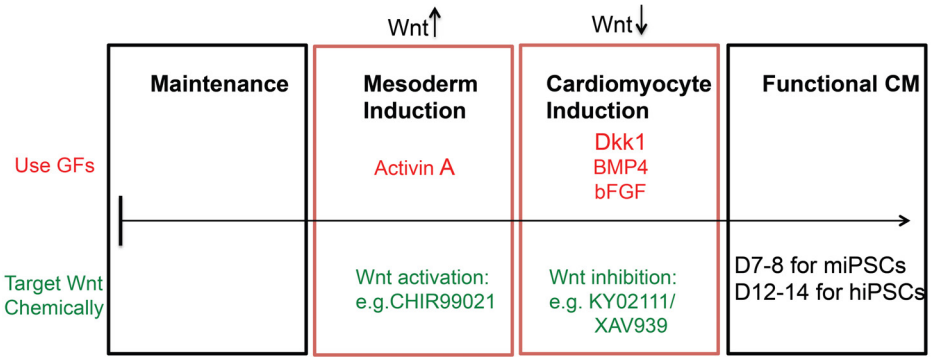

Figure 2: General timeline and molecules used to differentiate PSCs into cardiomyocytes. Firstly, mesodermal specification has to be induced followed by further induction of cardiomyocyte specification, mediated mainly through sequential Wnt activation and inhibition. This can be achieved chemically by using Wnt signaling modulators but it is also achievable by using several growth factors including Activin A, BMP4, bFGF and Dkk-1. It usually takes around 7-8 days for murine PSCs and 12-14 days for human PSCs to differentiate into cardiomyocytes. CHIR99021: chemical Wnt activator, KY02111/XAV939: chemical Wnt inhibitor.

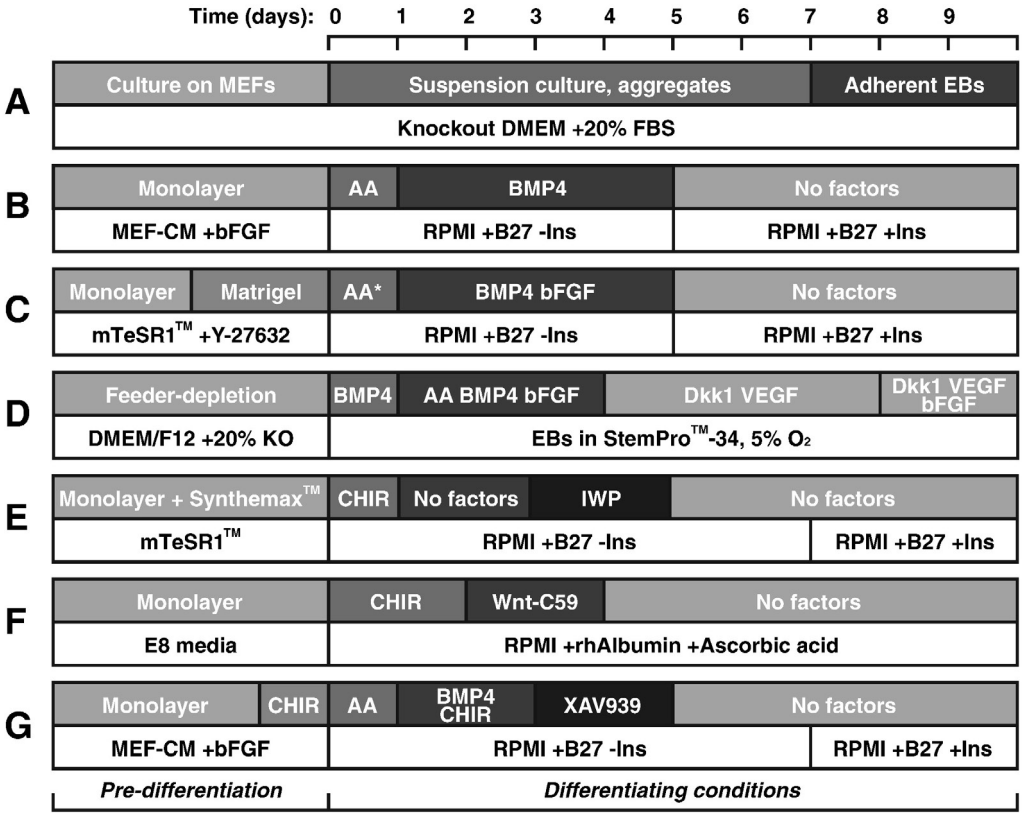

Figure 3: (A through G) Different differentiation protocols employed to directly guide pluripotent stem cells to a cardiomyocyte fate using 2D and 3D (EBs) approaches. Several growth factors such as Activin A (AA, AA* with Matrigel), BMP4, basic FGF (bFGF), VEGF, dickkopf homolog 1 (Dkk1), Insulin (Ins) and chemical Wnt modulators such CHIR99021 (CHIR), inhibitor of Wnt protein (IWP), Wnt-C59, XAV939 are used. MEF: mouse embryonic fibroblasts, KO: knockout serum replacement. Adapted from Hartman *et al.* [17].

The different differentiation protocols show, as expected, very different differentiation efficiencies. The relatively easy EB-based protocols usually have a very low efficiency. Early attempts showed that EBs with beating areas appeared in no more than 10% [4, 30] and have an additional caveat in that they develop a very heterogeneous cell population with ectodermal, mesodermal and endodermal origin [31]. More recent attempts with EB-based protocols show that between 90%-100% of EBs develop beating areas [32] but these protocols do not account for the actual number of cardiomyocytes, which is significantly lower. Other protocols such as guided differentiation methods using the growth factors Activin A, BMP4, bFGF, VEGF and Dkk-1 reach up to 50% [4, 33]. Importantly, Lian *et al.* [3] and Paige *et al.* [18] have shown that the differentiation efficiency varies greatly between pluripotent cell lines and even between experimental replicates of the same cell line. Efficiency usually ranges between 30%-90%. Other researchers, who used small-molecule activators and inhibitors of Wnt, such as CHIR99201, BIO, IWP-2 and IWP-4, Wnt-C59, KY02111 and XAV939 have reported efficiency rates of up to 98% [3, 17, 21].

1.2.1 The Wnt Signaling Pathway

After considerable effort, scientists were able to unravel the Wnt signaling pathway. The name is a combination of the names from the wingless (*wg*) and *Int-1* genes corresponding to the Drosophila (*wg*) and mouse (*Int-1*). Originally, it was observed to be important for polarity during larval development of the fly and was shown to be involved in correct spatial axis formation in Xenopus. Soon, it was found out that Wnt signaling was shared across invertebrate and vertebrate species and the different elements of the signaling cascade were identified including Dishevelled (Dsh), β-catenin (*armadillo* in invertebrates), glycogen synthase kinase 3 (GSK3, shaggy/zeste-white 3 in invertebrates) and adenomatous polyposis coli (APC) which was shown to interact with β-catenin [34, 35].

The activation of the pathway was identified to be a highly conserved family of secreted Wnt proteins of which roughly 20 have been identified in mammalian organisms. Currently, there are three different pathways identified that can be activated by Wnt proteins, namely the canonical pathway, the noncanonical planar cell polarity pathway, and the Wnt/Ca^{2+} pathway. Of these pathways, cardiac differentiation is believed to be mediated mainly by the best studied canonical Wnt pathway [32, 36].

To understand the canonical signaling pathway, it is necessary to know that in the inactivated state, a complex of several proteins including Axin, APC and the serine/threonine kinases GSK3β and casein kinase 1 (CK1) bind to β-catenin and phosphorylate it. In doing so, they mark β-catenin for ubiquitination followed by destruction in the proteasome. This process hinders the build up and translocation of β-catenin into the nucleus. The activation is started, if the canonical pathway is followed, by Wnt proteins binding to Frizzled (Fz) receptors, which are seven-pass transmembrane proteins with a cysteine-rich extracellular domain. Frizzled-receptors subsequently interact with the single-pass transmembrane coreceptors LRP5 and -6 and with Dsh and the GSK3β. In fact, Wnt signaling is also thought to bring about the GSK3β- and CK1-mediated phosphorylation of the LRP receptors thus creating docking sites for Axin, which in turn leaves the β-catenin destruction complex and ultimately stabilizes β-catenin. The accumulated β-catenin then translocates to the nucleus, dislodges the gene silencing protein Groucho from the transcription factors TCF/LEF and

leads to the transcription of the Wnt target genes. These target genes can be varied as they are determined by the developmental state of the target cell rather than universal Wnt targets. Interestingly, Wnt autoregulates itself to the point where several regulators of the Wnt pathway are themselves controlled by the β-catenin/TCF complex [34].

1.3 The Extracellular Matrix (ECM) and the ECM of the Heart

The extracellular Matrix (ECM) is comprised of an elaborate network of macromolecules that, together with cells, make up complex tissues. These macromolecules are a variety of different proteins and polysaccharides that are secreted by cells and their composition varies locally depending on the tissue. The three major classes of macromolecules are (1) highly charged polysaccharides called glycosaminoglycan (GAGs) that can also be covalently linked to proteins making them proteoglycans; (2) fibrous proteins, which are mainly members of the collagen-family; and (3) so called glycoproteins, which carry asparagine-linked oligosaccharides. GAGs and proteoglycans usually form the highly hydrated hydrogels in connective tissues, in which collagens and other proteins can be embedded. These hydrogels help to resist compressive forces, while allowing diffusion of nutrients. The collagen fibers strengthen the matrix and other fibrous proteins like elastin provide elasticity. Due to their many functions and variety, matrix proteins play an important role in a wide range of cellular processes such as cell proliferation, migration, settlement, differentiation and morphogenesis [37, 38, 39, 40].

In this thesis, a previously developed formulation of the ECM molecules Collagen I (Col I), Laminin-211 (LN), and Fibronectin (FN), optimized for cardiomyocyte differentiation (not yet published), was used to investigate the effects of ECM molecules on cardiomyocyte differentiation and as a potential delivery vehicle for other proteins [41].

1.3.1 Collagen

Collagens are fibrous proteins and are the most abundant proteins in mammals constituting 25% of the total protein mass. There are various different types of collagen molecules but they all share common features and a common primary function, namely to resist tensile forces. All collagen types share the triple-helical structure in which three α-chains are wrapped around each other and every third amino acid is Glycine. The most common collagen type is type I and as a member of the fibrillar collagens it forms into collagen fibrils after secretion and these fibrils in turn aggregate to form large bundles called collagen fibers. Other notable collagen types include types IX and XII as they are fibril-associated collagens that bind to collagen fibrils and are thought to attach the fibrils to each other. Collagen type IV is another noteworthy type as it forms networks that are a main part of the basal lamina of a cell [37]. Interestingly, different types of collagen have relatively high binding affinities for several growth factors. For instance, the fibrillar collagen type II is able to bind several growth factors from the TGF-β family including BMP2 but not others like BMP4 [42, 43]. Remarkably, a study found that collagen type IV and even collagen type I (to a lesser extent) bind BMP4 [44]. Collagen type I is also know to bind PlGF-2 [45].

1.3.2 Laminin

Laminin, a heterotrimer, is one of the main components of basal laminae and the organizer of the sheet structure. There are a variety of different types, each made up of three polypeptides called α, β and γ and they are joined by disulfide bonds into an asymmetrical cross-like structure. A great variety of types of laminin arise from different combinations of α, β and γ peptides, each named according to the numbers assigned to each one of the subunits. These different types create basal laminae with different properties. Laminin-111, for example, contains α1, β1, and γ1 subunits. Different tissues usually contain one main type of laminin. For example, laminin-332 is found in skin, laminin-211 in muscle, and laminin-411 in endothelial cells. Laminin is generally not known for binding growth factors but it has been shown that laminin is able to bind BMP4 [37, 44].

1.3.3 Fibronectin

Fibronectin is a very important glycoprotein that, among other things, is responsible for cell-ECM interactions as it contains a multitude of binding domains. It is a dimer composed of large subunits, which are composed of multiple small repeated domains, joined by disulfide bonds. The most commonly repeated domain is the so-called type III fibronectin repeat. Some of the varied binding domains include RGD sequences, fibrin binding domains, collagen binding domains, integrin binding domains and heparin binding domains. Fibronectin is also well known to bind several growth factors including bFGF, VEGF, PDGF, HGF [37, 42, 43, 45, 46, 47].

1.3.4 The ECM of the Heart

The heart ventricles, atria and valves form a very intricate system designed to move the blood throughout the body. Evidently, their development is similarly complex and involves the transition from a tube containing beating cells to the formation of distinct chambers and valves via cell proliferation, migration, and differentiation. It is not surprising that in light of that, the ECM of the developing heart is constantly changing as well. The ECM provides a plethora of signals ranging from structural support, mechanical cues and cell adhesion sites to sequestered soluble molecules such as growth factors. In fact, a changing cardiac ECM composition during cardiac development is critical for directing tissue specification. Thus, combining ECM molecules in a certain way can favor certain cellular states and may lead to a desirable balance between proliferation and differentiation that favors cardiomyocyte differentiation [38, 39, 48].

The ECM of the developing heart encompasses several glycoproteins, such as fibronectin, laminin, and vitronectin as well as the glycosaminoglycans hyaluronic acid and chondroitin sulfate. Moreover it also contains the collagen types I, III and IV. The most common ECM molecules in the heart are collagen I and III, providing structural support, collagen IV and laminin, which are a part of the basal lamina and help to align and polarize cells, and fibronectin, which helps cells attach to other ECM molecules such as collagen I, fibrin or heparin via integrins. Finally, elastin is also crucial for providing elasticity. A review of the ECM molecule expression and distribution in the developing heart was written by Jung *et al.* [38]. They identified that collagen I, collagen III and collagen IV are the main constituents

of the early development prior to embryonic day 11 (E11). Starting with E11, the atrial and interventricular septa begin to form and migrating epicardial cells cover the heart. This is the time when collagen IV and laminin localize in the “cardiac jelly” (an ECM layer between the primitive endocard and myocard). These two molecules are thought to facilitate mesenchymal cell migration into the endocardial cushions. Additionally, elastin and collagen VI emerge and fibronectin is localized in the endocardial and myocardial tubes. Elastin is highly expressed after E12.5, with the atrial septum forming and the outflow tract dividing into pulmonary and systemic branches. By E14.5, the fetal circulatory system is fully functional. With the ensuing developmental progression collagen I becomes circumferentially distributed around the heart to provide the needed structural and mechanical support. Cardiomyocyte proliferation decreases after E15.5 and comes to a halt by postnatal day 5. Fibronectin is significantly decreased after birth and elastin is also missing in these later stages. Laminin, however, is maintained after birth [38, 39].

1.3.5 The Glycosaminoglycan Heparin

Glycosaminoglycans (GAGs) and specifically heparin are involved in a variety of cellular processes, such as anticoagulation by inhibiting von Willebrand factor (vWF)-dependent platelet function [49]. Heparin, a well-known GAG is highly sulfated, linear polysaccharide with the highest negative charge density of any biological molecule [50]. It is commonly isolated from mast cells or mucosa and is most often used as an anticoagulant.

However, heparin and the structurally related heparan sulfate are also found covalently attached to proteins, forming proteoglycans, and mediating key processes by binding to regulatory proteins such as growth factors, cytokines and other signaling molecules. As a matter of fact, heparin has been shown to not only bind basic fibroblast growth factor (bFGF) but also stabilize its dimer and oligomer formation and thus protecting it from degradation [51]. Furthermore, heparin also non-covalently binds to and acts as a reservoir for a variety of other growth factors [52], such as bone morphogenetic protein-2 (BMP2) [53, 54], bone morphogenetic protein-4 (BMP4) [55] and Activin A [56]. This binding occurs primarily through binding of negatively charged groups on heparin to positively charged growth factors with a dissociation constant (KD) in the nM range [53, 54, 55, 56]. Interestingly, heparin also naturally binds to collagen with a KD in the nM range [57] and König *et al.* [58] showed that up to 86% of added heparin was stably attached to collagen.

Considering these biological characteristics of heparin, heparin was used in this thesis to functionalize collagen matrices in order to increase growth factor binding and stability as well as being able to efficiently deliver growth factors to cells.

Dimethyl Methylene Blue (DMMB)

In order to measure the amount of heparin in a solution, a dimethyl methylene blue assay was employed. This assay was first described by Farndale *et al.* [59] and is based on the fact that the dye 1,9-dimethylmethylene blue (DMMB) forms a complex with sulfated GAGs (sGAG) and causes a shift in color from blue towards purple. This color change can be measured spectrophotometrically at around 525 nm and, using known standard concentrations, it is possible to quantify the amount of sGAG in a solution. The assay was further modified

and improved by Farndale himself [60] to account for interference by polyanions such as hyaluronic acid, DNA and RNA. Moreover, Müller *et al.* [61] developed an indirect version of the original assay to overcome the disadvantage of obtaining falsified results due to precipitation of the sGAG-DMMB complex, which happens after approximately 10 min. In fact, this new method aims to use the amount of precipitate to determine the original amount of sGAG in a solution.

1.4 Polyethylene Glycol (PEG) Hydrogels and Native Chemical Ligation (NCL)

1.4.1 Polyethylene Glycol (PEG) Hydrogels

PEG is a readily water-soluble polymer that can be cross-linked with different strategies and is easily modified with functional groups. PEG hydrogels make up the majority of hydrogel-based approaches in medicine because of its exceptional biocompatibility, based on its high hydrophilicity and thus non-fouling surface that makes it non-immunogenic. In fact, the highly swollen hydrogels mimic soft tissue, allow for diffusion of nutrients and waste substances and have been used in a variety of tissue engineering approaches including cartilage, bone and vascular tissue engineering. The fact that it is easily modified allows for a multitude of different hydrogels properties in regard to mesh size, swelling ratio, type of cross-linking and degradability. Generally, PEGs basic structure is either linear or multi-armed. The basic end groups of the PEG chains are two hydroxyl end groups that can be easily exchanged for functional groups such as methyloxyl, carboxyl, amine, thiol, azide, vinyl sulfone, acetylene, and acrylate groups. Three main types of cross-linking methods have been used to make PEG hydrogels. Namely, radiation of PEG polymers, free radical polymerization of PEG acrylates, and specific chemical reactions including condensation, Michael-type addition, Click chemistry, native chemical ligation and enzymatic reactions with the most common method being photo-polymerization [62, 63].

PEG hydrogels without further functionalization, however, have a major drawback in that they exhibit minimal or no intrinsic biological activity and are not easily degradable. It has been reported that certain cell types show little viability due to the inert characteristics of PEG. Therefore it is important to incorporate e.g. enzymatically degradable cross-links for controlled elimination from a patient, cell adhesion molecules such as the RGD peptide sequence or encapsulate extracellular matrix (ECM) molecules [62, 63].

1.4.2 Native Chemical Ligation (NCL)

Native chemical ligation (NCL) is a technique originally used in protein synthesis. It enables researchers to covalently link peptides with a peptide bond and allows for complete control over the covalent protein structure. In an aqueous solution, a chemoselective reaction occurs between two unprotected peptides, which is not fully elucidated but is believed to occur according to the schematic seen in Figure 5. The result is a single native peptide bond-linked (covalently-linked) product. The suggested mechanism by which chemical ligation links two molecules covalently and chemoselectively follows. First, one molecule has to carry a C-terminal thioester and the other peptide an N-terminal cysteine. Then, the thiol group of the cysteine attacks the thioester which results in a thioester-linked intermediate, a reaction that is still fully reversible, that furthermore spontaneously rearranges, through

a favorable five-membered ring nucleophilic attack by the cysteine α-amino group, to form a native amide bond and ligate the two peptides. This last reaction is irreversible [41, 64, 65].

A key feature of this native chemical ligation is that the reaction occurs at a specific N-terminal cysteine residue and it does not matter how many additional cysteine residues are present in either one of the molecules. This remarkable selectivity makes it a promising target for the use in hydrogel or scaffold formation as no side reactions that may harm cells will occur [41, 64, 65].

This chemistry, seen in Figure 4, was used in this thesis to selectively cross-link PEG precursors without the use of UV light or toxic photoinitiators into a PEG hydrogel that can contain cells and ECM molecules. Furthermore, the selective chemistry of NCL does not alter ECM or growth factor (GF) presentation to the cells as no other reactions beside the NCL occur during hydrogel formation [41].

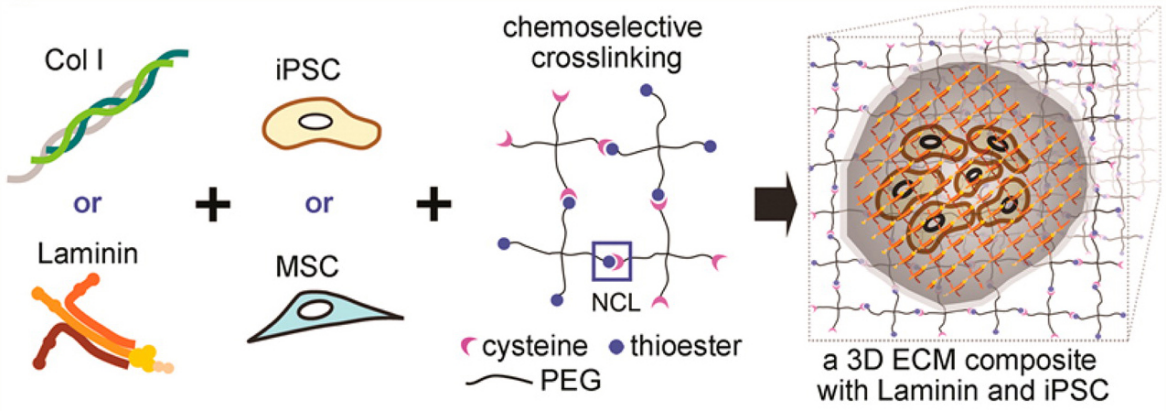

Figure 4: Schematic representation of the produced 3D hydrogels cross-linked by native chemical ligation (NCL) containing cells (e.g. iPS cells or mesenchymal stem cells (MSC) and ECM molecules such as collagen I and/or laminin. Adapted from [41].

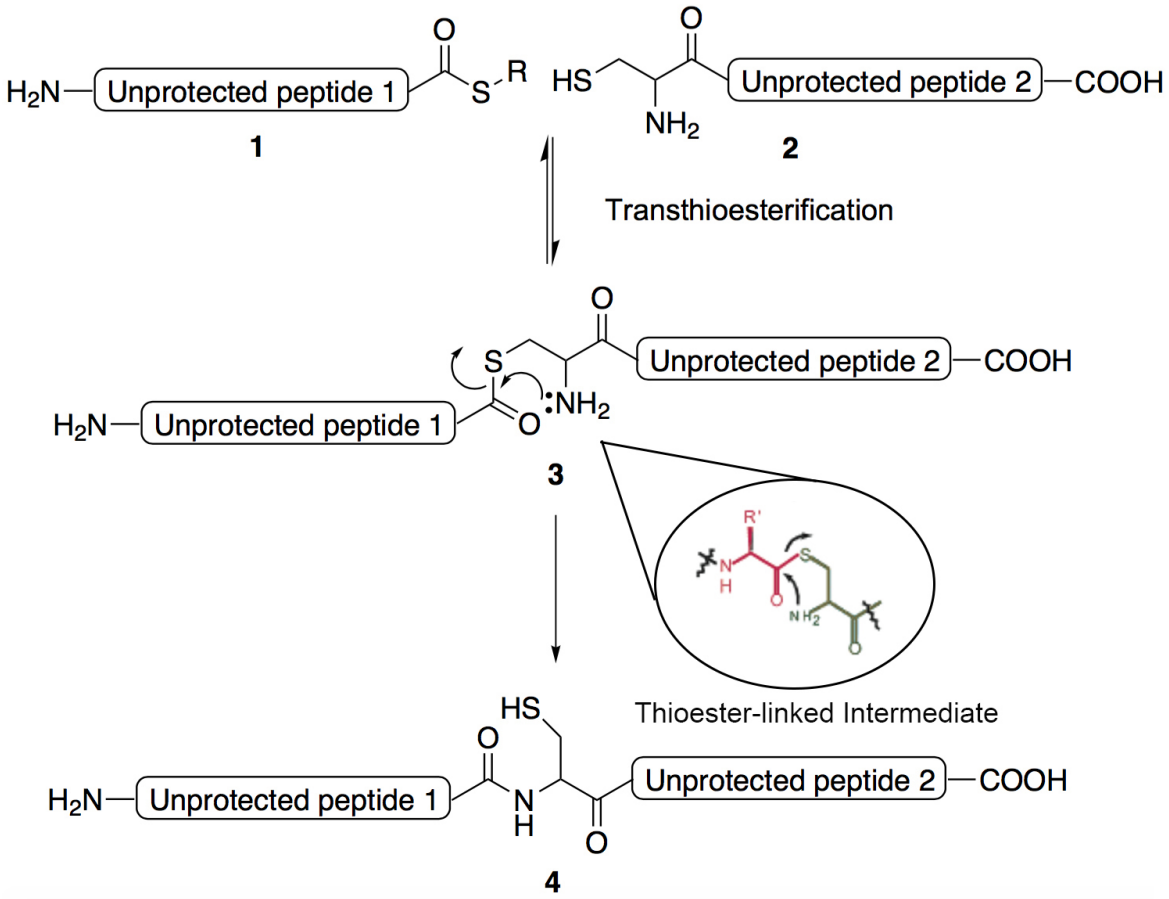

Figure 5: Suggested mechanism of native chemical ligation. An unprotected peptide (1) with a C terminal thioester is reacted with an unprotected peptide (2) containing an N-terminal cysteine resulting in a transthioesterification and the formation of a thioester-linked intermediate (3). This reaction is fully reversible. However, a favorable nucleophilic attack of the cysteine α-amino group will occur that leads to the formation of an irreversible (covalent) peptide (amide) bond (4). Adapted from [66] and [64].

Summing up, discrepancies in efficiency between differentiation methods and even cell lines, introduced in section 1.2, still exist and it is thus important to elucidate the mechanisms by which pluripotent stem cells are differentiated to be able to translate these protocols into a clinical setting. Furthermore, it is imperative to develop all differentiation protocols by starting with animal cells/models to study the aforementioned mechanisms prior to translation to human use and eventual clinical implementation. Only by following this process can we guarantee a fully understood and safe differentiation protocol. In this thesis, I utilized murine iPS cells and developed a new cardiac differentiation protocol that excels through its simplicity. Some of the characteristics of the novel protocol are elucidated and compared to existing protocols. Moreover, a possible underlying mechanism is investigated. As a second part of the thesis, the effects of ECM-bound growth factors on cardiac differentiation in three-dimensional PEG hydrogels are examined.

2 Methods

2.1 Cell Culture

2.1.1 Murine Induced Pluripotent Stem Cells (miPS cells)

miPS cells were obtained from Deepak Srivastava at the Gladstone Institute of Cardiovascular Disease (designated in this thesis as iPS#1). These cells originate from tail tips of NKX2-5-GFP mice and they were reprogrammed by the infection with Oct4, Sox2, Klf4 and c-Myc [67]. miPS cells were cultured according to Jung *et al.* [41] by culturing them feeder-free on gelatinized (0.1%, Cat#: G1890, Sigma-Aldrich, St. Louis, MO) 6-well-plates in GMEM (Cat#: 51492C, Sigma-Aldrich) supplemented with 10% fetal bovine serum (Cat#: 26140, Gibco, Carlsbad, CA, FBS), 2 mM L-glutamine (Cat#: 25030-81, Gibco), 1X nonessential amino acids (Cat#: 11140-050, Gibco) and 0.1 mM β-mercaptoethanol (Cat#: 194705, MP Biomedicals, Santa Ana, CA).

A second line of miPS cells (miPS cells JBL6, designated in this thesis as iPS#2) was obtained from James Dutton and the Stem Cell Institute of the University of Minnesota and cultured according to their protocol [68] until the SECD-Protocol in section 2.2.1 was initiated. They were cultured on murine embryonic fibroblasts (STO cells, Cat#: ATCC-CRL-1503, ATCC, Manassas, VA) that had been mitotically inactivated with Mitomycin C (Cat#: SC-3514B, Santa Cruz Biotechnology, Dallas, TX).

miPS cells were seeded at 3.68×10^3 cells/cm^2, the medium was supplemented with 10^6 units/ml leukemia inhibitory factor (LIF, Cat#: ESG1107, EMD Millipore, Billerica, MA) to yield a final concentration of 2000 U/ml and the cells were harvested at 60%$-$70% confluence with 0.05% Trypsin/EDTA in HBSS (Cat#: 25300-054, Gibco). Cells were pelleted using a centrifuge (Thermo Electron Corp., IEC CL31R Multispeed) at 300$\times$g for 5 min. Supernatant was removed and miPSCs were resuspended in fresh medium.

2.1.2 Murine Embryonic Stem Cells (mESCs)

mESCs (HM1-aMHC::GFP mESCs, previously published in [69])) were cultured similar to Squirrell *et al.* [70] by culturing them feeder-free on gelatinized (0.1%, Cat#: G1890, Sigma-Aldrich) 6-well-plates in DMEM-Glutamax (Cat#: 10569, Gibco) supplemented with 10% fetal bovine serum (Cat#: 26140, Gibco, Carlsbad, CA, FBS), 0.1 mM β-mercaptoethanol (Cat#: 194705, MP Biomedicals), 1X nonessential amino acids (Cat#: 11140-050, Gibco), and 1X penicillin/streptomycin (Cat#: 15140-122, Gibco). mESCs were seeded at 3.68$\times$103 cells/cm2 and the medium was supplemented with 106 units/ml leukemia inhibitory factor (LIF, Cat#: ESG1107, EMD Millipore, Billerica, MA) to yield a final concentration of 2000 U/ml. Furthermore, 10 ng/ml BMP4 (Cat#: 315-27, Peprotech, Rocky Hill, NJ) were also added. Cells were harvested at 60%$-$70% confluence with 0.05% Trypsin/EDTA in HBSS (Cat#: 25300-054, Gibco). Cells were pelleted using a centrifuge (Thermo Electron Corp., IEC CL31R Multispeed) at 300$\times$g for 5 min. Supernatant was removed and miPSCs were resuspended in fresh medium.

2.2 Cardiac Differentiation Protocols

2.2.1 Newly Developed "Simple but Efficient Cardiomyocyte Differentiation" (SECD)-Protocol

Cardiac differentiation was carried out by a newly developed and entirely novel approach. Differentiating miPSC colonies were selected and aspirated, the remaining cells detached, counted and seeded at 3.68×10^3 cells/cm^2 (7000 cells/24-well) and at 18.4×10^3 cells/cm^2 for iPS#2 into gelatinized (0.1%) 24-wells in 1 ml of medium on Day 0. Until Day 4, 1 ml medium was changed every 48h on Day 2 and 4. Then, amount of medium and changing frequency were altered to 2 ml medium every 24h until Day 16 at the latest. Cells were then taken and fixed or further processed.

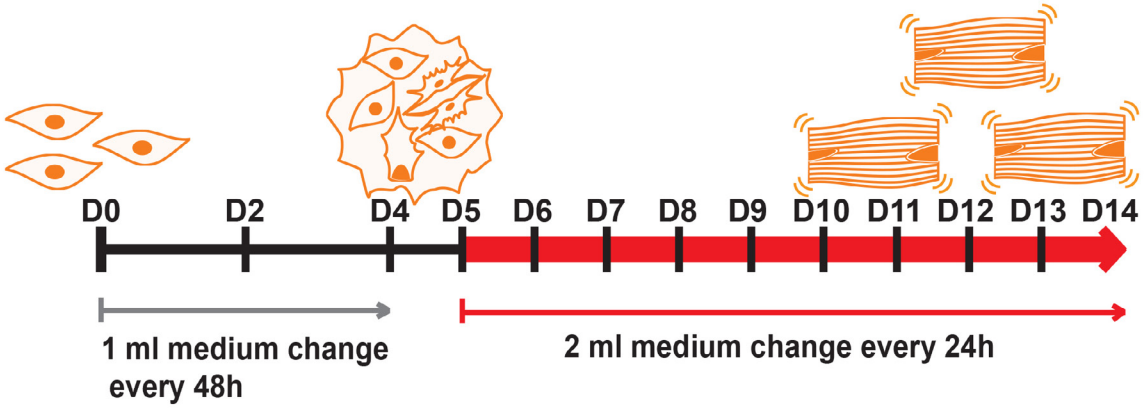

Figure 6: Schematic of the newly developed cardiac differentiation protocol. miPS cells were seeded into a 24-well and 1 ml medium added on Day 0 (D0). The medium was changed (1 ml) on Day 2 and Day 4 and switched to 2 ml from Day 5 onward. Additionally, the frequency of medium change was increased to every 24h. Cells were fixed or further processed on Day 14. First, cells were seeded as singularized cells that displayed colonies of differentiating cells by Days 3 and 4 and ultimately led to the emergence of clearly visible and beating cardiomyocytes between Days 10 and 14.

2.2.2 3D Differentiation Protocols

Embryoid Body Formation

Differentiating miPSC colonies were selected and aspirated, the remaining cells detached, counted and 160,000 cells resuspended in 1 ml growth medium. The cell suspension was subsequently diluted 1:10 by adding another 9 ml of medium to obtain a concentration of 16,000 cells/ml. The cell suspension was then transferred to a boat and 30 μl drops (containing 480 cells) were pipetted onto the lid of a non-cell culture treated petri dish (Cat#: 25384-302, VWR, Radnor, PA) using a multichannel pipette (Research Plus 8-channel pipette, Eppendorf, Hamburg, Germany). 60 EBs were added per lid and the lids were then put on top of the corresponding dish containing 25 ml PBS and incubated at 37°C and 5% CO_2.

Cardiac Differentiation Protocol Based on Wang *et al.* [22]

The cardiac differentiation was conducted according to Wang et al. [22]. Briefly, EBs were cultured in IMDM (Cat#: 30-2005, ATCC, Manassas, VA) supplemented with 20% FBS (Cat#: 26140, Gibco, Carlsbad, CA), 1.6 mM L-glutamine (Cat#: 25030-81, Gibco), 1X nonessential amino acids (Cat#: 11140-050, Gibco), 0.08 mM β-mercaptoethanol (Cat#: 194705, MP Biomedicals) and 2 μM dorsomorphin (Cat#: P5499, Sigma-Aldrich). EBs were transferred to a bacterial petri dish after 2 days in hanging drop culture and thus kept in suspension until Day 4 when the EBs were transferred to gelatinized 6-wells and allowed to attach. XAV939 (Cat#: X3004, Sigma-Aldrich) was added from Day 3 to Day 5. Medium was subsequently changed every 48h.

Cardiac Differentiation Protocol Based on van Laake *et al.* [67], Kwon *et al.* [36]

The cardiac differentiation was conducted according to van Laake *et al.* [67] and Kwon *et al.* [36]. Briefly, EBs were cultured in GMEM (Cat#: G5154, Sigma-Aldrich), supplemented with 20% FBS (Cat#: SH30071.3, GE Healthcare Bio-Sciences, Pittsburg, PA), 1 mM β-mercaptoethanol (MP Biomedicals), 2 mM L-glutamine (Gibco) and 0.1 mM non essential amino acids (Gibco). EBs were formed and left in hanging drop culture until day 3, when they were transferred onto a gelatin coated 6-well-plate. 150 ng/ml Wnt3a (Cat#: 1324-WN, R&D Systems, Minneapolis, MN) were added between days 4 and 6 and medium was changed every 72h.

2.3 Poly Ethylene Glycol (PEG) Hydrogel Formation

2.3.1 Chemicals

The utilized materials are listed below and are based on Jung *et al.* [41]. Four-armed, MW: 20K poly ethylene glycol (PEG-4A) with amine end groups was bought from Layson Bio (Cat#: 4arm-NH2-20k, Arab, AL). Ethyl-3-mercaptopropionate (EMP) was purchased from TCI America (Cat#: M1038, Portland, OR) and Benzotriazol-1-yl-oxy-tris (dimethylamino)-phosphonium hexafluorophosphate (BOP) was purchased from Peptide International (Cat#: KBP-1060-PI, Louisville, KY). The protected cysteine (Boc-Cys(Trt)-OH) was procured from EMD Millipore (Cat#: 853005, EMD Millipore) whereas diethyl ether, acetonitrile, trifluoroacetic acid (TFA), dichloromethane (DCM) and methanol were purchased from Fisher Scientific (Fisher Scientific, Hanover Park, IL). Additionally, anhydrous ethyl acetate, succinic anhydride, N,N-diisopropylethylamine (DIEA), 4-dimethylaminopyridine (DMAP), triisopropylsilane (TIS), 1,2-ethanedithiol (EDT), and pyridine were purchased from Sigma-Aldrich.

2.3.2 Synthesis of 4-Armed PEG Terminated with Either Thioester or Cysteine Groups

Both types of PEG-4A were synthesized according to protocols developed and used by Hu *et al.* [71] and Jung *et al.* [41] and consisted of the following steps.

Synthesis of Ethyl 3-Mercaptopropionate-Succinic Acid (EMP-SA)

Firstly, Ethyl 3-Mercaptopropionate-Succinic Acid (EMP-SA) was synthesized by adding 2g of 20 mM succinic anhydride (SA) and 0.122 g of 1 mM DMAP to 25 ml of acetonitrile-pyridine (9:1) in a round bottom flask. The mixture was put under a vacuum and filled with Argon (Ar) for 5 min. Secondly, 2.78 ml of 22 mM EMP was added to the mixture and again it was exposed to a vacuum and filled with Ar for 30 min. Then, it was stirred at room temperature overnight. Acetonitrile was subsequently removed by rotary evaporation (Büchi Rotovapor R-200, BÜCHI Labortechnik AG, Flawil, Switzerland) on the next day. Then, 50 ml of ethyl acetate were added to the flask and the mixture was moved to a separation funnel in order to wash and extract the organic phase. By adding 30 ml of 0.1 N HCL and subsequent mixing of the mixture I was able to separate the organic phase from the rest, which was let go by opening up the bottom valve of the separation funnel long enough to only keep the organic phase. This washing step was repeated 3 times. It was repeated a 4^{th}, 5^{th}, and 6^{th} time with Milli-Q water. The remaining aqueous phase was eventually transferred to a capped Erlenmeyer flask containing anhydrous $MgSO_4$ to remove water. The mixture was then stirred for 20 min until $MgSO_4$ became a clearly visible crystalline powder followed by a filtering step to remove the powder. Finally, the remaining mixture was transferred back to a round bottom flask and concentrated by drying it in the rotary evaporator. It was then stored at -20 °C for at least 80h until white crystalline EMP-SA formed in the round bottom flask.

Synthesis of 4-Armed PEG–Thioester or PEG–Cysteine

0.117 g of 0.5 mM EMP-SA were added to 2 ml of DCM containing PEG-4A (1 g, 0.2 mM amine), 0.111 g of 0.25 mM BOP, and 0.174 ml of 1 mM DIEA in a scintillation vial. This mixture was now termed PEG-Thioester. Moreover, 0.07 g of 0.15 mM Boc-Cys(Trt)-OH in 4 mL of DCM were added to PEG-4A (0.5 g, 0.1 mM amine) with 0.067 g of 0.15 mM BOP and 0.0265 mL of 0.15 mM DIEA to a scintillation vial. This mixture is termed PEG-Cys and the following procedures were done for both PEG-Thioester and PEG-Cys.

The mixtures were shaken for 2h, transferred to a 50 ml conical tube and concentrated using a stream of Ar until all the DCM was gone. The mixtures were then dissolved in 50 ml of methanol and stored at -20 °C overnight. This was followed up by vortexing thoroughly before centrifuging the solutions at -9 °C and 1600×g for 20 min. The liquid was decanted and fresh methanol was added to the conical tubes. These were vortexed until the solution turned clear and placed into a cooler with dry ice for 30 min. These centrifugation, decanting and cooling steps were repeated 3 times. Once the methanol was decanted the 3^{rd} time, 30 ml of ethyl ether were added to the conical tubes and they were once again vortexed and centrifuged at -9 °C and 1600×g for 20 min. Finally, the ethyl ether was decanted, PEG-Thioester and PEG-Cys were dried with Argon, the 50 ml conical tubes sealed with parafilm (Parafilm, Neenah, WI, made holes in parafilm with needle) and put into dry ice for 30 min before lyophilizing them.

After lyophilization, the side chain protecting group of cysteine had to be removed and was done so by dissolving the protected lyophilized PEG-Cys in a deprotection cocktail composed of TFA/TIS/EDT in a volumetric ratio of 28:1:1 for 2h at room temperature. This

cocktail was then removed again using the rotary evaporator and the previously described methanol and ethyl ether washing steps. The deprotected PEG-Cys was dissolved in 25 mL of 0.01 M NH_4HCO_3 buffer per 0.2 mM of PEG-amines, resulting in TFA salt-free conjugates and this neutralized PEG-Cys was frozen and lyophilized.

2.3.3 Hydrogel Formation to Encapsulate Cells and ECM

Firstly, Jangwook P. Jung and colleagues had previously determined, that the optimal concentrations of ECM molecules in the gel for cardiac differentiation were 1.15 mg/ml collagen I (ColI), 0.45 mg/ml laminin (LN) and 0.28 mg/ml fibronectin (FN) (not yet published). Secondly, literature research regarding cardiac differentiation led us to the use of a final concentration of 10 μg/ml heparin [53], 10 ng/ml bFGF [3] and 0.5 ng/ml BMP4 [26] as final growth factor concentrations in the gels.

Before polymerization, certain elements had to be mixed together in a defined manner to successfully obtain the PEG hydrogels and this mixture can be seen in Table 1.

Elements	Volume
Medium/ECM Molecules/Cells	18.6 μl
PEG-Cys (in α-MEM)	7.26 μl
PEG-Thioester (in α-MEM + 35 mM $NaHCO_3$)	7.26 μl
Total Volume	33.12 μl

Table 1: Formula for PEG hydrogel formation (per gel)

First and in order to encapsulate cells and ECM molecules in a PEG hydrogel, the correct amounts of PEG-Cys and PEG-Thioester had to be weighed in to achieve a concentration of 184 mg/ml. Subsequently, ECM molecules, heparin and growth factors had to be mixed and incubated for 1h on ice in order for the growth factors to bind. In the meantime, dialysis tubes (Cat#: 69562, Pierce, Rockford, IL), later used for casting of the gels, and a blade were UV sterilized. Then, miPS cells were harvested according to section 2.1.1 and 3.3×10^5 cells were added to Eppendorf tubes (1 per gel), and spun down at 200$\times$g and 37°C for 5 min. During that time, PEG-Cys and PEG-Thioester were dissolved in α-MEM and α-MEM + 35 mM $NaHCO_3$ respectively, vortexed, spun down for 2 min at max speed, vortexed again, sonicated and finally spun down once more before being ready to use. Cells were subsequently taken and the supernatant removed followed by the final mixing according to Table 1. In more detail, ECM mixtures and growth factors were taken and used to resuspend the cell pellets in the Eppendorf tubes. Afterward, PEG-Cys and PEG-Thioester were combined in a new Eppendorf tube, the ECM/growth factor/cell mixture was added to them and finally 30 μl of this final mixture were cast into a dialysis tube. The gels in the dialysis tubes were subsequently transferred to an incubator to complete the polymerization at 37 °C, 5% CO2 for 30 min. Once they were polymerized, they were changed to a 48-well containing 500 μl of fresh media for washing and left for 30 min in the incubator. This washing step was repeated three times followed by casting of the gels into a 24 well containing 1 ml medium. The casting was performed by cutting the dialysis membrane with a needle and gently transferring the gels to the 24 well containing fresh medium. Medium was then changed every

24h making sure that the hydrogels floated on top of the medium.

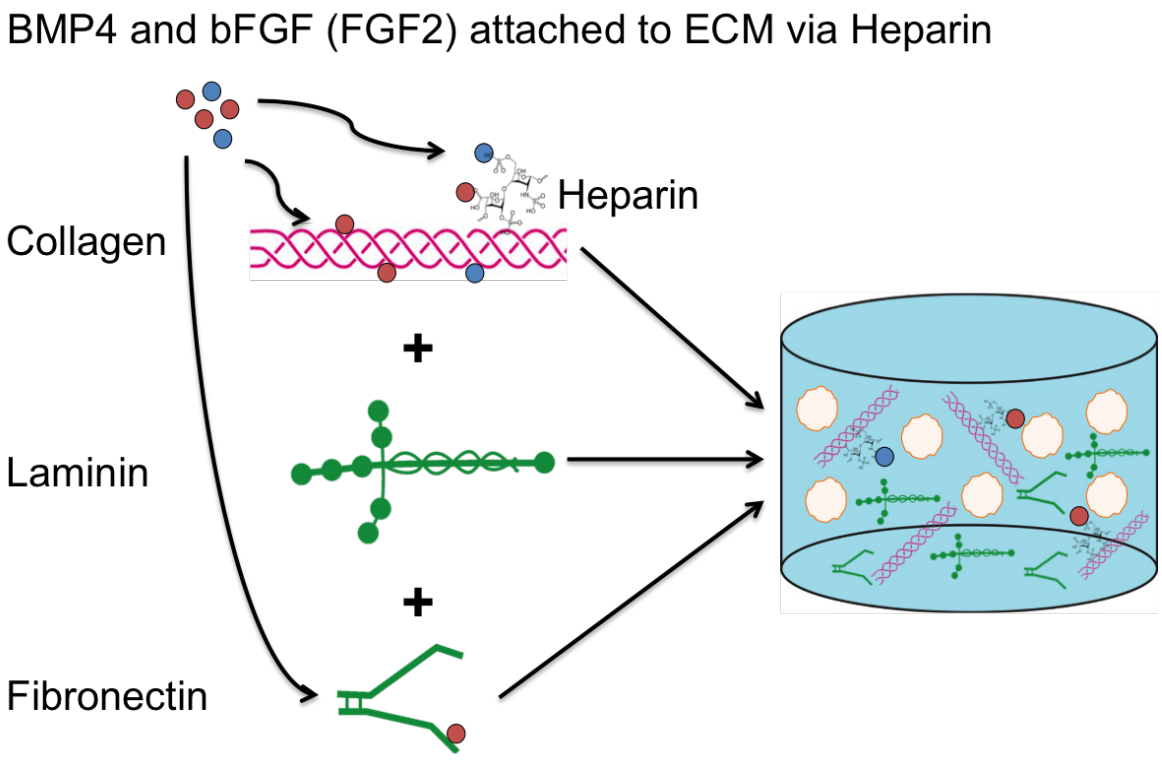

Figure 7: Schematic drawing of the concept of encapsulating the ECM molecules collagen I (Col I), laminin (LN) and fibronectin (FN) with bound growth factors (bFGF to FN and BMP4 to Col I/Heparin) in a PEG hydrogel together with miPS cells.

2.4 Characterization of miPS Cells and miPS Cell-Derived Cardiomyocytes

2.4.1 Immunofluorescence

Antibodies

Primary Antibodies: Oct3/4 (Mouse IgG, Cat#: SC5279, Santa Cruz Biotechnology, Dallas, TX, 1:200), cTnT (Mouse IgG, Cat#: MS-295-P0, Thermo Scientific, Fremont, CA, 1:200). Secondary Antibody: Goat IgG Texas Red (Goat α mouse, Cat#: 31500, Pierce, Waltham, MA, 1:1000). For Actin staining, the Millipore focal adhesion staining kit was used (Cat#: FAK100, EMD Millipore, Billerica, MA).

Staining and Imaging

Firstly, cells were fixed. To this end, medium was aspirated, cells were washed twice with 1X Phosphate Buffered Saline (PBS, Cat#: BP399-1, Fisher Scientific, Waltham, Massachusetts) and fixed with 4% Paraformaldehyde (PFA, Cat#: 15710, Electron Microscopy Sciences, Hatfield, Pennsylvania) for 15 min on a rocker (VWR, Radnor, Pennsylvania). After incubation with 4% PFA it was aspirated, cells were washed twice with PBS and they

were stored in the dark and at 4°C.

In order to stain the cells, antibody dilutions were prepared on the first day in a BSA (Cat#: 126575, Calbiochem, San Diego, California), Glycine (Cat#: G7403, Sigma-Aldrich), Goat Serum (Cat#: 16210064, Invitrogen/Life Technologies, Carlsbad, CA), and Triton X-100 (Cat#: T8787, Sigma-Aldrich) solution (BGST) and left overnight at 4°C.

The next day, PBS was aspirated and replaced with 0.2% Triton X-100 (Sigma-Aldrich, 100 μl in 50 ml PBS) and the cells were left in this solution for 1h on the rocker. Afterwards, cells were washed twice with PBS and PBS was replaced with a 5% nonfat dry milk (Cat#: 170-6404, Bio-Rad, Hercules, California, 2.5 g in 50 ml) solution. This blocking solution was left on for 2h on a rocker. Cells were subsequently washed with PBS twice again and covered with the primary antibody solution, which was left on overnight at 4°C. On the next day, the primary antibody solution was aspirated and cells were washed with a 0.2% Tween-20 (Cat#: 655204, Calbiochem, 100 μl in 50 ml) solution twice for 5 min each (on rocker) followed by a 5 min wash with PBS (on rocker). This washing step was followed up by the incubation with the secondary antibody solution for 1.5h at room temperature. Finally, the secondary antibody solution was discarded and the cells washed twice with a 0.2% Tween-20 solution for 5 min each before a last washing step of 5 min with PBS was carried out on a rocker. In order to stain the nuclei, a 0.1 μg/ml DAPI (Cat#: D9542, Sigma-Aldrich)/2.5% DAPCO (Cat#: D27802, Sigma-Aldrich) solution was finally added for 5 min before it was replaced by PBS and the cells were stored in the dark and at 4°C for imaging.

Imaging was done on a confocal microscope (Olympus IX81, Olympus Corporation, Tokyo, Japan) using MetaMorph (Molecular Devices LLC, Sunnyvale, CA) software. Images were background subtracted and processed using FIJI (v2.0.0-rc-31/1.49v, LOCI, Madison, WI) and Photoshop (version CS6, Adobe, San Jose, CA) software. Additionally, image measurements were taken with FIJI resulting in values for covered area and integrated density of the signal. In order to obtain results normalized to DAPI, area ratios and integrated density ratios were calculated by dividing the values of the signal of interest by the values of the DAPI signal.

2.4.2 Pluripotency

To show the pluripotent status of the miPS cells a staining for the pluripotency marker Oct3/4 was performed essentially as described in section 2.4.1.

2.4.3 Cardiac Differentiation - cTnT Staining

In order to show the successful differentiation of miPS cells, a cardiac Troponin T (cTnT) staining was performed essentially as described in section 2.4.1.

2.4.4 Cardiac Differentiation – Wnt Activation (β-Catenin Staining)

In order to show the Wnt activation status of iPS cells undergoing cardiac differentiation with the SECD-Protocol, a staining for β-Catenin (Rabbit IgG, Cat#: 8814, Cell Signaling

Technologies, Boston, MA) was performed essentially as described by the manufacturer. In brief, cells were blocked for 60 min with a blocking buffer consisting of PBS, Triton X-100 (0.3%) and serum (5%) from the host of the secondary antibody (goat α rabbit, Cat#: A21244, Invitrogen, Carlsbad, CA). Then, the cells were incubated with the primary antibody overnight at 4°C followed by washing with PBS and incubation with the secondary antibody for 1.5 h. Finally, and after another washing with PBS, 0.1 μg/ml DAPI (Cat#: D9542, Sigma-Aldrich) was added for 5 min, aspirated and cells stored at 4°C until they were analyzed. Images were taken by a confocal microscope (Olympus IX81, Olympus Corporation, Tokyo, Japan) using MetaMorph (Molecular Devices LLC, Sunnyvale, California) software. In order to analyze the amount of β-Catenin, seven representative images/day were taken (N=7) and analyzed for the integrated density and area ratio between β-Catenin signal and DAPI signal with FIJI (v2.0.0-rc-31/1.49v, LOCI, Madison, WI). For nuclear quantification, three areas of interest were taken from three image (N=9) and analyzed in the above way.

2.5 Growth Factor and Heparin Binding Assays

2.5.1 Collagen Binding and Fibronectin Binding

The following assay was developed in order to test the binding of BMP4 (Cat#: 315-27, Peprotech, Rocky Hill, NJ) and bFGF (Cat#: 450-33, Peprotech), and/or heparin (Cat#: H3393, Sigma-Aldrich) to collagen I (Cat#: 354249, Corning Inc., Corning, NY, ColI) or fibronectin (Cat#: F1141, Sigma-Aldrich, FN). For the collagen-binding assay 251.72 μl of GMEM (without FBS) were mixed with 48.28 μl of collagen stock-solution (8.7 mg/ml), added to a 24-well and left to polymerize for 30 min at room temperature to obtain a 1.4 mg/ml collagen layer. Alternatively, collagen matrices were also left to polymerize for 30 min in an Eppendorf tube (Eppendorf, Hamburg, Germany) to obtain a 3D collagen matrix. For the fibronectin-binding assay 200 μl of a 47.5 μg/ml fibronectin solution were added to a 24-well for 10 min to yield a surface concentration of 5 μg/cm^2. Then, 1 ml of GMEM (without FBS) containing growth factors and/or heparin in the desired concentrations (10 ng/ml for bFGF, 0.8 ng/ml BMP4 and 10 μg/ml heparin) was subsequently added on top of either collagen I or fibronectin and incubated for 30 min on a rocker at room temperature. Supernatants were taken and used for further analysis using a GF-ELISA or a DMMB-Assay.

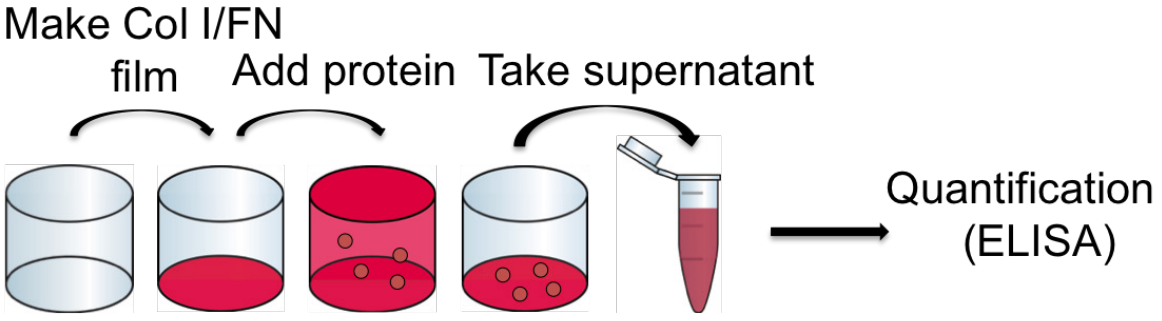

Figure 8: Schematic representation of the developed protocol to assess collagen binding of growth factors and heparin and fibronectin binding (bFGF only). Firstly, a collagen I (Col1) or fibronectin (FN) layer is made by polymerization for 30 (Col1) or 10 min (FN). Secondly, the protein is added on top and the supernatant is taken after another 30 min of incubation time on a rocker and analyzed by enzyme linked immunosorbent assay (ELISA) in described in section 2.5.2.

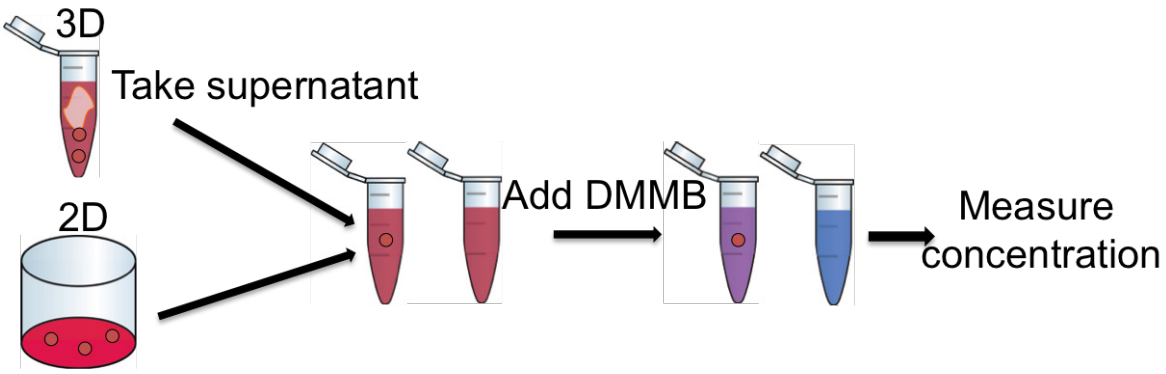

Figure 9: Schematic representation of the developed protocol to assess collagen binding of heparin. Firstly, a collagen I layer or 3D matrix is made by polymerization for 30 min in a 24 well or an Eppendorf tube. Secondly, heparin is added on top and the supernatant is taken after another 30 min of incubation time on a rocker and analyzed by the DMMB-assay described in section 2.5.3 measuring the optical density (OD).

2.5.2 Enzyme-linked Immunosorbent Assay (ELISA)

In order to quantify the amount of free antigen in the supernatant taken from the assay in section 2.5.1, enzyme-linked immunosorbent assays (ELISAs) for bFGF (Cat#: MFB00, R&D Systems, Minneapolis, MN) and BMP4 (Cat#: SEA014Mu, Cloud Clone Corp., Houston, TX) were performed according to the manufacturers instruction. A brief description is provided below.

bFGF ELISA

The principle of this assay is the sandwich technique. Antibodies against bFGF were immobilized on the bottom of the wells and upon adding of the samples and standards bind the free bFGF. Subsequently, an enzyme-linked antibody against bFGF is added and after removal of excess antibody, a substrate solution is added. The enzyme causes this solution to turn blue and after addition of a stop solution it turns yellow. The intensity of the color is then proportional to the amount of the initially bound bFGF. The color intensity is measured spectrophotometrically, using a BioTek Cytation3 spectrophotometer (BioTek Instruments Inc., Winooski, Vermont), at 450 nm. Rigorous washing was performed in between the addition of the several solutions.

BMP4 ELISA

The principle of this assay is the sandwich technique. Antibodies against BMP4 were immobilized on the bottom of the wells and upon adding of the samples and standards bind the free BMP4. Subsequently, a biotin-conjugated antibody against BMP4 is added and after removal of excess antibody, Avidin conjugated to the enzyme horseradish peroxidase (HRP) is added. HRP changes the color of a previously added substrate solution to blue and after addition of a stop solution it turns yellow. The intensity of the color is then proportional to the amount of the initially bound BMP4. The color intensity is measured spectrophotometrically, using a BioTek Cytation3 spectrophotometer (BioTek Instruments Inc., Winooski, Vermont),

at 450 nm. Rigorous washing was performed in between the addition of the different solutions.

2.5.3 Dimethyl Methylene Blue Assay (DMMB)

The DMMB solution was prepared as follows: 0.8 mg of DMMB (1,9-Dimethyl-Methylene Blue zinc chloride double salt, Cat#: 341088, Sigma-Aldrich), 152 mg Glycine (Cat#: G7403, Sigma-Aldrich), 80 mg NaCl (Cat#: S3014, Sigma-Aldrich) and 1.9 ml of 0.1 M Acetic Acid (Cat#: A9967, Sigma-Aldrich) were added to a 50 ml conical tube (Cat#: 339652, Nalge-Nunc, Rochester, New York) and this conical tube was filled up to 50 ml with ddH_2O. This solution was filtered through a 0.45 μm filter (Cat#: SLHV033RS, EMD Millipore, Billerica, MA) and stored in the dark. It was not used if precipitate had formed.

After performing the collagen binding as described in section 2.5.1, the supernatant was taken, filtered through a 0.2 μm filter (Cat#: 09-720-3, Fisher Scientific) and 20 μl of that sample were added to a 96-well plate. Standards were prepared in parallel by using a 500 μg/ml standard stock and the following dilutions depicted in Table 2.
Finally, 200 μl of DMMB-Solution were added to each well, the plate was shaken for 5 sec and the absorbance was measured at 525 nm using a spectrophotometer (Cytation3, BioTek Instruments Inc., Winooski, Vermont) [58, 72].

Standard [μg/ml]	μl of Stock	Standard	μl of H_2O
10	20		0
7.5	15		5
5	10		10
2.5	5		15
1.25	2.5		17.5
0	0		0

Table 2: Representation of the standard dilutions made for the DMMB-Assay.

2.5.4 Statistics

In order to analyze the data, Graphpad Prism 5 software (GraphPad Software, Inc., La Jolly, CA) was used. Data was firstly analyzed for normality using the D'Agostino and Pearson omnibus or the Shapiro-Wilk normality test where applicable. The data was subsequently subjected to either a parametric (One-Way ANOVA with Tukey's *post-hoc* test) or nonparametric (Kruskal-Wallis test with Dunn's *post-hoc* test) test based on whether the data was normally distributed. For grouped analyses, data was tested with a Two-Way ANOVA followed by a Bonferroni's *post-hoc* test. Finally, for the comparison of the SECD-Protocol and the EB-based protocol regarding global cTnT expression, a Mann-Whitney test was employed. Differences were considered significant if p-value$<$0.05. Results are always given as mean $\pm$ SD.

3 Results

3.1 Oct3/4 Staining Confirms Pluripotent Status of miPS Cells

In order to confirm the pluripotent status of the utilized murine iPS cells (iPS#1), cells were stained with Oct3/4 and, on average, 91.2% of the cells clearly expressed Oct3/4 (Figure 10 (A)). Cells showed the typical colonies of pluripotent cells and demonstrated the clear and pervasive nature of Oct3/4 expression in the iPS cultures prior to differentiation (representative image in Figure 10 (B)).

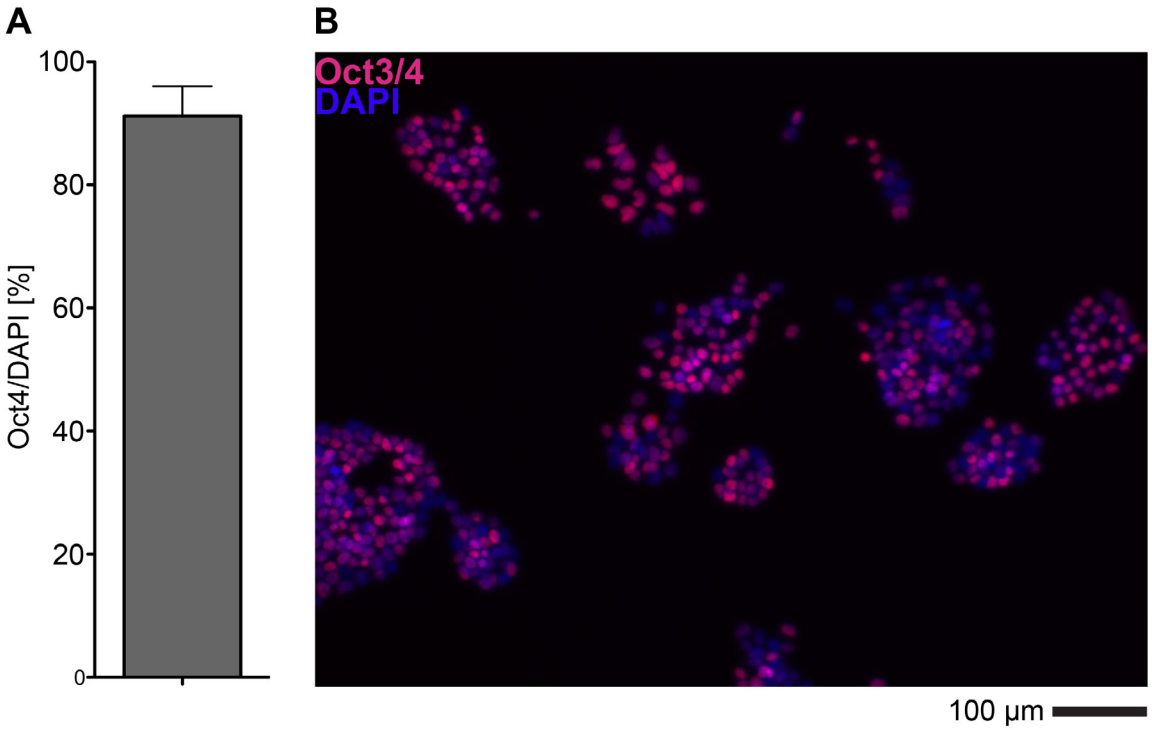

Figure 10: Oct3/4 staining confirms the pluripotent state of the miPS cells. (A) 91.2% of the iPS cells express the pluripotency marker Oct3/4 (Pink). (B) Representative image of the pluripotent iPS cell colonies expressing Oct3/4. Nuclei were stained with DAPI (Blue); N=3.

3.2 Use of SECD-Protocol Leads to Significant Cardiomyocyte Generation from miPS Cells (2D)

Using the SECD-Protocol I was able to show significant cardiac differentiation of miPS cells. A morphological study over the course of the protocol can be seen in Figure 11 and showed the developing monolayer starting from a sparse seeding density on day 1 and leading to the final confluent layer of contracting cardiomyocytes. Furthermore, I found that starting on days 6/7 and through day 14, cells started to build 3-dimensional structures in addition to just growing in a monolayer. In fact, most of the developing 3-dimensional structures exhibited strongly beating areas. The clearly visble blurring of the encircled regions indicated contraction of miPS-derived cardiomyocytes (Figure 12 (B)) and was

juxtaposed to the resting state (Figure 12 (B)).

During the development of the SECD-Protocol, beating areas were counted in conditions that differed in the amount and the timing of the medium change. Firstly, the amount of observed beating areas increased until it reached a maximum on Day 13 and subsequently fell (Figure 13 (A) and (B)). Secondly, starting off by exchanging only 1 ml of medium until Day 4 and performing the switch to exchanging 2 ml of medium from Day 5 on, led to a significant increase in beating areas (Figure 13 (A)). Thirdly, increasing the serum content in the medium from 10% to 20% did not significantly change the amount of observed beating areas until Day 14, if 2 ml of medium were consistently exchanged. The conditions that did include the switch from 1-2 ml on Day 5 and had a higher serum content (20%) also showed a higher mean number of beating areas than the 20% condition without the switch and a significant increase in beating areas on days 11 and 13. I moreover confirmed the observation that the number of beating areas rose until Day 13 and decreased thereafter, in multiple replicates performed at different time points (Figure 13 (B)). It also shows that the number of beating areas on Day 13 was significantly higher than any other day of the protocol except Day 12. Likewise, the number of beating areas significantly decreased after Days 12 and 13 but did not differ from Day 11 and was still significantly higher than on Day 10 and Day 9 (Figure 13 (B)).

In order to further characterize the obtained contracting cells and ultimately prove the rise of miPS-derived cardiomyocytes, they were stained for cTnT. I confirmed the nearly ubiquitous and efficient expression of the cardiomyocyte marker cTnT in the observed beating areas for miPS cells (Figure 14). The clearly depicted characteristic thread-like striations of cTnT expression in miPS-derived cardiomyocytes is also visible (Figure 14). In addition, mESCs and a second line of miPS cells (iPS#2) were also subjected to the SECD-Protocol and stained for cTnT. The resulting representative images of ESC and iPS#2, seen in Figure 14, showed that mESC and iPS#2 only displayed several smaller cTnT-positive areas. Stitching 243 images together into Figure 15 provided a global look at the differentiated areas of a 24-well. Evidently, cardiac differentiation was predominantly observed on an outer ring around the well. Contrary to these outer areas, most of the middle section of the well did not show the same high degree of differentiation even though several smaller cTnT-positive areas were visible.

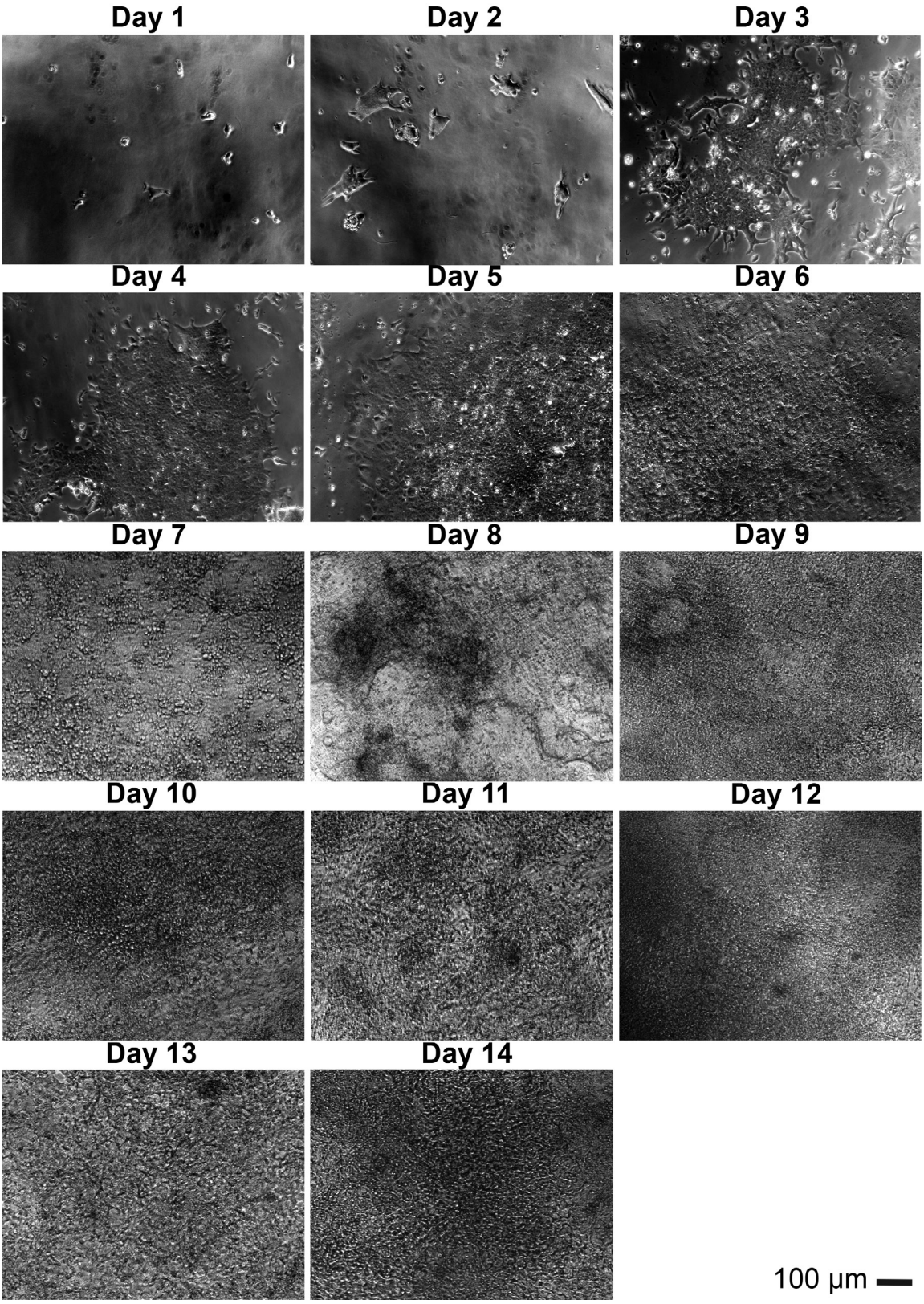

Figure 11: Developing morphology of iPS cells during SECD-Protocol. Representative images of the typical morphology observed in miPS cells undergoing the SECD-Protocol show the gradual increase in cell number until confluency ($\sim$ Day 7) and the subsequent morphology until cardiomyocytes are formed ($\sim$ Day 13). After reaching confluency, cells in some regions also start building 3D structures (e.g. seen from Day 8 on).

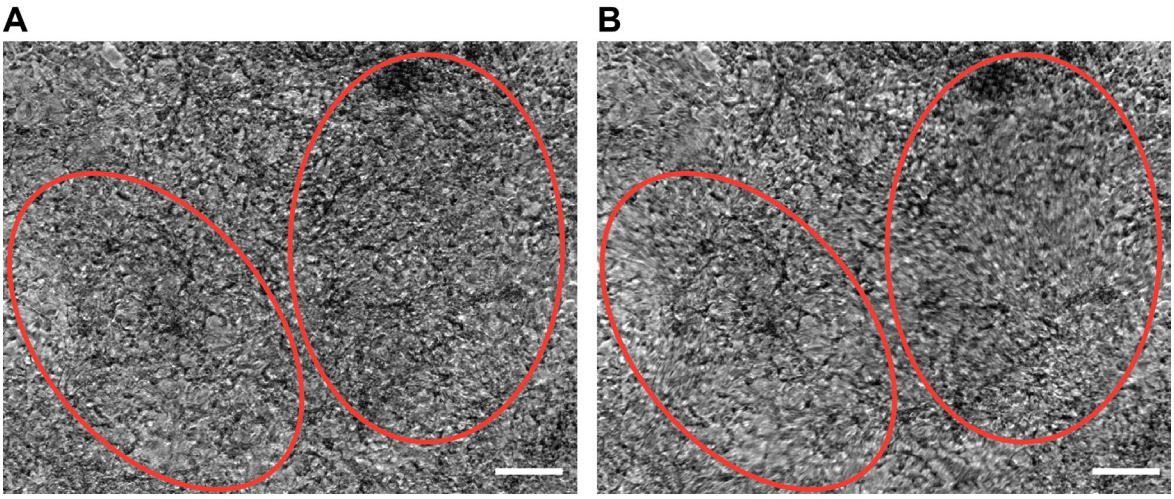

Figure 12: Beating iPS-derived cardiomyocytes generated with the SECD-Protocol. Resting state (A) and contracting state (B) are juxtaposed. Red circles show clear distortions suggestive of contracting cardiomyocytes. Scale bar = 100 μm.

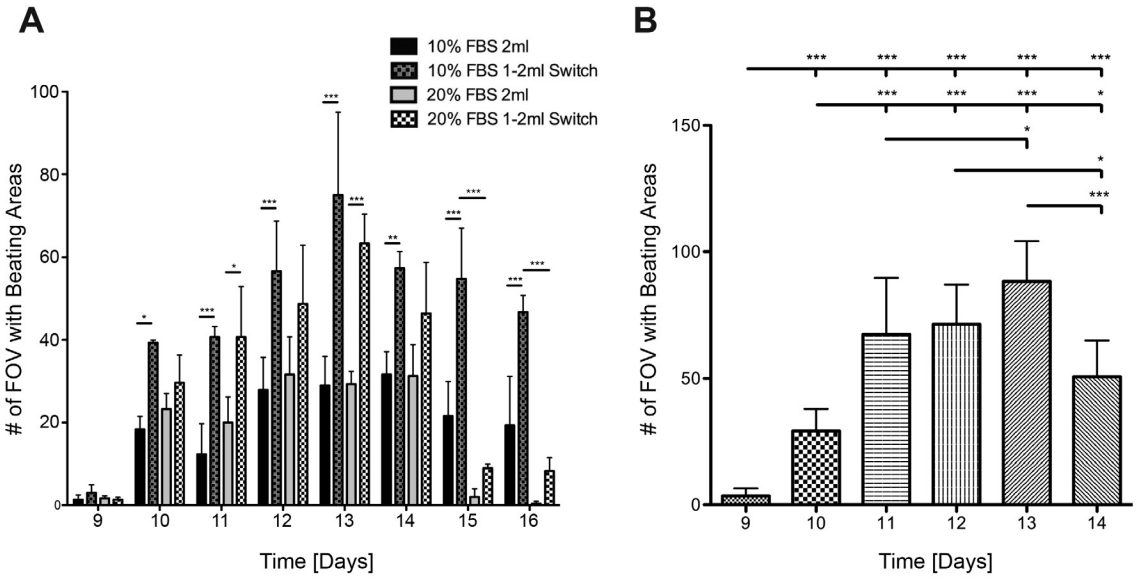

Figure 13: Quantification of beating areas shows a dramatic increase until day 13 of culture and subsequently falls starting at day 14 when using the SECD-Protocol. Moreover, the use of 10% serum and performing the switch from 1 ml to 2 ml medium during culture is necessary for the highest efficiency in cardiomyocyte differentiation (A). Conditions that include the switch demonstrate significantly increased numbers of beating areas regardless of the serum content. Furthermore, panel (B) shows the number of beating areas in multiple replicates subjected to the protocol at different timepoints. (A) N=3, (B) N=12 for Days 9, 10, 11, 12, 13 and N=8 for Day 14. * = $p<0.05$, ** = $p<0.01$, *** = $p<0.001$.

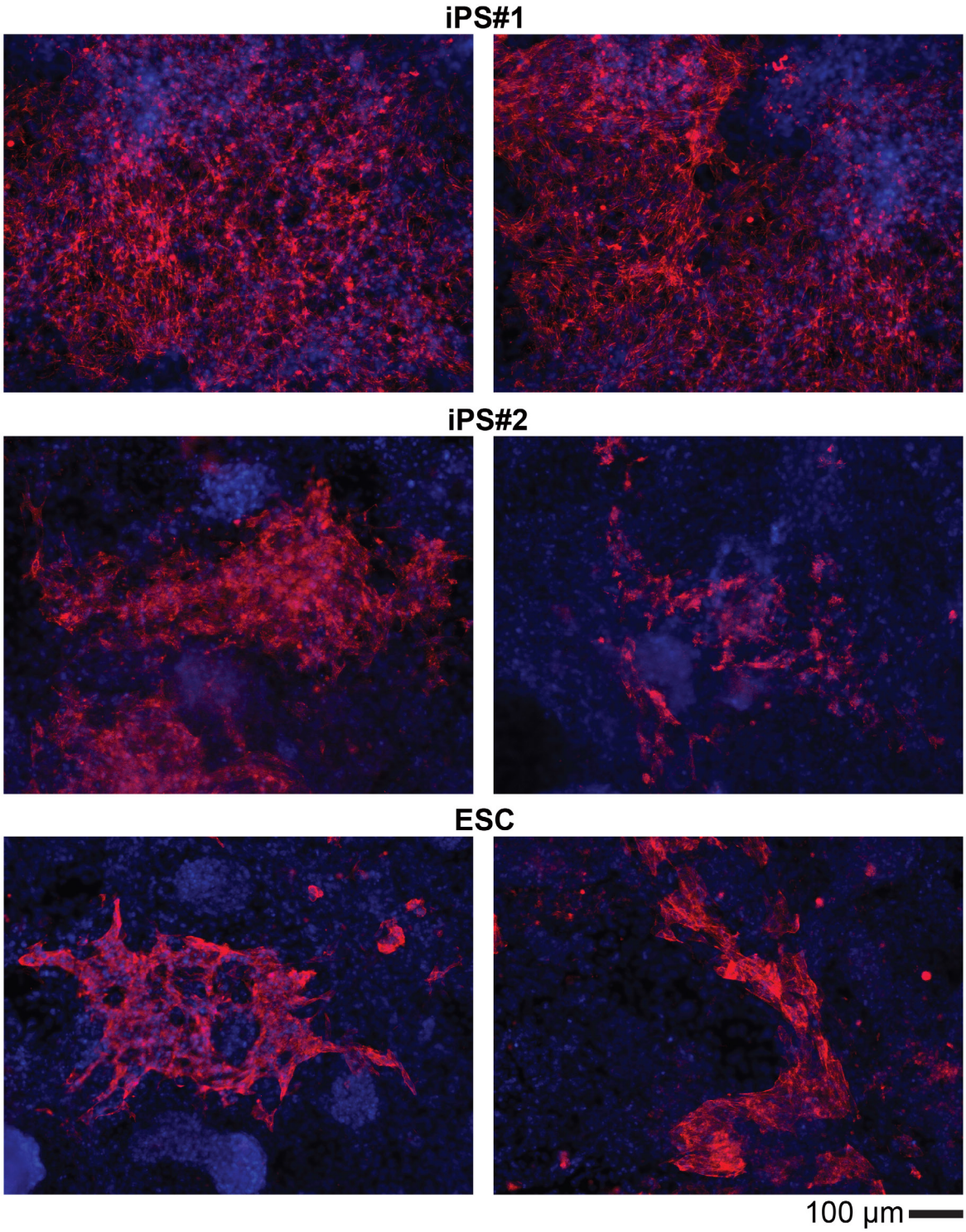

Figure 14: iPS cells (iPS#1) are efficiently differentiated into cardiomyocytes using the SECD-Protocol while a second miPS cell line (iPS#2) and ESCs show several smaller differentiated regions. Representative images of cTnT-positive cells (Red) indicative of iPS- and ESC-derived cardiomyocytes generated with the SECD-Protocol. While the primary iPS cells [67] show efficient differentiation into cardiomyocytes in certain regions, ESCs and iPS#2 do not and instead show several smaller cTnT-positive areas. Staining performed on Day 14.
Nuclei (DAPI) = Blue.

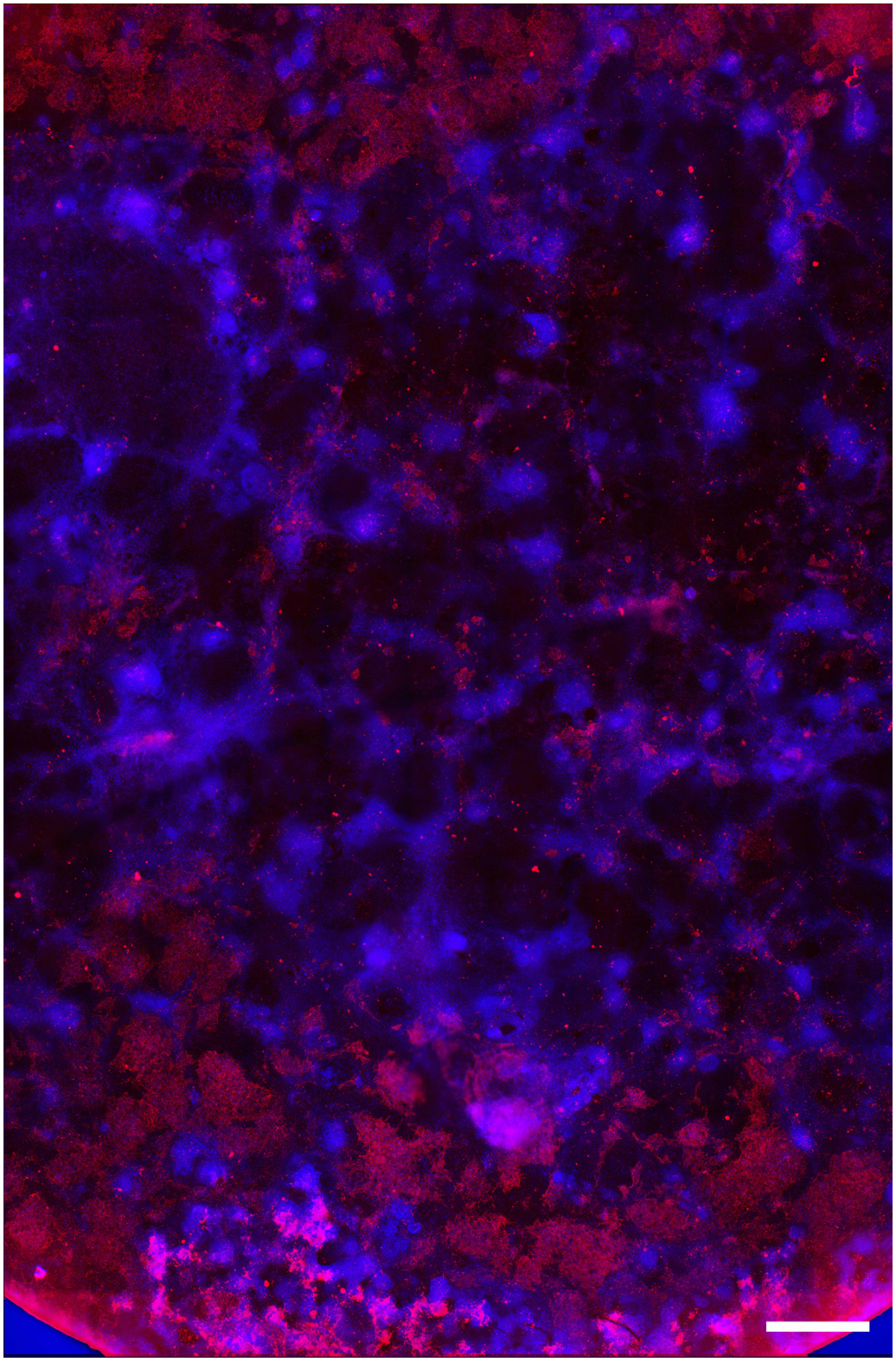

Figure 15: SECD-Protocol shows particularly efficient cardiac differentiation at the outer ring of the well. This image was stitched together from 243 single images to provide a global picture of cTnT-positive cells (Red) indicative of iPS-derived cardiomyocytes generated with the SECD-Protocol. Staining performed on Day 14. Nuclei were stained with DAPI (Blue), Scale bar = 1000 μm.

3.3 Quantification of Wnt-Signaling During Cardiac Differentiation with the SECD-Protocol Reveals an Initial Increase and Subsequent Drop in Active β-Catenin

Overall and nuclear amounts of dephosphorylated, and thus active, β-Catenin were quantified in the hopes of elucidating the mechanism by which the SECD-Protocol exerts its cardiomyogenic stimulus. The resulting area ratios between the β-Catenin-positive and the nuclear DAPI signals, seen in Figure 16, remained very close to 1 in the nuclear quantification (A) and only differed from 1 on Days 2 and 3 of the SECD-Protocol in the quantification of the global signal (C). In fact, only the amount of global Day 2 signal ratio differed significantly from Days 4, 5, 6, 8, 9 and 10. Day 2 and 3 in the quantification of the total signal ratio also exhibited a high standard deviation.

The integrated density ratio between the active β-Catenin signal and the DAPI signal was also quantified (Figure 16 (B) and (D)). It showed that active β-Catenin remained on a plateau for Days 2, 3 and 4 of the SECD-Protocol and subsequently increased in the nuclei and overall until Days 6 and 7. Eventually and from Day 8 through Day 10, active β-Catenin levels fell back to a similar level as on Days 2, 3 and 4. The nuclear levels of β-Catenin showed significant differences during the course of the SECD-Protocol. Firstly, Day 2, 3 and 4 differed significantly from Day 7. Secondly, Day 3 differed significantly from Day 7 and Day 4 from Days 6 and 7. Moreover, the amount of β-Catenin on days 5, 6 and 7 was markedly and significantly higher than the amount on Days 8, 9 and 10. The integrated density ratios of the total quantifications showed the same trend as the nuclear quantification revealing lower levels on days 2, 3 and 4, higher levels on days 5, 6 and 7 and again low levels on days 8, 9 and 10. Indeed, Day 2 was significantly lower than Days 5, 6 and 7 and β-Catenin levels on Days 5, 6 and 7 were significantly elevated compared to Days 8, 9 and 10.

The results from the quantification can be seen in representative images showing the sequential increase of signal associated with activated β-Catenin until Day 7 and subsequent decrease starting on Day 8 (Figure 17).

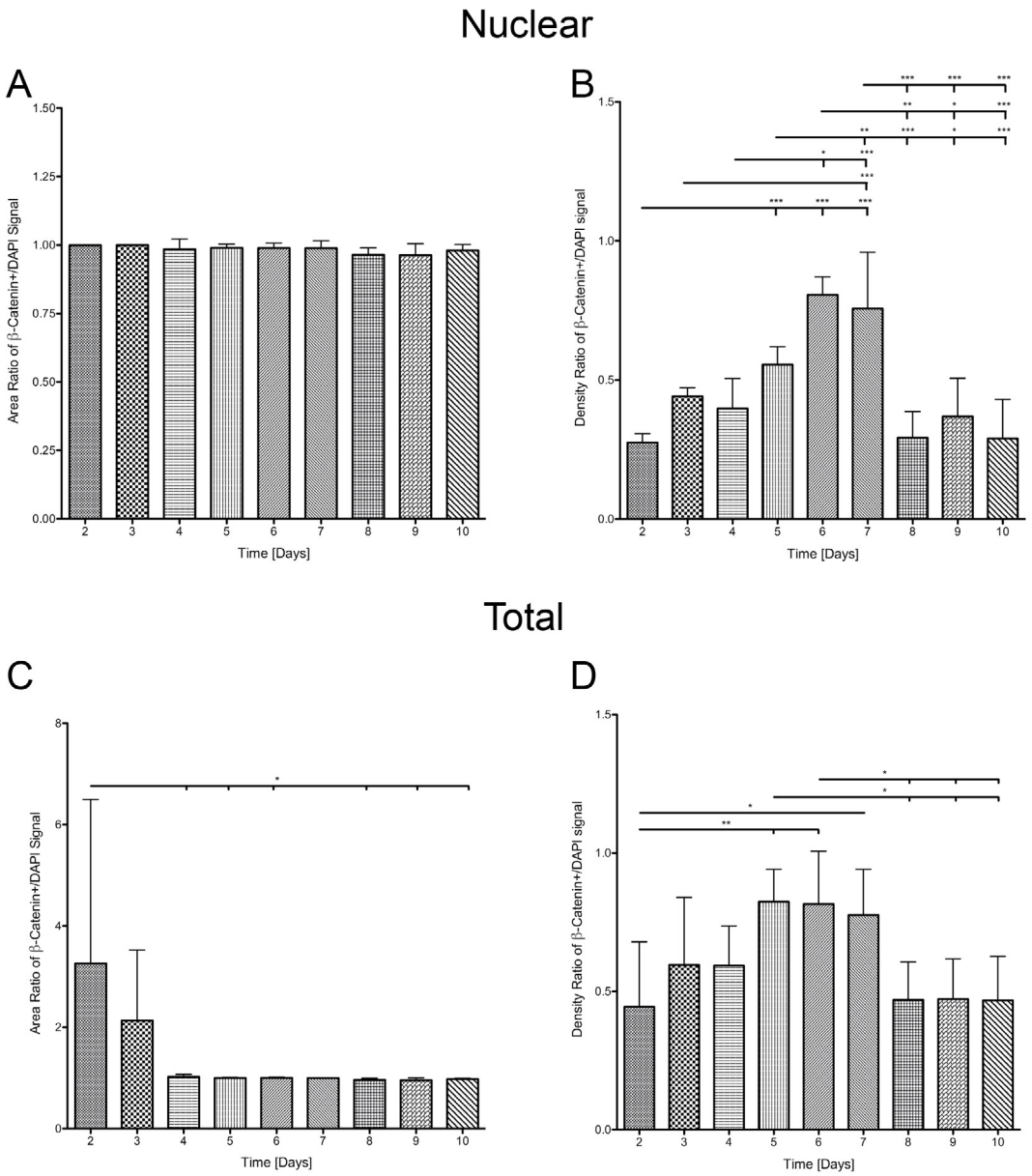

Figure 16: Active β-Catenin levels show a sequential activation (rise until Day 7) and inactivation (decrease starting on Day 8) of Wnt-Signaling. Nuclear area ratio (A) and nuclear integrated density ratio (B) between β-Catenin and DAPI signals show a significant increase until day 7 and subsequent decrease starting on Day 8 and maintained through Day 10. The nuclear area ratio shows that the nuclear area was completely covered by β-Catenin signal. (C) and (D) show the total area and integrated density ratios and display the same trend. N=9 for (A) and (B) and N=7 for (C) and (D). * = $p<0.05$, ** = $p<0.01$, *** = $p<0.001$.

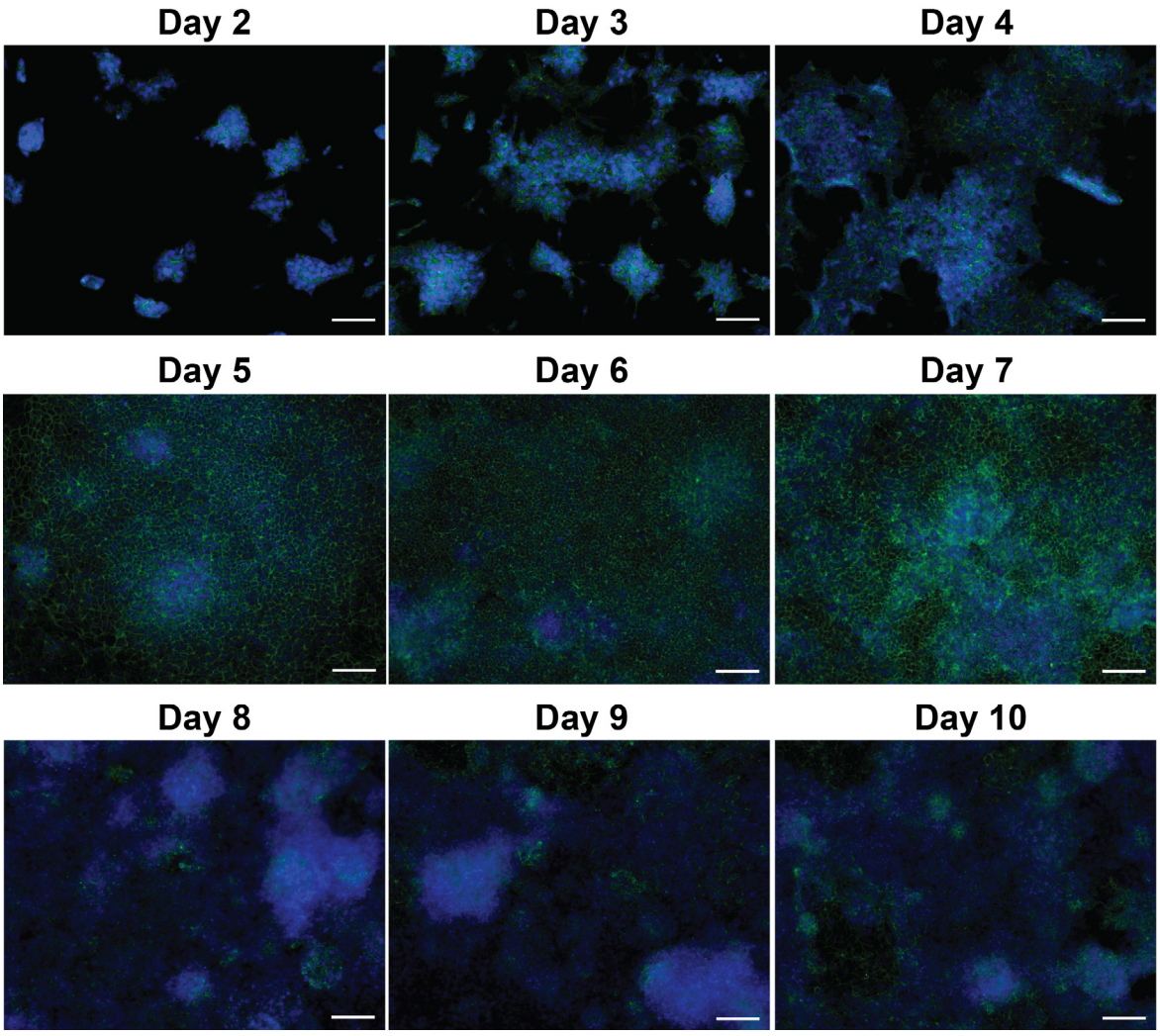

Figure 17: Representative images of the active β-Catenin staining (green) performed during the SECD-Protocol. Active β-Catenin levels show a sequential activation (rise in signal until Day 7) and inactivation (decrease in signal starting on Day 8) of Wnt-Signaling. Nuclei stained with DAPI (blue), Scale bar = 100 μm.

3.4 Directed Differentiation into Cardiomyocytes Utilizing Standard EB-based Protocols Showed Contrasting Results (3D)

miPS cells were subjected to standard cardiomyocyte differentiation protocols based on Wang *et al.* [22] and Kwon *et al.* [36], in order to determine the inherent potential of miPS cells to differentiate into cardiomyocytes and to compare it to the SECD-Protocol. These protocols employ EB formation and the Wnt-modulating molecules Wnt3a and XAV939.

Employing the protocol from Wang *et al.* [22], I was not able to obtain any beating areas (quantified in Figure 20 (A)) and cells instead showed multiple distinct morphologies within the EB outgrowth, depicted in Figure 18. Cells displayed mesenchymal-like morphologies (Figure 18 (B)), flat, cobblestone-like morphologies (Figure 18 (C)) and other cells contained what appeared to be fat vacuoles (Figure 18 (D)).

Conversely, cTnT-stainings of EBs subjected to the protocol of Kwon *et al.* [36], seen in Figure 19, revealed that there were several cTnT-positive regions. A global picture of the entire EB and its surroundings showing multiple cTnT-positive regions concentrated in the center region of the EB was obtained by stitching single images together to show an entire EB area (Figure 21). The outer areas only show spotty cTnT expression, if any.

Furthermore, starting on Day 7, between 90% and 100% of EBs developed beating areas if stimulated with Wnt3a, as described by Kwon *et al.* [36] (as seen in Figure 20 (A)). These beating areas were maintained through Day 12.

Conversely, addition of small molecule activators (CHIR99021) and inhibitors (XAV939) of Wnt signaling led to differences in the emergence of contracting areas (Figure 20 (B)). Stimulation with CHIR99021 for the same period as previously stimulated with Wnt3a clearly showed a significant overall drop in the number of beating areas that emerged between Days 8 and 12. EBs subjected to the differentiation protocol based on Wang *et al.* [22] and utilizing the small molecule Wnt inhibitor XAV939 between Days 3 and 5 did not show any contracting regions at any time during their culture. However, changing the medium from IMDM to GMEM 51492C resulted in appearance of beating regions on Day 9. Furthermore, beginning on Day 10 and through Day 12, 90% to 100% of the EBs displayed beating areas and their number did not differ thereafter from the protocols employing Wnt3a as a stimulant.

The resulting quantification of the area ratio of the cTnT-positive area of global stiches including the ones seen in Figure 15 and Figure 21 is seen in Figure 22. The cTnT signal was set in relation to the nuclei and the quantification revealed a significantly higher area ratio in the newly developed SECD-Protocol compared to the EB-based protocol by Kwon *et al.* [36].

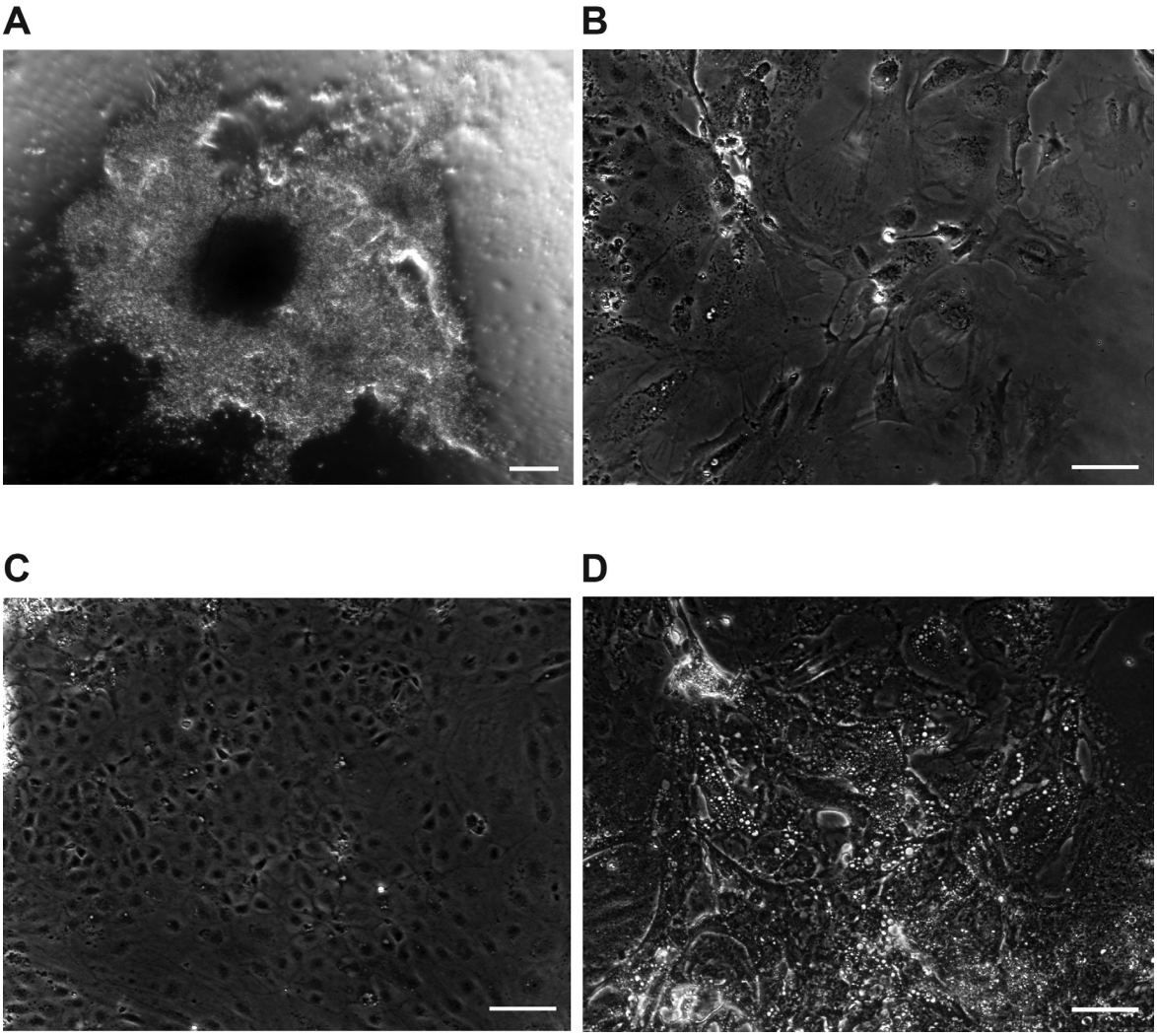

Figure 18: EBs subjected to the protocol of Wang *et al.* [22] did not show any contracting regions but iPS cells instead displayed morphologies characteristic of other cell types. (A) provides a top view of the EB and the outgrowing cells and (B) shows cells extending multiple filopodia in a mesenchymal-like morphology. Cells in (C) exhibit a flat and cobblestone-like morphology and (D) shows several cells that appear to contain fat vacuoles. Images from Day 10 of culture. Scale bars 200 μm for (A) and 100 μm for (B, C, D).

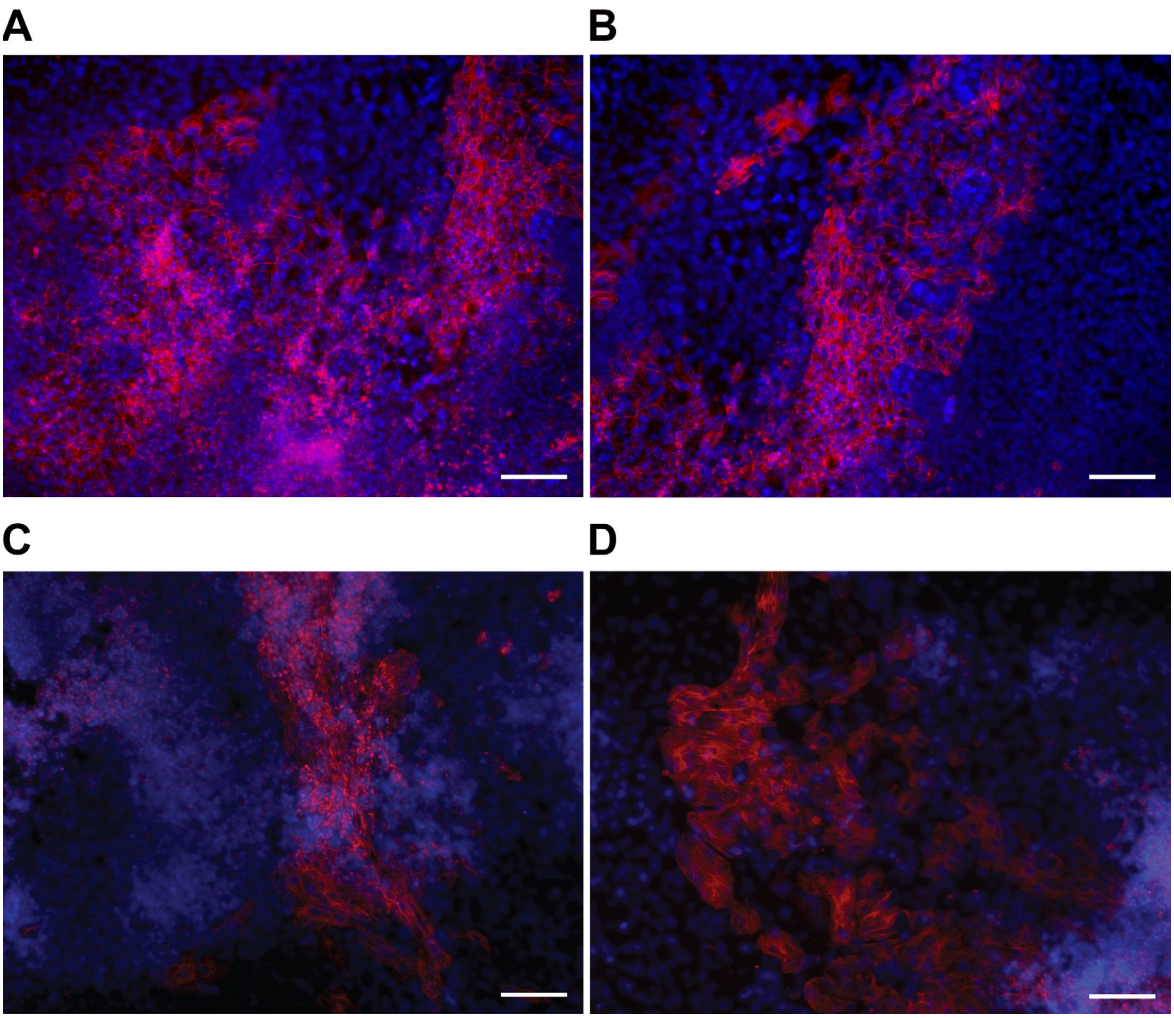

Figure 19: The EB-based protocol by Kwon *et al.* [36] leads to several, however heterogenous, cTnT-positive regions (Red) over the course of 12 days using miPS cells. Representative images in (A), (B), (C) and (D) show heterogenous cTnT-positive areas ranging from high cTnT-staining (A) in some areas to areas with low cTnT-staining ((B), (C) and (D)). Nuclei were stained with DAPI (Blue); Scale bar = 100 μm.

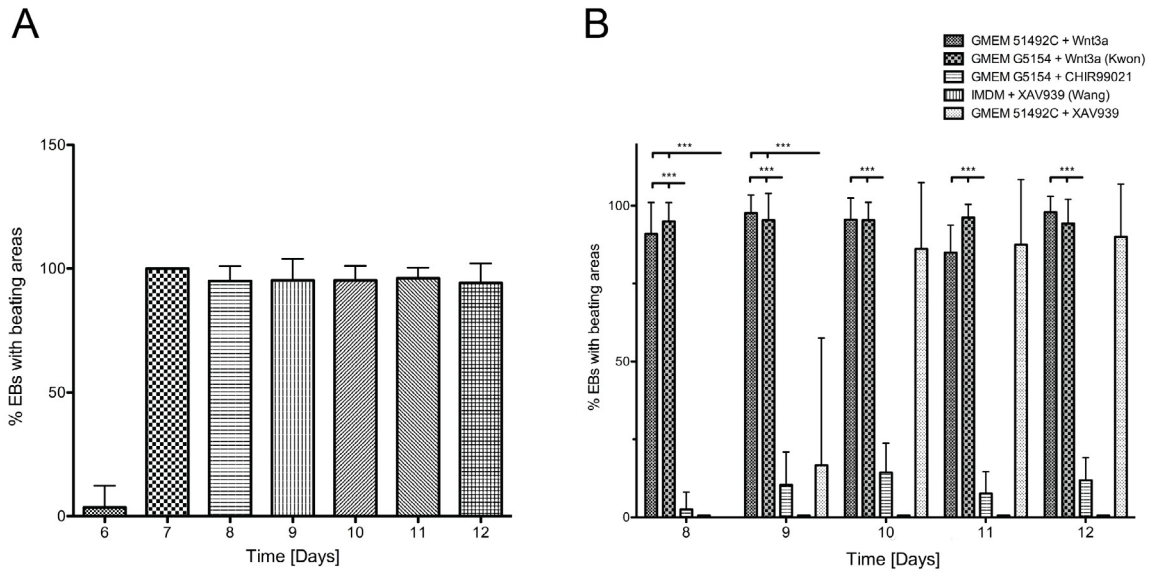

Figure 20: Different EB-based cardiac differentiation protocols show very diverse efficiency. (A) Percentage of EBs with beating areas after undergoing the original van Laake *et al.* [67], Kwon *et al.* [36] protocol. EBs were treated with Wnt3a between days 4-6 and between 90%-100% of the EBs had beating areas after 7 days. (B) Percentage of EBs with beating areas after several modifications (the Wnt activator CHIR99021 instead of Wnt3a) to the original Kwon-protocol compared to the Wang *et al.* [22] protocol using IMDM instead of GMEM and the Wnt inhibitor XAV939 between days 3-5. N=6 for (A) and (B). * = $p<0.05$, ** = $p<0.01$, *** = $p<0.001$.

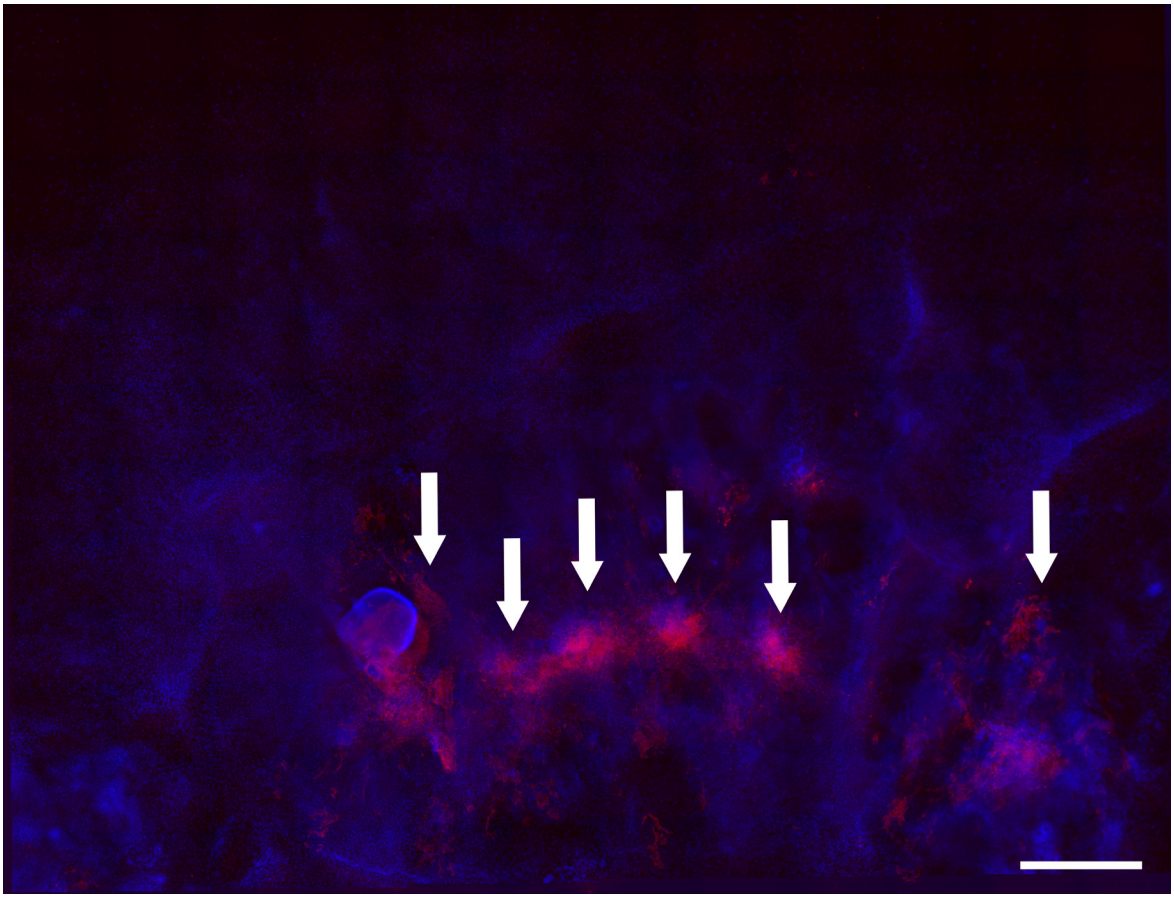

Figure 21: The EB-based protocol by Kwon *et al.* [36] leads to several cTnT-positive regions over the course of 12 days (white arrows). This image was stitched together from 145 images and provides a global picture of cTnT-positive cells (Red) indicative of miPS-derived cardiomyocytes. Staining performed on Day 12. Nuclei were stained with DAPI (Blue), Scale bar = 1000 μm.

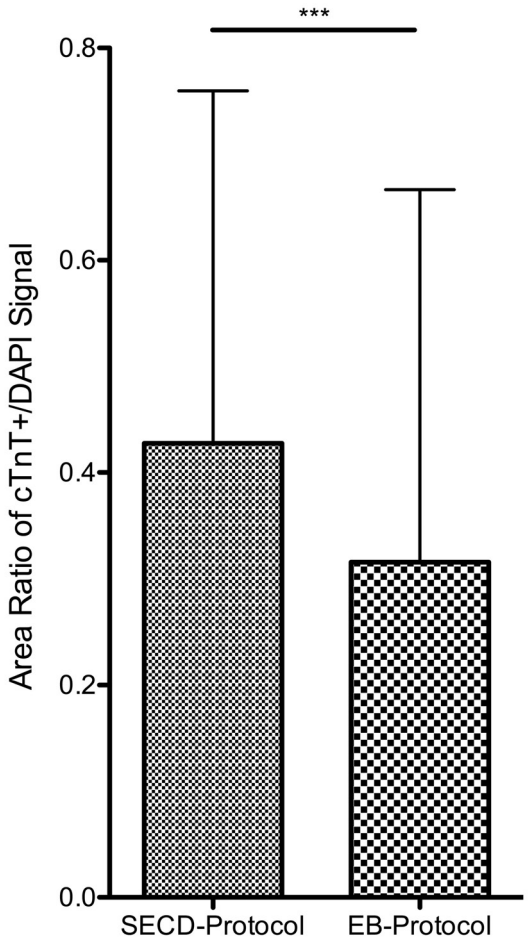

Figure 22: Quantification of area ratio of cTnT-positive signal, normalized to DAPI, confirms that the newly developed SECD-Protocol produces a significantly higher number of cardiomyocytes compared to a standard EB-based protocol (based on Kwon *et. al.* [36]). The entire well/EB area was scanned and the area of cTnT-positive signal of each single image was measured. These measurements were then set in relation to the DAPI signal to obtain the area ratio. Well subjected to the SECD-Protocol contained 240 measured images and 3 analyzed EB-regions made up a total of 418 images. *** = $p<0.001$.

3.5 Successful PEG-Hydrogel Formation Encapsulates Cells and ECM Molecules and miPS Cells Remain Viable in PEG Hydrogel Culture

Firstly, the hydrogel formation was successful and that cells and ECM molecules were successfully entrapped in the hydrogels (Figure 24). In the PEG condition, miPS colonies appear as clearly visible white spots inside the hydrogel (Figure 24 (A)). Moreover, and as visualized in the conditions encompassing ECM molecules in addition to miPS cells ("+++", "opt" and "opt + GF"), combinations of cells and ECM molecules reveal a more pronounced white matrix inside the hydrogel ((Figure 24 (A))).

Secondly, it was confirmed that medium readily diffuses into the hydrogel as indicated by the red coloration of the hydrogels brought about by the phenol red indicator in the medium (Figure 24 (B)). In fact, to show that I was able to readily grow iPS cells in the manufactured PEG hydrogels, cells were encapsulated in them and observed during culture. miPS cells grew normally and showed typical colony formation and actin staining (as seen in Figure 23 (A) and (B)).

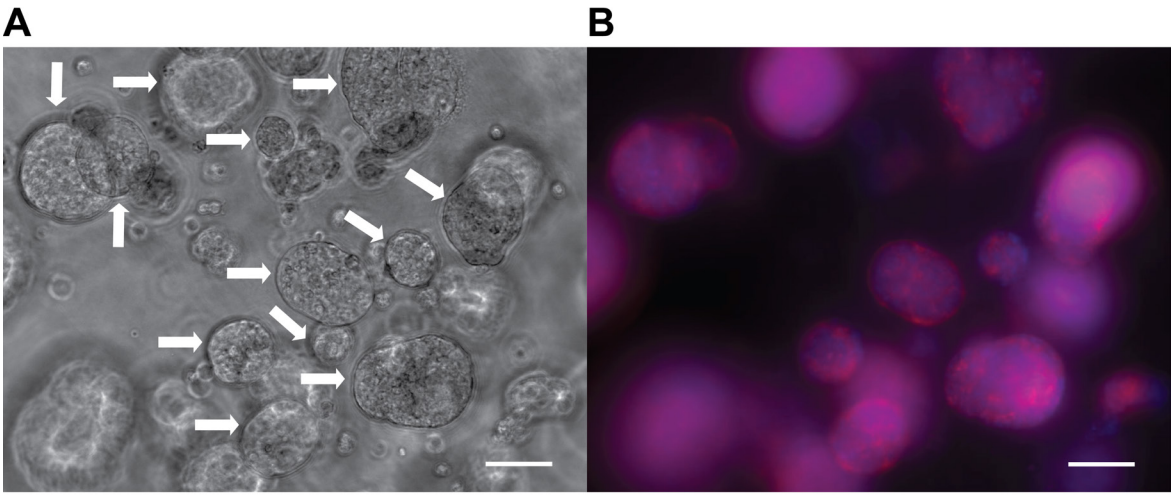

Figure 23: miPS-cell-colonies (white arrows show representative colonies) remain viable in PEG hydrogels. (A) Phase contrast image of the typical iPS cell colonies in a PEG hydrogel. (B) Corresponding image showing nuclear (DAPI) staining in blue and cytoskeletal (F-actin/Phalloidin) staining in pink. Scale bar = 100 μm.

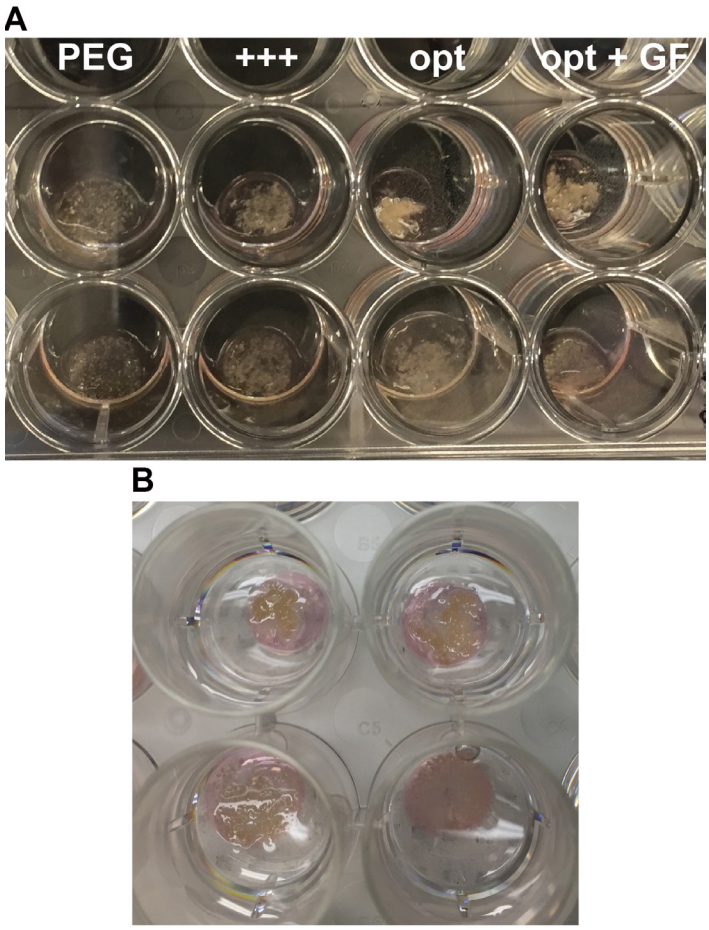

Figure 24: Hydrogel formation and cell/ECM entrapment was successful. (A) shows clearly visible cells in the PEG only condition, whereas hydrogels additionally containing different ECM formulations (”+++”, ”opt”, ”opt + GF”) reveal a more pronounced white matrix (composed of cells and ECM molecules) inside the hydrogel. The distinct color of phenol red in the medium, seen in (B), confirms the efficient incorporation of medium into the hydrogels. “+++”: Hydrogel contains Col I, LN, and FN. “Opt” contains an ECM composition of Col I, LN and FN optimized for cardiomyocyte differentiation. “Opt + GF” contains optimized composition of ECM with bound BMP4 & bFGF.

3.6 Growth Factors and Heparin Showed an Inherent Ability to Non-Covalently Bind to ECM Molecules

To test the hypothesis that growth factors can enhance cardiac differentiation in a 3D hydrogel containing miPS cells and ECM molecules, I first showed that the growth factors have an inherent ability to attach non-covalently to collagen I + heparin and fibronectin with the developed assays found in sections 2.5.1 and 2.5.3.

bFGF showed a mean concentration of 4.602 ng/ml in the supernatant taken from a collagen I matrix and showed a similar mean supernatant concentration (5.171 ng/ml) when heparin was added (as observed in Figure 25 (A)). Additionally, bFGF did not show up in the conditions where it was not added. No statistical differences could be observed between the heparin containing condition and the heparin free condition.

The resulting retention rates for bFGF when added to a fibronectin coated cell culture well are shown in Figure 25 (B). When incubated on a fibronectin coated well, bFGF demonstrated a mean concentration of 5.756 ng/ml in the supernatant. Also, bFGF showed a not significantly different but higher mean supernatant concentration (7.253 ng/ml) when heparin was added and did not show up in the conditions where it was not added. No statistical differences could be observed between the heparin containing and heparin free condition.

BMP4 retention results (shown in Figure 25 (C)) visualize the complete retention of the added concentration of BMP4 on a collagen I matrix including the condition that encompassed heparin.

The retention of heparin itself to collagen I was tested using the developed protocol of section 2.5.3 on 2D and 3D collagen matrices (Figure 25 (D)). Heparin exhibited a mean concentration of 0.877 μg/ml in the supernatant incubated on a 2D collagen matrix and 0.354 μg/ml in the supernatant originating from a 3D collagen matrix. Moreover, there was a significant difference in concentration if heparin was added to a 3D matrix compared to the control that did not contain heparin. In a 2D environment, no significant difference could be observed between the supernatants that originally contained heparin and the one that did not.

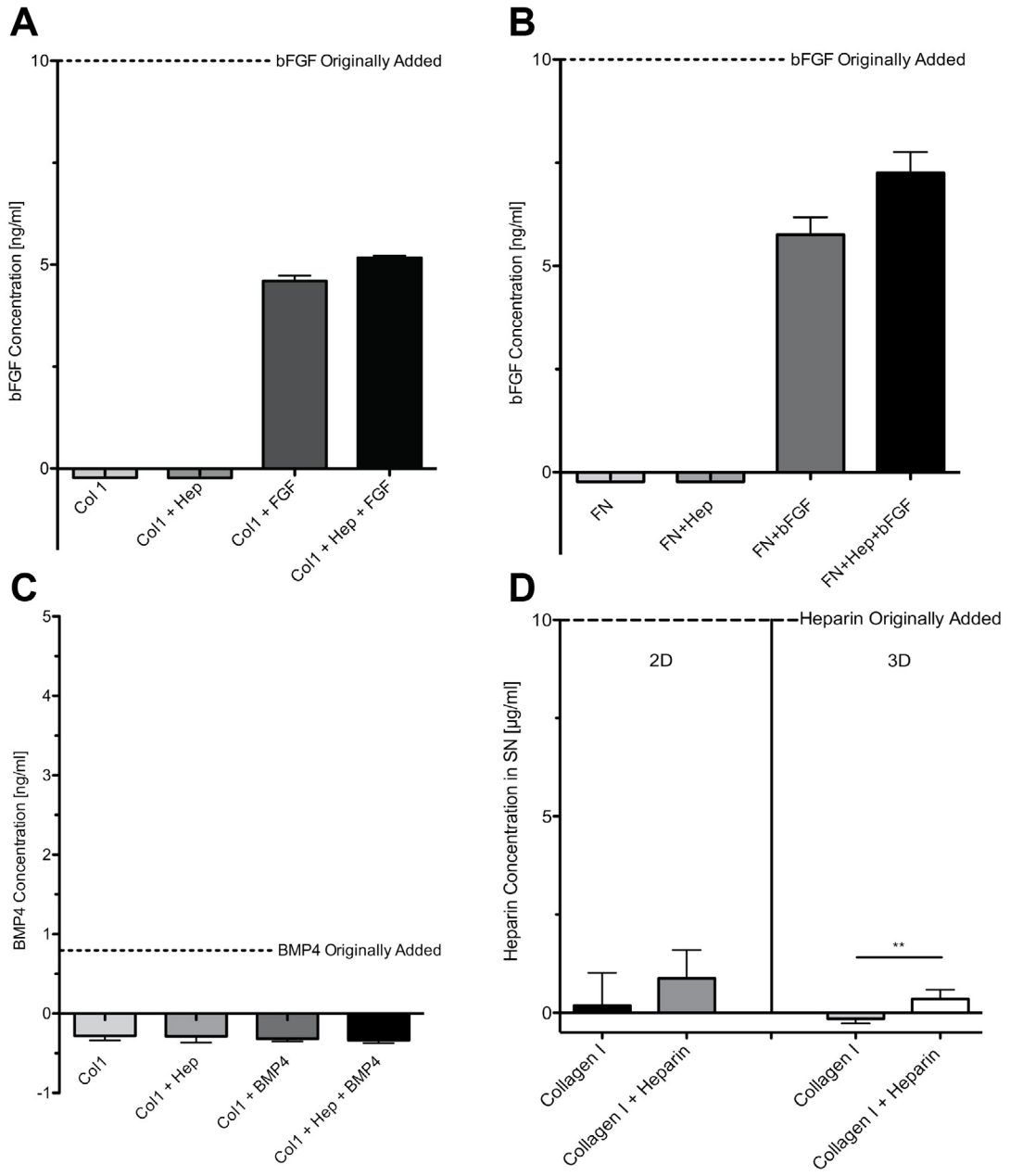

Figure 25: Growth factors and heparin are effectively retained on collagen/fibronectin matrices. (A) ELISA results of the supernatant incubated with a collagen matrix, showing that 4.602 ng/ml of bFGF was still present. If incubated on collagen + heparin 5.171 ng/ml were still present. A similar trend can be seen if bFGF is incubated on a fibronectin-coated surface (B) showing that slightly less than half of bFGF is retained on fibronectin (5.756 ng/ml after incubation on fibronectin and 7.253 ng/ml on fibronectin + heparin). Panel (C), however, shows that all of BMP4 is retained on the collagen matrix. Panel (D) depicts the DMMB results showing that almost all heparin is retained on the collagen films (2D, 0.877 μg/ml) and matrices (3D, 0.354 μg/ml). Dotted lines show the original concentration of protein of interest/heparin added. N=2 for A, B, C and N$\geq$4 for D. ** = p$<$0.01.

3.7 Attaching Growth Factors Non-Covalently to ECM Molecules Encapsulated in PEG Hydrogels Enhances the cTnT Expression of miPS Cells Undergoing Cardiac Differentiation

miPS cells were encapsulated in PEG hydrogels together with bFGF non-covalently coupled to fibronectin and BMP4 non-covalently attached to collagen I + heparin to determine the impact of the ECM-bound growth factors on cardiomyogenic specification. miPS cells cultured in plain PEG hydrogels did not exhibit noticeable cTnT expression after 14 days, as seen in Figure 26 and globally in Figure 27. However, if encapsulated together with collagen I, laminin and fibronectin they showed some positive cTnT staining, as evidenced in the "+++" condition of Figure 26. Moreover, Figure 27 and the respective view of the whole hydrogel confirmed the above statement. Cells also showed a significant amount of cTnT expression when cultured in an ECM formulation consisting of the previously mentioned elements, however optimized for cardiac differentiation ("opt"). On top of that, even stronger cTnT staining can be observed in the "opt + GF" conditions of Figure 26 and Figure 27 that incorporate the growth factors into the optimized ECM formulation. The latter figure visualizes the overall distribution and expression of cTnT throughout the entire hydrogel.

The quantification of cTnT expression in the form of area ratios Figure 28 (A) and integrated density ratios Figure 28 (B) between cTnT-positive signal and nuclear staining (DAPI) for miPS cells encapsulated in "PEG", "+++", "opt" and "opt + GF" was performed. The area ratio (in Figure 28 (A)) was increased when ECM was encapsulated together with miPS cells followed by a further increase if the optimized formulation was used. The cTnT/DAPI area ratio was subsequently further increased when cultured with the optimized ECM formulation and the attached growth factors. As a matter of fact, cTnT/DAPI area ratio was significantly increased in the "opt + GF" condition compared to the PEG condition. The integrated density ratio of cTnT signal normalized to DAPI, demonstrated a trend comparable to the area ratio (Figure 28 (B)). The "opt + GF" condition differed significantly from the PEG condition and maintained the highest mean ratio of all conditions. The integrated density ratio was non-significantly increased in the "+++" condition compared to "PEG" and showed a higher mean ratio compared to "opt". However, "opt" displayed a higher standard deviation.

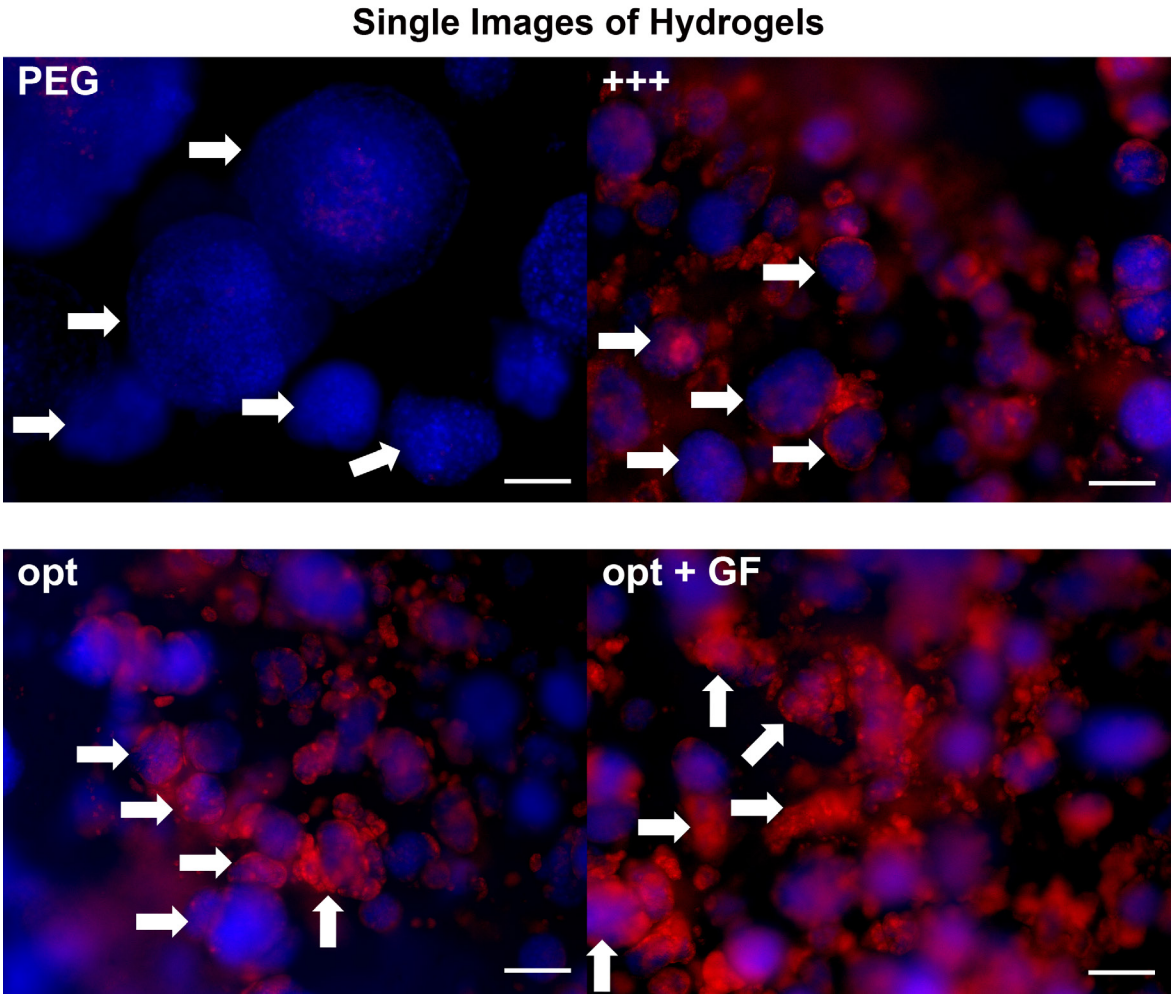

Figure 26: Attachment of GFs to ECM molecules encapsulated with miPS cells (white arrows demonstrate representative cell colonies) during a 14-day culture period in PEG hydrogels demonstrates stronger cTnT signal compared to the controls. Different ECM formulations (”+++”, ”opt”) or ”PEG” only are shown. “+++”: Hydrogel contains Col I, LN, and FN. “Opt” contains an ECM composition of Col I, LN and FN optimized for cardiomyocyte differentiation. “Opt + GF” contains optimized composition of ECM with bound BMP4 & bFGF. Scale bar = 100 μm.

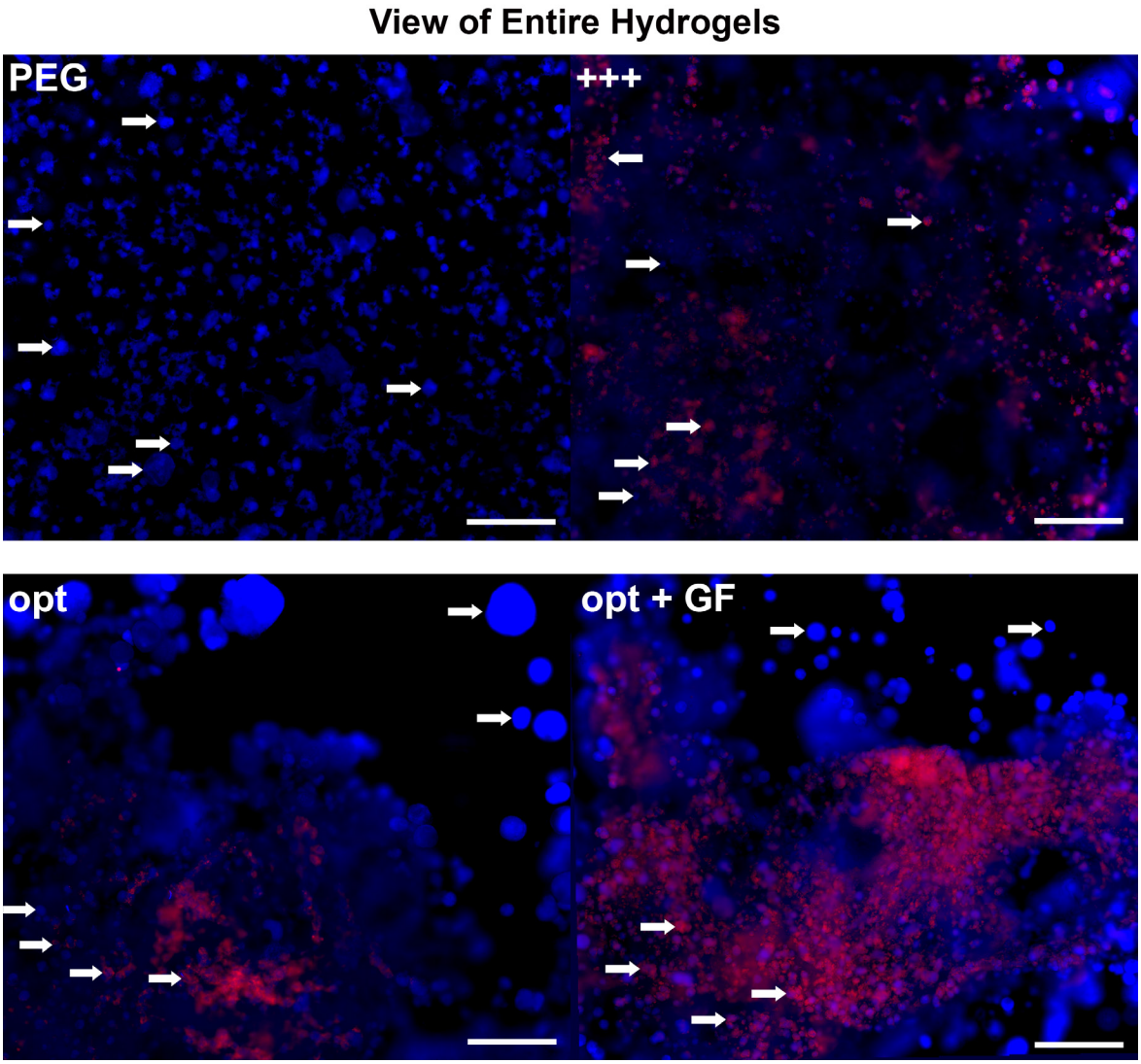

Figure 27: Stitched images of the entire hydrogel confirm the fact that attachment of GFs to ECM molecules encapsulated with miPS cells (white arrows demonstrate representative cell colonies) in PEG hydrogels demonstrates stronger cTnT signal compared to the controls. These images show the entire hydrogel and were stitched together from 72 single images. Different ECM formulations (”+++”, ”opt”) or ”PEG” only are shown. “+++”: Hydrogel contains Col I, LN, and FN. “Opt” contains an ECM composition of Col I, LN and FN optimized for cardiomyocyte differentiation. “Opt + GF” contains optimized composition of ECM with bound BMP4 & bFGF. Scale bar = 1000 μm.

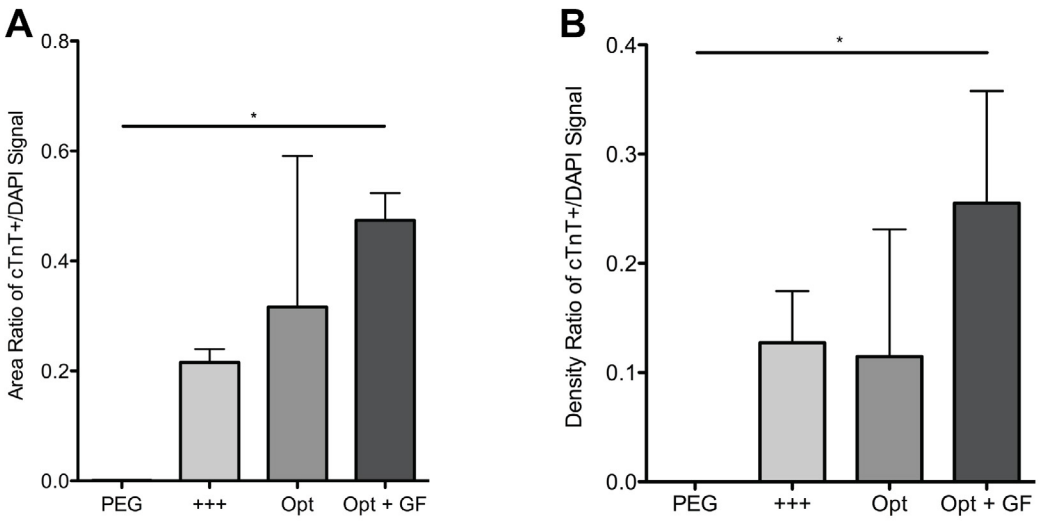

Figure 28: Quantification of area ratio (A) and integrated density ratio (B) of cTnT-positive signal normalized to DAPI confirms that attaching GFs to the ECM/Cells in a PEG-Hydrogel promotes cardiomyocyte differentiation. N= 4 for ”Opt + GF” and ”PEG”, N=3 for ”+++” and N=2 for ”Opt”. * = $p<0.05$, ** = $p<0.01$, *** = $p<0.001$.

4 Discussion

In this thesis, a new and efficient differentiation protocol for at least one iPS cell line was developed and characterized and it was discovered that it is possible to attach bFGF and BMP4 to ECM molecules, which leads to an increased cardiomyocyte generation in a 3D environment.

Firstly, the pluripotency of the used iPS cell line [67] was confirmed in Figure 10 by the cells displaying the typical embryonic stem cell colony-forming morphology and the Oct3/4 staining, a transcription factor that aids in maintaining pluripotency [6, 3].

Here I show a newly developed cardiomyocyte differentiation protocol based solely on the timely exchange of a specific amount of medium that led to iPS-derived cells that showed multiple characteristics of cardiomyocytes. Not only did the protocol give rise to over 100 contracting areas at its peak, around Day 13 of the protocol (seen in Figure 13), but these beating regions also displayed extensive beating spanning multiple entire fields of view (as seen in Figure 12). These beating areas were similar if not equivalent to the beating areas obtained by other leading protocols in the field reporting up to 98% efficacy such as Lian *et al.* [3, 32] for human iPS-derived cardiomyocytes and Kattman *et al.* [26] or Hao *et al.* [73] for murine iPS-derived cardiomyocytes. Interestingly, these protocols employing murine iPS or ES cells usually show that cardiomyocyte differentiation is complete at about the eighth day, whereas the described protocol in this thesis shows differentiation reaches its completion at about Day 13. The reason for that could potentially be that the protocol described here lacks any specific stimulation by bioactive molecules, outside of the serum in the cell culture medium, which would most likely speed up the process of differentiation. In fact, most protocols for cardiac differentiation of murine iPS cells employ up to 20% of serum and/or other supplements such as B27 in addition to the stimulating molecules [21, 22, 26, 73, 74]. The developed protocol also differs from most other protocols in that the seeding density is kept relatively low at 7000 cells/24 well. This most likely also contributes to the delayed differentiation (the progression can be seen in Figure 11) but may indeed be another key factor driving the differentiation. Evidence seen in Figure 16 suggests that Wnt signaling increases until Day 7 of the protocol and subsequently decreases significantly. The evidence is particularly compelling as both nuclear and overall quantification resulted in the increase prior to the decrease in active β-catenin. The fact that the seeding density is low likely stimulated cellular proliferation, and thus also kept Wnt signaling active. Incidentally, cells also reached confluency around Day 7, seen in Figure 11, and starting on Day 8, Wnt signaling decreased in line with the potential stop in proliferation due to contact inhibition. This trend can also be seen in the representative images taken during the SECD-Protocol in Figure 17.

Intriguingly, cardiac differentiation of the miPS cells seemed to function best in the outer regions of the 24 well as depicted in Figure 15, which was stitched together from 243 single images to provide a comprehensive view of the differentiation. The reasons for this phenomenon could be manifold, but it is likely the interplay between the right seeding density, speed of proliferation and thus also modulation of Wnt-signaling, and timely contact inhibition that provides the necessary framework for surprisingly efficient cardiac differentiation. As a matter of fact, Ma *et al.* [75] already showed that differentiation is mediated, in no small part, by the mechanical and physical environment as they created

self-organizing cardiac microchambers mediated by geometric confinement and thus spatially confined mechanical stress. Another interesting report by Rosowski *et al.* [76] recently showed that cells at the edges of pluripotent colonies start differentiating first and remain on the perimeter of the colony. This is due to stronger mechanical interactions with the ECM at the border, which correlates well with the observed differentiation efficiency of the SECD-Protocol in the outer regions of the well.

It is also noteworthy that this SECD-protocol yielded significantly better results than several established EB-based protocols (seen in Figure 18, Figure 19, Figure 21 and Figure 20 and quantified in Figure 22) which have been the traditional cardiac differentiation method for miPS/mES cells [22, 26, 73, 74]. In fact, the protocol based on Wang *et al.* [22] failed to produce any tangible results at all while using their Wnt-inhibitor, namely XAV939, with our culture medium resulted in delayed emergence of cardiomyocytes. Moreover, another chemical modulator (activator) of the Wnt-signaling pathway, CHIR99021, that significantly promoted cardiac differentiation in human iPS cell lines [3, 32] only led to a minimal development of contracting areas in the used murine iPS cells (seen in Figure 20). These findings highlight the fact that cardiac differentiation protocols still remain highly heterogeneous in regard to successful cardiomyocyte differentiation and may involve significant species-specific differences. There are also significant differences between iPS cells themselves and other pluripotent cell lines such as ES cells as neither a second iPS cell line (iPS#2, [68]), nor a murine ESC line [69] were able to show the same degree of differentiation. One possible explanation for the selective functionality of the SECD-Protocol seen with the primarily used iPS cell line could be that the iPS generation process, involving the transfection with the four reprogramming factors Oct-4, Sox-2, Klf4 and c-Myc, included a GFP reporter gene in the NKX2.5 locus [67]. The introduction of the GFP gene could have promoted the ability of these cells to differentiate into cardiomyocytes by, for instance, opening up the NKX2.5 gene, an early cardiac transcription factor. Nevertheless, van Laake *et al.* [67] also analyzed the transcriptomes of multiple iPS and ES cells and their derived cardiomyocytes and showed that the genome wide mRNA analysis displayed very high similarities. Indeed, only 195 of 28,853 transcripts differed significantly between ES and iPS and of those 195 only 38 genes were increased more than 2-fold [67]. Similar findings were also obtained by Gupta *et al.* [77]. In light of these findings it seems unlikely that the observed heterogeneity in terms of differentiation can be attributed solely to the gene expression, albeit still possible.

Regardless of the observed heterogeneity, the SECD-protocol yielded significant cardiomyocyte generation in the primarily used miPS cell line [67] that rivals and arguably even surpasses the cardiomyocyte generation observed with the protocol proposed by Kwon *et al.* [36] (Figure 15 vs. Figure 20). In fact, quantification of entire well/EB area, seen in Figure 22, confirms that the SECD protocol yields a higher cardiomyocyte number. This holds especially true, considering the fact that the 3D cell aggregations produced with EBs unfortunately yields prominent false positive signals because it falsely retained some of the secondary antibody. The true cTnT-positive regions display the characteristic striated structures observed in Figure 14 and Figure 18. While some truly positive cTnT signals can be seen in the global view of the EB in Figure 20, they do not compare to the results achieved by the SECD-protocol, especially compared to the outer regions of the well, seen in Figure 15.

As visualized in Figure 24, PEG hydrogels including entrapped cells and ECM molecules were successfully generated and these gels allowed for easy diffusion of the medium and maintained a reasonable cell culture environment as indicated by the viable cells seen in Figure 23. A more detailed analysis of the environment can be obtained from [41].

Generally, many options for the incorporation of growth factors or proteins into a 3D scaffold exist including covalent attachment [78, 79, 80] and non-covalent, affinity-based, attachment with the help of e.g. Heparin [53], or ECM molecules such as collagen [81, 82] reviewed in [83]. However, covalent modification likely also modifies the bioactivity and thus a mechanism that non-covalently binds proteins, such as attaching them to heparin and collagen is preferred. Indeed, and as discussed in section 1.3.5, heparin not only binds growth factors but also may increase their bioactivity. Moreover, several growth factors including bFGF bind to fibronectin [47]. This is why it was tested whether bFGF and BMP4 could be non-covalently attached to fibronectin and heparin respectively (seen in Figure 25). Interestingly, about half of bFGF was retained on fibronectin and even showed a slightly better retention on a collagen film. Moreover, BMP4 was completely retained on the collagen + heparin matrix. The differences between the two growth factors observed here can likely be attributed to the higher initial concentration of bFGF compared to the concentration of BMP4. Importantly I was also able to show the efficient attachment of heparin to collagen matrices regardless of the dimensionality of the matrix. Nearly all heparin was retained on collagen, which confirms the reported high affinity between heparin and collagen [57].

The non-covalent attachment of bFGF to fibronectin and BMP4 to collagen + heparin showed a higher degree of differentiation based on cTnT-expression, as seen in Figure 26 and globally in Figure 27. These appearances were confirmed when the quantification of the overall cTnT signal resulted in the highest mean area and integrated density ratio normalized to the nuclei (Figure 28 (A) and (B) respectively). While the only significant difference observed was between the cells encapsulated in ”PEG” only and the cells in PEG + optimized ECM formulation (”opt + GF”), the trend shows that ”PEG” only does not induce cardiomyocyte differentiation but that adding ECM (”+++”), optimizing its composition (”opt”) and finally adding the growth factors (”opt + GF”) continually increased the rate of differentiation. It should be noted, however, that the opt condition displayed a relatively high standard deviation, which is partly because 2 out of 4 gels were unfortunately lost during the process of staining leaving only 2 data points.

In conclusion, I was able to develop a novel simple and most importantly surprisingly efficient protocol for cardiomyocyte differentiation for at least one iPS cell line and determined that it is at least partially mediated by the Wnt signaling pathway. Nevertheless, other pluripotent lines did not show similarly efficient cardiac differentiation. Additionally, I was able to effectively and non-covalently attach bFGF and BMP4 to collagen, fibronectin and heparin and showed that it is beneficial for cardiac differentiation of one iPS cell line in a 3D environment. These results are very promising for future applications and I envision a set-up that employs similar combinations of scaffold, factors and cells to serve as an effective means to not only deliver stem cells or associated progeny to damaged cardiac tissue but are also able to spur cardiomyocyte differentiation of transplanted or recipient cells.

List of Figures

1 The differentiation path from pluripotent stem cell to cardiovascular cell, including differentiation into cardiomyocytes. Pluripotent stem cells can be harvested from the inner cell mass (ICM) of a blastocyst or obtained by reprogramming of somatic cells with the Yamanaka factors. Cells first undergo specification into a multipotent cardiovascular progenitor cell and can then further differentiate into cardiomyocytes (and even differentiate further into ventricular, atrial and nodal cardiomyocytes, endothelial cells and smooth muscle cells). Image adapted from Hartman *et al.* [17] 9
2 General timeline and molecules used to differentiate PSCs into cardiomyocytes. Firstly, mesodermal specification has to be induced followed by further induction of cardiomyocyte specification, mediated mainly through sequential Wnt activation and inhibition. This can be achieved chemically by using Wnt signaling modulators but it is also achievable by using several growth factors including Activin A, BMP4, bFGF and Dkk-1. It usually takes around 7-8 days for murine PSCs and 12-14 days for human PSCs to differentiate into cardiomyocytes. CHIR99021: chemical Wnt activator, KY02111/XAV939: chemical Wnt inhibitor. 11
3 (A through G) Different differentiation protocols employed to directly guide pluripotent stem cells to a cardiomyocyte fate using 2D and 3D (EBs) approaches. Several growth factors such as Activin A (AA, AA* with Matrigel), BMP4, basic FGF (bFGF), VEGF, dickkopf homolog 1 (Dkk1), Insulin (Ins) and chemical Wnt modulators such CHIR99021 (CHIR), inhibitor of Wnt protein (IWP), Wnt-C59, XAV939 are used. MEF: mouse embryonic fibroblasts, KO: knockout serum replacement. Adapted from Hartman *et al.* [17]. 11
4 Schematic representation of the produced 3D hydrogels cross-linked by native chemical ligation (NCL) containing cells (e.g. iPS cells or mesenchymal stem cells (MSC) and ECM molecules such as collagen I and/or laminin. Adapted from [41]. 17
5 Suggested mechanism of native chemical ligation. An unprotected peptide (1) with a C terminal thioester is reacted with an unprotected peptide (2) containing an N-terminal cysteine resulting in a transthioesterification and the formation of a thioester-linked intermediate (3). This reaction is fully reversible. However, a favorable nucleophilic attack of the cysteine α-amino group will occur that leads to the formation of an irreversible (covalent) peptide (amide) bond (4). Adapted from [66] and [64]. 18
6 Schematic of the newly developed cardiac differentiation protocol. miPS cells were seeded into a 24-well and 1 ml medium added on Day 0 (D0). The medium was changed (1 ml) on Day 2 and Day 4 and switched to 2 ml from Day 5 onward. Additionally, the frequency of medium change was increased to every 24h. Cells were fixed or further processed on Day 14. First, cells were seeded as singularized cells that displayed colonies of differentiating cells by Days 3 and 4 and ultimately led to the emergence of clearly visible and beating cardiomyocytes between Days 10 and 14. 20

7 Schematic drawing of the concept of encapsulating the ECM molecules collagen I (Col I), laminin (LN) and fibronectin (FN) with bound growth factors (bFGF to FN and BMP4 to Col I/Heparin) in a PEG hydrogel together with miPS cells. 24
8 Schematic representation of the developed protocol to assess collagen binding of growth factors and heparin and fibronectin binding (bFGF only). Firstly, a collagen I (Col1) or fibronectin (FN) layer is made by polymerization for 30 (Col1) or 10 min (FN). Secondly, the protein is added on top and the supernatant is taken after another 30 min of incubation time on a rocker and analyzed by enzyme linked immunosorbent assay (ELISA) in described in section 2.5.2. 26
9 Schematic representation of the developed protocol to assess collagen binding of heparin. Firstly, a collagen I layer or 3D matrix is made by polymerization for 30 min in a 24 well or an Eppendorf tube. Secondly, heparin is added on top and the supernatant is taken after another 30 min of incubation time on a rocker and analyzed by the DMMB-assay described in section 2.5.3 measuring the optical density (OD). 27
10 Oct3/4 staining confirms the pluripotent state of the miPS cells. (A) 91.2% of the iPS cells express the pluripotency marker Oct3/4 (Pink). (B) Representative image of the pluripotent iPS cell colonies expressing Oct3/4. Nuclei were stained with DAPI (Blue); N=3. 29
11 Developing morphology of iPS cells during SECD-Protocol. Representative images of the typical morphology observed in miPS cells undergoing the SECD-Protocol show the gradual increase in cell number until confluency ($\sim$ Day 7) and the subsequent morphology until cardiomyocytes are formed ($\sim$ Day 13). After reaching confluency, cells in some regions also start building 3D structures (e.g. seen from Day 8 on). 31
12 Beating iPS-derived cardiomyocytes generated with the SECD-Protocol. Resting state (A) and contracting state (B) are juxtaposed. Red circles show clear distortions suggestive of contracting cardiomyocytes. Scale bar = 100 μm. 32
13 Quantification of beating areas shows a dramatic increase until day 13 of culture and subsequently falls starting at day 14 when using the SECD-Protocol. Moreover, the use of 10% serum and performing the switch from 1 ml to 2 ml medium during culture is necessary for the highest efficiency in cardiomyocyte differentiation (A). Conditions that include the switch demonstrate significantly increased numbers of beating areas regardless of the serum content. Furthermore, panel (B) shows the number of beating areas in multiple replicates subjected to the protocol at different timepoints. (A) N=3, (B) N=12 for Days 9, 10, 11, 12, 13 and N=8 for Day 14. * = $p<0.05$, ** = $p<0.01$, *** = $p<0.001$. 32

14 iPS cells (iPS#1) are efficiently differentiated into cardiomyocytes using the SECD-Protocol while a second miPS cell line (iPS#2) and ESCs show several smaller differentiated regions. Representative images of cTnT-positive cells (Red) indicative of iPS- and ESC-derived cardiomyocytes generated with the SECD-Protocol. While the primary iPS cells [67] show efficient differentiation into cardiomyocytes in certain regions, ESCs and iPS#2 do not and instead show several smaller cTnT-positive areas. Staining performed on Day 14. Nuclei (DAPI) = Blue. 33
15 SECD-Protocol shows particularly efficient cardiac differentiation at the outer ring of the well. This image was stitched together from 243 single images to provide a global picture of cTnT-positive cells (Red) indicative of iPS-derived cardiomyocytes generated with the SECD-Protocol. Staining performed on Day 14. Nuclei were stained with DAPI (Blue), Scale bar = 1000 μm. 34
16 Active β-Catenin levels show a sequential activation (rise until Day 7) and inactivation (decrease starting on Day 8) of Wnt-Signaling. Nuclear area ratio (A) and nuclear integrated density ratio (B) between β-Catenin and DAPI signals show a significant increase until day 7 and subsequent decrease starting on Day 8 and maintained through Day 10. The nuclear area ratio shows that the nuclear area was completely covered by β-Catenin signal. (C) and (D) show the total area and integrated density ratios and display the same trend. N=9 for (A) and (B) and N=7 for (C) and (D). * = $p<0.05$, ** = $p<0.01$, *** = $p<0.001$. 36
17 Representative images of the active β-Catenin staining (green) performed during the SECD-Protocol. Active β-Catenin levels show a sequential activation (rise in signal until Day 7) and inactivation (decrease in signal starting on Day 8) of Wnt-Signaling. Nuclei stained with DAPI (blue), Scale bar = 100 μm. 37
18 EBs subjected to the protocol of Wang *et al.* [22] did not show any contracting regions but iPS cells instead displayed morphologies characteristic of other cell types. (A) provides a top view of the EB and the outgrowing cells and (B) shows cells extending multiple filopodia in a mesenchymal-like morphology. Cells in (C) exhibit a flat and cobblestone-like morphology and (D) shows several cells that appear to contain fat vacuoles. Images from Day 10 of culture. Scale bars 200 μm for (A) and 100 μm for (B, C, D). 39
19 The EB-based protocol by Kwon *et al.* [36] leads to several, however heterogenous, cTnT-positive regions (Red) over the course of 12 days using miPS cells. Representative images in (A), (B), (C) and (D) show heterogenous cTnT-positive areas ranging from high cTnT-staining (A) in some areas to areas with low cTnT-staining ((B), (C) and (D)). Nuclei were stained with DAPI (Blue); Scale bar = 100 μm. 40

20 Different EB-based cardiac differentiation protocols show very diverse efficiency. (A) Percentage of EBs with beating areas after undergoing the original van Laake *et al.* [67], Kwon *et al.* [36] protocol. EBs were treated with Wnt3a between days 4-6 and between 90%-100% of the EBs had beating areas after 7 days. (B) Percentage of EBs with beating areas after several modifications (the Wnt activator CHIR99021 instead of Wnt3a) to the original Kwon-protocol compared to the Wang *et al.* [22] protocol using IMDM instead of GMEM and the Wnt inhibitor XAV939 between days 3-5. N=6 for (A) and (B). * = $p<0.05$, ** = $p<0.01$, *** = $p<0.001$. 41
21 The EB-based protocol by Kwon *et al.* [36] leads to several cTnT-positive regions over the course of 12 days (white arrows). This image was stitched together from 145 images and provides a global picture of cTnT-positive cells (Red) indicative of miPS-derived cardiomyocytes. Staining performed on Day 12. Nuclei were stained with DAPI (Blue), Scale bar = 1000 μm. 42
22 Quantification of area ratio of cTnT-positive signal, normalized to DAPI, confirms that the newly developed SECD-Protocol produces a significantly higher number of cardiomyocytes compared to a standard EB-based protocol (based on Kwon *et. al.* [36]). The entire well/EB area was scanned and the area of cTnT-positive signal of each single image was measured. These measurements were then set in relation to the DAPI signal to obtain the area ratio. Well subjected to the SECD-Protocol contained 240 measured images and 3 analyzed EB-regions made up a total of 418 images. *** = $p<0.001$. . . 43
23 miPS-cell-colonies (white arrows show representative colonies) remain viable in PEG hydrogels. (A) Phase contrast image of the typical iPS cell colonies in a PEG hydrogel. (B) Corresponding image showing nuclear (DAPI) staining in blue and cytoskeletal (F-actin/Phalloidin) staining in pink. Scale bar = 100 μm. 44
24 Hydrogel formation and cell/ECM entrapment was successful. (A) shows clearly visible cells in the PEG only condition, whereas hydrogels additionally containing different ECM formulations (”+++”, ”opt”, ”opt + GF”) reveal a more pronounced white matrix (composed of cells and ECM molecules) inside the hydrogel. The distinct color of phenol red in the medium, seen in (B), confirms the efficient incorporation of medium into the hydrogels. “+++”: Hydrogel contains Col I, LN, and FN. “Opt” contains an ECM composition of Col I, LN and FN optimized for cardiomyocyte differentiation. “Opt + GF” contains optimized composition of ECM with bound BMP4 & bFGF. 45

25 Growth factors and heparin are effectively retained on collagen/fibronectin matrices. (A) ELISA results of the supernatant incubated with a collagen matrix, showing that 4.602 ng/ml of bFGF was still present. If incubated on collagen + heparin 5.171 ng/ml were still present. A similar trend can be seen if bFGF is incubated on a fibronectin-coated surface (B) showing that slightly less than half of bFGF is retained on fibronectin (5.756 ng/ml after incubation on fibronectin and 7.253 ng/ml on fibronectin + heparin). Panel (C), however, shows that all of BMP4 is retained on the collagen matrix. Panel (D) depicts the DMMB results showing that almost all heparin is retained on the collagen films (2D, 0.877 μg/ml) and matrices (3D, 0.354 μg/ml). Dotted lines show the original concentration of protein of interest/heparin added. N=2 for A, B, C and N$\geq$4 for D. ** = p$<$0.01. 47
26 Attachment of GFs to ECM molecules encapsulated with miPS cells (white arrows demonstrate representative cell colonies) during a 14-day culture period in PEG hydrogels demonstrates stronger cTnT signal compared to the controls. Different ECM formulations (”+++”, ”opt”) or ”PEG” only are shown. “+++”: Hydrogel contains Col I, LN, and FN. “Opt” contains an ECM composition of Col I, LN and FN optimized for cardiomyocyte differentiation. “Opt + GF” contains optimized composition of ECM with bound BMP4 & bFGF. Scale bar = 100 μm. 49
27 Stitched images of the entire hydrogel confirm the fact that attachment of GFs to ECM molecules encapsulated with miPS cells (white arrows demonstrate representative cell colonies) in PEG hydrogels demonstrates stronger cTnT signal compared to the controls. These images show the entire hydrogel and were stitched together from 72 single images. Different ECM formulations (”+++”, ”opt”) or ”PEG” only are shown. “+++”: Hydrogel contains Col I, LN, and FN. “Opt” contains an ECM composition of Col I, LN and FN optimized for cardiomyocyte differentiation. “Opt + GF” contains optimized composition of ECM with bound BMP4 & bFGF. Scale bar = 1000 μm. 50
28 Quantification of area ratio (A) and integrated density ratio (B) of cTnT-positive signal normalized to DAPI confirms that attaching GFs to the ECM/Cells in a PEG-Hydrogel promotes cardiomyocyte differentiation. N= 4 for ”Opt + GF” and ”PEG”, N=3 for ”+++” and N=2 for ”Opt”. * = p$<$0.05, ** = p$<$0.01, *** = p$<$0.001. 51

List of Tables

1 Formula for PEG hydrogel formation (per gel) 23
2 Representation of the standard dilutions made for the DMMB-Assay. 28

List of Abbreviations

CVD Cardiovascular Diseases
CMs Cardiomyocytes
PSCs Pluripotent Stem Cells
iPS Cells induced Pluripotent Stem Cells
ECM Extracellular Matrix
PEG Polyethylene Glycol
ESCs Embryonic Stem Cells
miRNA micro RNA
SeV Sendai Virus
ALS Amyotrophic Lateral Sclerosis
HLA Human Leukocyte Antigen
mESCs murine Embryonic Stem Cells
EBs Embryoid Bodies
hPSC human Pluripotent Stem Cells
α-MHC α-Myosin Heavy Chain
β-MHC β-Myosin Heavy Chain
cTnI cardiac Troponin I
cTnT cardiac Troponin T
Mlc-2a/2v Myosin Light Chain 2a/2v
ICM Inner Cell Mass
Dkk-1 Dickkopf homolog-1
BMP Bone Morphogenetic Protein
FGF Fibroblast Growth Factor
bFGF basic Fibroblast Growth Factor
VEGF Vascular Endothelial Growth Factor
IMDM Iscove's Modified Dulbecco's Media
RPMI Roswell Park Memorial Institute Medium
GMEM Glasgow Minimum Essential Medium
DMEM Dulbecco's Modified Eagle's Medium
GAGs Glycosaminoglycans
sGAGs sulfated Glycosaminoglycans
Col I Collagen I
LN Laminin
FN Fibronectin
DMMB Dimethyl Methylene Blue
NCL Native Chemical Ligation
GFs Growth Factors
MSCs Mesenchymal Stem Cells

References

[1] A. S. Go, D. Mozaffarian, V. L. Roger, E. J. Benjamin, J. D. Berry, W. B. Borden, D. M. Bravata, S. Dai, E. S. Ford, C. S. Fox, S. Franco, H. J. Fullerton, C. Gillespie, S. M. Hailpern, J. A. Heit, V. J. Howard, M. D. Huffman, B. M. Kissela, S. J. Kittner, D. T. Lackland, J. H. Lichtman, L. D. Lisabeth, D. Magid, G. M. Marcus, A. Marelli, D. B. Matchar, D. K. McGuire, E. R. Mohler, C. S. Moy, M. E. Mussolino, G. Nichol, N. P. Paynter, P. J. Schreiner, P. D. Sorlie, J. Stein, T. N. Turan, S. S. Virani, N. D. Wong, D. Woo, M. B. Turner, and on behalf of the American Heart Association Statistics Committee and Stroke Statistics Subcommittee, "Heart disease and stroke statistics–2013 update: a report from the American Heart Association.," *Circulation*, vol. 127, pp. e6–e245, Jan. 2013.

[2] R. C. Addis and J. A. Epstein, "Induced regeneration–the progress and promise of direct reprogramming for heart repair.," *Nature Medicine*, vol. 19, pp. 829–836, July 2013.

[3] X. Lian, J. Zhang, S. M. Azarin, K. Zhu, L. B. Hazeltine, X. Bao, C. Hsiao, T. J. Kamp, and S. P. Palecek, "Directed cardiomyocyte differentiation from human pluripotent stem cells by modulating Wnt/β-catenin signaling under fully defined conditions," *Nature Protocols*, vol. 8, pp. 162–175, Dec. 2012.

[4] K. Rajala, M. Pekkanen-Mattila, and K. Aalto-Setälä, "Cardiac Differentiation of Pluripotent Stem Cells," *Stem Cells International*, vol. 2011, no. 21, pp. 1–12, 2011.

[5] L. A. Sanz, S. K. Kota, and R. Feil, "Genome-wide DNA demethylation in mammals.," *Genome biology*, vol. 11, no. 3, p. 110, 2010.

[6] K. Takahashi and S. Yamanaka, "Induction of pluripotent stem cells from mouse embryonic and adult fibroblast cultures by defined factors.," *Cell*, vol. 126, pp. 663–676, Aug. 2006.

[7] R. Lanza and A. Atala, *Essentials of Stem Cell Biology*. Elsevier Inc., third edition ed.

[8] T. Seki, S. Yuasa, M. Oda, T. Egashira, K. Yae, D. Kusumoto, H. Nakata, S. Tohyama, H. Hashimoto, M. Kodaira, Y. Okada, H. Seimiya, N. Fusaki, M. Hasegawa, and K. Fukuda, "Generation of induced pluripotent stem cells from human terminally differentiated circulating T cells.," *Cell Stem Cell*, vol. 7, pp. 11–14, July 2010.

[9] K. Okita, T. Yamakawa, Y. Matsumura, Y. Sato, N. Amano, A. Watanabe, N. Goshima, and S. Yamanaka, "An efficient nonviral method to generate integration-free human-induced pluripotent stem cells from cord blood and peripheral blood cells.," *Stem Cells*, vol. 31, pp. 458–466, Mar. 2013.

[10] Y. Fujie, N. Fusaki, T. Katayama, M. Hamasaki, Y. Soejima, M. Soga, H. Ban, M. Hasegawa, S. Yamashita, S. Kimura, S. Suzuki, T. Matsuzawa, H. Akari, and T. Era, "New type of Sendai virus vector provides transgene-free iPS cells derived from chimpanzee blood.," *PLoS ONE*, vol. 9, no. 12, p. e113052, 2014.

[11] W. Li, H. Zhou, R. Abujarour, S. Zhu, J. Young Joo, T. Lin, E. Hao, H. R. Schöler, A. Hayek, and S. Ding, "Generation of human-induced pluripotent stem cells in the absence of exogenous Sox2.," *Stem Cells*, vol. 27, pp. 2992–3000, Dec. 2009.

[12] Y. Yoshida, K. Takahashi, K. Okita, T. Ichisaka, and S. Yamanaka, "Hypoxia enhances the generation of induced pluripotent stem cells.," *Cell Stem Cell*, vol. 5, pp. 237–241, Sept. 2009.

[13] G. Amabile and A. Meissner, "Induced pluripotent stem cells: current progress and potential for regenerative medicine.," *Trends in molecular medicine*, vol. 15, pp. 59–68, Feb. 2009.

[14] F. Nakajima, K. Tokunaga, and N. Nakatsuji, "Human leukocyte antigen matching estimations in a hypothetical bank of human embryonic stem cell lines in the Japanese population for use in cell transplantation therapy.," *Stem Cells*, vol. 25, pp. 983–985, Apr. 2007.

[15] C. J. Taylor, E. M. Bolton, S. Pocock, L. D. Sharples, R. A. Pedersen, and J. A. Bradley, "Banking on human embryonic stem cells: estimating the number of donor cell lines needed for HLA matching," *The Lancet*, vol. 366, pp. 2019–2025, Dec. 2005.

[16] T. C. Doetschman, H. Eistetter, M. Katz, W. Schmidt, and R. Kemler, "The in vitro development of blastocyst-derived embryonic stem cell lines: formation of visceral yolk sac, blood islands and myocardium.," *Journal of embryology and experimental morphology*, vol. 87, pp. 27–45, June 1985.

[17] M. E. Hartman, D.-F. Dai, and M. A. Laflamme, "Human pluripotent stem cells: Prospects and challenges as a source of cardiomyocytes for in vitro modeling and cell-based cardiac repair.," *Advanced drug delivery reviews*, May 2015.

[18] S. L. Paige, T. Osugi, O. K. Afanasiev, L. Pabon, H. Reinecke, and C. E. Murry, "Endogenous Wnt/β-Catenin Signaling Is Required for Cardiac Differentiation in Human Embryonic Stem Cells," *PLoS ONE*, vol. 5, pp. e11134–8, June 2010.

[19] E. Cagavi, O. Bartulos, C. Y. Suh, B. Sun, Z. Yue, Z. Jiang, L. Yue, and Y. Qyang, "Functional Cardiomyocytes Derived from Isl1 Cardiac Progenitors via Bmp4 Stimulation," *PLoS ONE*, vol. 9, pp. e110752–21, Dec. 2014.

[20] M. F. Taha, M. R. Valojerdi, and S. J. Mowla, "Effect of bone morphogenetic protein-4 (BMP-4) on cardiomyocyte differentiation from mouse embryonic stem cell.," *International Journal of Cardiology*, vol. 120, pp. 92–101, Aug. 2007.

[21] I. Minami, K. Yamada, T. G. Otsuji, T. Yamamoto, Y. Shen, S. Otsuka, S. Kadota, N. Morone, M. Barve, Y. Asai, T. Tenkova-Heuser, J. E. Heuser, M. Uesugi, K. Aiba, and N. Nakatsuji, "A Small Molecule that Promotes Cardiac Differentiation of Human Pluripotent Stem Cells under Defined, Cytokine- and Xeno-free Conditions," *CellReports*, vol. 2, pp. 1448–1460, Nov. 2012.

[22] H. Wang, J. Hao, and C. C. Hong, "Cardiac Induction of Embryonic Stem Cells by a Small Molecule Inhibitor of Wnt/β-Catenin Signaling," *ACS chemical biology*, vol. 6, pp. 192–197, Feb. 2011.

[23] P. W. Burridge, E. Matsa, P. Shukla, Z. C. Lin, J. M. Churko, A. D. Ebert, F. Lan, S. Diecke, B. Huber, N. M. Mordwinkin, J. R. Plews, O. J. Abilez, B. Cui, J. D. Gold, and J. C. Wu, "Chemically defined generation of human cardiomyocytes," *Nature Methods*, vol. 11, pp. 855–860, June 2014.

[24] H. Masumoto, T. Ikuno, M. Takeda, H. Fukushima, A. Marui, S. Katayama, T. Shimizu, T. Ikeda, T. Okano, R. Sakata, and J. K. Yamashita, "Human iPS cell-engineered cardiac tissue sheets with cardiomyocytes and vascular cells for cardiac regeneration," *Scientific Reports*, vol. 4, pp. 6716–7, Oct. 2014.

[25] M. Kennedy, S. L. D'Souza, M. Lynch-Kattman, S. Schwantz, and G. Keller, "Development of the hemangioblast defines the onset of hematopoiesis in human ES cell differentiation cultures.," *Blood*, vol. 109, pp. 2679–2687, Apr. 2007.

[26] S. J. Kattman, A. D. Witty, M. Gagliardi, N. C. Dubois, M. Niapour, A. Hotta, J. Ellis, and G. Keller, "Stage-Specific Optimization of Activin/Nodal and BMP Signaling Promotes Cardiac Differentiation of Mouse and Human Pluripotent Stem Cell Lines," *Stem Cell*, vol. 8, pp. 228–240, Feb. 2011.

[27] D. Ivanyuk, G. Budash, Y. Zheng, J. A. Gaspar, U. Chaudhari, A. Fatima, S. Bahmanpour, V. K. Grin, A. G. Popandopulo, A. Sachinidis, J. Hescheler, and T. Šarić, "Ascorbic Acid-Induced Cardiac Differentiation of Murine Pluripotent Stem Cells: Transcriptional Profiling and Effect of a Small Molecule Synergist of Wnt/β-Catenin Signaling Pathway.," *Cellular physiology and biochemistry : international journal of experimental cellular physiology, biochemistry, and pharmacology*, vol. 36, no. 2, pp. 810–830, 2015.

[28] C. P. Jackman, I. Y. Shadrin, A. L. Carlson, and N. Bursac, "Human Cardiac Tissue Engineering: From Pluripotent Stem Cells to Heart Repair.," *Current opinion in chemical engineering*, vol. 7, pp. 57–64, Feb. 2015.

[29] M. Zhang, J. S. Schulte, A. Heinick, I. Piccini, J. Rao, R. Quaranta, D. Zeuschner, D. Malan, K.-P. Kim, A. Röpke, P. Sasse, M. Araúzo-Bravo, G. Seebohm, H. Schöler, L. Fabritz, P. Kirchhof, F. U. Müller, and B. Greber, "Universal cardiac induction of human pluripotent stem cells in two and three-dimensional formats: implications for in vitro maturation.," *Stem Cells*, vol. 33, pp. 1456–1469, May 2015.

[30] I. Kehat, D. Kenyagin-Karsenti, M. Snir, H. Segev, M. Amit, A. Gepstein, E. Livne, O. Binah, J. Itskovitz-Eldor, and L. Gepstein, "Human embryonic stem cells can differentiate into myocytes with structural and functional properties of cardiomyocytes.," *Journal of Clinical Investigation*, vol. 108, pp. 407–414, Aug. 2001.

[31] B. Valamehr, S. J. Jonas, J. Polleux, R. Qiao, S. Guo, E. H. Gschweng, B. Stiles, K. Kam, T.-J. M. Luo, O. N. Witte, X. Liu, B. Dunn, and H. Wu, "Hydrophobic surfaces for enhanced differentiation of embryonic stem cell-derived embryoid bodies.," *Proceedings of the National Academy of Sciences of the United States of America*, vol. 105, pp. 14459–14464, Sept. 2008.

[32] X. Lian, C. Hsiao, G. Wilson, K. Zhu, L. B. Hazeltine, S. M. Azarin, K. K. Raval, J. Zhang, T. J. Kamp, and S. P. Palecek, "Robust cardiomyocyte differentiation from human pluripotent stem cells via temporal modulation of canonical Wnt signaling.,"

Proceedings of the National Academy of Sciences of the United States of America, vol. 109, pp. E1848–57, July 2012.

[33] L. Yang, M. H. Soonpaa, E. D. Adler, T. K. Roepke, S. J. Kattman, M. Kennedy, E. Henckaerts, K. Bonham, G. W. Abbott, R. M. Linden, L. J. Field, and G. M. Keller, "Human cardiovascular progenitor cells develop from a KDR+ embryonic-stem-cell-derived population.," *Nature*, vol. 453, pp. 524–528, May 2008.

[34] H. Clevers, "Wnt/beta-catenin signaling in development and disease.," *Cell*, vol. 127, pp. 469–480, Nov. 2006.

[35] J. Roose and H. Clevers, "TCF transcription factors: molecular switches in carcinogenesis.," *Biochimica et biophysica acta*, vol. 1424, pp. M23–37, Oct. 1999.

[36] C. Kwon, J. Arnold, E. C. Hsiao, M. M. Taketo, B. R. Conklin, and D. Srivastava, "Canonical Wnt signaling is a positive regulator of mammalian cardiac progenitors.," *Proceedings of the National Academy of Sciences of the United States of America*, vol. 104, pp. 10894–10899, June 2007.

[37] B. Alberts, A. Johnson, J. Lewis, D. Morgan, M. Raff, K. Roberts, and P. Walter, *Molecular Biology of the Cell*. New York: Garland Science, sixth edition ed., 2015.

[38] J. P. Jung, J. M. Squirrell, G. E. Lyons, K. W. Eliceiri, and B. M. Ogle, "Imaging cardiac extracellular matrices: a blueprint for regeneration," *Trends in Biotechnology*, vol. 30, pp. 233–240, Apr. 2012.

[39] K. P. Hanson, J. P. Jung, Q. A. Tran, S.-P. P. Hsu, R. Iida, V. Ajeti, P. J. Campagnola, K. W. Eliceiri, J. M. Squirrell, G. E. Lyons, and B. M. Ogle, "Spatial and Temporal Analysis of Extracellular Matrix Proteins in the Developing Murine Heart: A Blueprint for Regeneration," *Tissue engineering. Part A*, vol. 19, pp. 1132–1143, May 2013.

[40] J. H. Collier, J. S. Rudra, J. Z. Gasiorowski, and J. P. Jung, "Multi-component extracellular matrices based on peptide self-assembly," *Chemical Society Reviews*, vol. 39, no. 9, p. 3413, 2010.

[41] J. P. Jung, A. J. Sprangers, J. R. Byce, J. Su, J. M. Squirrell, P. B. Messersmith, K. W. Eliceiri, and B. M. Ogle, "ECM-incorporated hydrogels cross-linked via native chemical ligation to engineer stem cell microenvironments.," *Biomacromolecules*, vol. 14, pp. 3102–3111, Sept. 2013.

[42] R. O. Hynes, "The extracellular matrix: not just pretty fibrils.," *Science*, vol. 326, pp. 1216–1219, Nov. 2009.

[43] J. Zhu and R. A. F. Clark, "Fibronectin at select sites binds multiple growth factors and enhances their activity: expansion of the collaborative ECM-GF paradigm.," *The Journal of investigative dermatology*, vol. 134, pp. 895–901, Apr. 2014.

[44] V. M. Paralkar, B. S. Weeks, Y. M. Yu, H. K. Kleinman, and A. H. Reddi, "Recombinant human bone morphogenetic protein 2B stimulates PC12 cell differentiation: potentiation and binding to type IV collagen.," *The Journal of cell biology*, vol. 119, pp. 1721–1728, Dec. 1992.

[45] M. M. Martino, P. S. Briquez, E. Güç, F. Tortelli, W. W. Kilarski, S. Metzger, J. J. Rice, G. A. Kuhn, R. Müller, M. A. Swartz, and J. A. Hubbell, "Growth factors engineered for super-affinity to the extracellular matrix enhance tissue healing.," *Science*, vol. 343, pp. 885–888, Feb. 2014.

[46] P. S. Briquez, J. A. Hubbell, and M. M. Martino, "Extracellular Matrix-Inspired Growth Factor Delivery Systems for Skin Wound Healing," *Advances in Wound Care*, pp. 150127064149004–11, Jan. 2015.

[47] M. M. Martino and J. A. Hubbell, "The 12th-14th type III repeats of fibronectin function as a highly promiscuous growth factor-binding domain.," *FASEB journal : official publication of the Federation of American Societies for Experimental Biology*, vol. 24, pp. 4711–4721, Dec. 2010.

[48] L. W. van Laake, E. G. van Donselaar, J. Monshouwer-Kloots, C. Schreurs, R. Passier, B. M. Humbel, P. A. Doevendans, A. Sonnenberg, A. J. Verkleij, and C. L. Mummery, "Extracellular matrix formation after transplantation of human embryonic stem cell-derived cardiomyocytes.," *Cellular and molecular life sciences : CMLS*, vol. 67, pp. 277–290, Jan. 2010.

[49] M. Sobel, P. M. McNeill, P. L. Carlson, J. C. Kermode, B. Adelman, R. Conroy, and D. Marques, "Heparin inhibition of von Willebrand factor-dependent platelet function in vitro and in vivo.," *Journal of Clinical Investigation*, vol. 87, pp. 1787–1793, May 1991.

[50] A. L. Lehninger, D. L. D. L. . Nelson, and M. M. Cox, *Lehninger principles of biochemistry*. New York : W.H. Freeman, 2013.

[51] G. Venkataraman, V. Sasisekharan, A. B. Herr, D. M. Ornitz, G. Waksman, C. L. Cooney, R. Langer, and R. Sasisekharan, "Preferential self-association of basic fibroblast growth factor is stabilized by heparin during receptor dimerization and activation.," *Proceedings of the National Academy of Sciences of the United States of America*, vol. 93, pp. 845–850, Jan. 1996.

[52] R. Goetz and M. Mohammadi, "Exploring mechanisms of FGF signalling through the lens of structural biology.," *Nature Reviews Molecular Cell Biology*, vol. 14, pp. 166–180, Mar. 2013.

[53] M. R. Johnson, J. D. Boerckel, K. M. Dupont, and R. E. Guldberg, "Functional restoration of critically sized segmental defects with bone morphogenetic protein-2 and heparin treatment.," *Clinical orthopaedics and related research*, vol. 469, pp. 3111–3117, Nov. 2011.

[54] M. H. Hettiaratchi, T. Miller, J. S. Temenoff, R. E. Guldberg, and T. C. McDevitt, "Heparin microparticle effects on presentation and bioactivity of bone morphogenetic protein-2.," *Biomaterials*, vol. 35, pp. 7228–7238, Aug. 2014.

[55] Y. J. Choi, J. Y. Lee, J. H. Park, J. B. Park, J. S. Suh, Y. S. Choi, S. J. Lee, C.-P. Chung, and Y. J. Park, "The identification of a heparin binding domain peptide from bone morphogenetic protein-4 and its role on osteogenesis.," *Biomaterials*, vol. 31, pp. 7226–7238, Oct. 2010.

[56] S. Li, C. Shimono, N. Norioka, I. Nakano, T. Okubo, Y. Yagi, M. Hayashi, Y. Sato, H. Fujisaki, S. Hattori, N. Sugiura, K. Kimata, and K. Sekiguchi, "Activin A binds to perlecan through its pro-region that has heparin/heparan sulfate binding activity.," *The Journal of biological chemistry*, vol. 285, pp. 36645–36655, Nov. 2010.

[57] S. M. Sweeney, C. A. Guy, G. B. Fields, and J. D. San Antonio, "Defining the domains of type I collagen involved in heparin-binding and endothelial tube formation.," *Proceedings of the National Academy of Sciences of the United States of America*, vol. 95, pp. 7275–7280, June 1998.

[58] U. König, A. Lode, P. B. Welzel, Y. Ueda, S. Knaack, A. Henß, A. Hauswald, and M. Gelinsky, "Heparinization of a biomimetic bone matrix: integration of heparin during matrix synthesis versus adsorptive post surface modification.," *Journal of materials science. Materials in medicine*, vol. 25, pp. 607–621, Mar. 2014.

[59] R. W. Farndale, C. A. Sayers, and A. J. Barrett, "A direct spectrophotometric microassay for sulfated glycosaminoglycans in cartilage cultures.," *Connective tissue research*, vol. 9, no. 4, pp. 247–248, 1982.

[60] R. W. Farndale, D. J. Buttle, and A. J. Barrett, "Improved quantitation and discrimination of sulphated glycosaminoglycans by use of dimethylmethylene blue.," *Biochimica et biophysica acta*, vol. 883, pp. 173–177, Sept. 1986.

[61] G. Müller and M. Hanschke, "Quantitative and qualitative analyses of proteoglycans in cartilage extracts by precipitation with 1,9-dimethylmethylene blue.," *Connective tissue research*, vol. 33, no. 4, pp. 243–248, 1996.

[62] U. Meyer, T. Meyer, J. Handschel, and H. P. Wiesmann, eds., *Fundamentals of tissue engineering and regenerative medicine*. Berlin : Springer, 2009.

[63] J. Zhu, "Bioactive modification of poly(ethylene glycol) hydrogels for tissue engineering.," *Biomaterials*, vol. 31, pp. 4639–4656, June 2010.

[64] E. C. B. Johnson and S. B. H. Kent, "Insights into the Mechanism and Catalysis of the Native Chemical Ligation Reaction," *Journal of the American Chemical Society*, vol. 128, pp. 6640–6646, May 2006.

[65] P. E. Dawson and S. B. Kent, "Synthesis of native proteins by chemical ligation.," *Annual review of biochemistry*, vol. 69, no. 1, pp. 923–960, 2000.

[66] "Native Chemical Ligation (NCL) mechanism," en.wikipedia.org [Online]. [Accessed: 04-Aug-2015]."

[67] L. W. van Laake, L. Qian, P. Cheng, Y. Huang, E. C. Hsiao, B. R. Conklin, and D. Srivastava, "Reporter-Based Isolation of Induced Pluripotent Stem Cell- and Embryonic Stem Cell-Derived Cardiac Progenitors Reveals Limited Gene Expression Variance," *Circulation Research*, vol. 107, pp. 340–347, Aug. 2010.

[68] D. Terzic, J. R. Maxon, L. Krevitt, C. DiBartolomeo, T. Goyal, W. C. Low, J. R. Dutton, and A. M. Parr, "Directed Differentiation of Oligodendrocyte Progenitor Cells From Mouse Induced Pluripotent Stem Cells.," *Cell transplantation*, May 2015.

[69] D. G. Buschke, J. M. Squirrell, H. Ansari, M. A. Smith, C. T. Rueden, J. C. Williams, G. E. Lyons, T. J. Kamp, K. W. Eliceiri, and B. M. Ogle, "Multiphoton Flow Cytometry to Assess Intrinsic and Extrinsic Fluorescence in Cellular Aggregates: Applications to Stem Cells," *Microscopy and Microanalysis*, vol. 17, pp. 540–554, Aug. 2010.

[70] J. M. Squirrell, J. J. Fong, C. A. Ariza, A. Mael, K. Meyer, N. K. Shevde, A. Roopra, G. E. Lyons, T. J. Kamp, K. W. Eliceiri, and B. M. Ogle, "Endogenous Fluorescence Signatures in Living Pluripotent Stem Cells Change with Loss of Potency," *PLoS ONE*, vol. 7, p. e43708, Aug. 2012.

[71] B.-H. Hu, J. Su, and P. B. Messersmith, "Hydrogels cross-linked by native chemical ligation.," *Biomacromolecules*, vol. 10, pp. 2194–2200, Aug. 2009.

[72] V. Coulson-Thomas and T. Ferreira Gesteira, "V. Coulson-Thomas and T. Ferreira Gesteira, "Dimethylmethylene Blue Assay (DMMB)," 20-Sep-2014.)," Sept. 2014.

[73] J. Hao, M. A. Daleo, C. K. Murphy, P. B. Yu, J. N. Ho, J. Hu, R. T. Peterson, A. K. Hatzopoulos, and C. C. Hong, "Dorsomorphin, a Selective Small Molecule Inhibitor of BMP Signaling, Promotes Cardiomyogenesis in Embryonic Stem Cells," *PLoS ONE*, vol. 3, pp. e2904–8, Aug. 2008.

[74] P. Gadue, T. L. Huber, P. J. Paddison, and G. M. Keller, "Wnt and TGF-beta signaling are required for the induction of an in vitro model of primitive streak formation using embryonic stem cells.," *Proceedings of the National Academy of Sciences of the United States of America*, vol. 103, pp. 16806–16811, Nov. 2006.

[75] Z. Ma, J. Wang, P. Loskill, N. Huebsch, S. Koo, F. L. Svedlund, N. C. Marks, E. W. Hua, C. P. Grigoropoulos, B. R. Conklin, and K. E. Healy, "Self-organizing human cardiac microchambers mediated by geometric confinement," *Nat Commun*, vol. 6, p. 7413, 2015.

[76] K. A. Rosowski, A. F. Mertz, S. Norcross, E. R. Dufresne, and V. Horsley, "Edges of human embryonic stem cell colonies display distinct mechanical properties and differentiation potential," *Sci Rep*, vol. 5, p. 14218, 2015.

[77] M. K. Gupta, D. J. Illich, A. Gaarz, M. Matzkies, F. Nguemo, K. Pfannkuche, H. Liang, S. Classen, M. Reppel, J. L. Schultze, J. Hescheler, and T. Šarić, "Global transcriptional profiles of beating clusters derived from human induced pluripotent stem cells and embryonic stem cells are highly similar.," *BMC developmental biology*, vol. 10, no. 1, p. 98, 2010.

[78] B. V. Sridhar, N. R. Doyle, M. A. Randolph, and K. S. Anseth, "Covalently tethered TGF-β1 with encapsulated chondrocytes in a PEG hydrogel system enhances extracellular matrix production," *Journal of biomedical materials research. Part A*, pp. n/a–n/a, Feb. 2014.

[79] J. E. Saik, D. J. Gould, E. M. Watkins, M. E. Dickinson, and J. L. West, "Covalently immobilized platelet-derived growth factor-BB promotes angiogenesis in biomimetic poly(ethylene glycol) hydrogels.," *Acta Biomaterialia*, vol. 7, pp. 133–143, Jan. 2011.

[80] J. E. Leslie-Barbick, J. J. Moon, and J. L. West, “Covalently-immobilized vascular endothelial growth factor promotes endothelial cell tubulogenesis in poly(ethylene glycol) diacrylate hydrogels.,” *Journal of Biomaterials Science, Polymer Edition*, vol. 20, no. 12, pp. 1763–1779, 2009.

[81] Y. Li and S. M. Yu, “Targeting and mimicking collagens via triple helical peptide assembly.,” *Current opinion in chemical biology*, vol. 17, pp. 968–975, Dec. 2013.

[82] Y. Li, C. A. Foss, D. D. Summerfield, J. J. Doyle, C. M. Torok, H. C. Dietz, M. G. Pomper, and S. M. Yu, “Targeting collagen strands by photo-triggered triple-helix hybridization.,” *Proceedings of the National Academy of Sciences of the United States of America*, vol. 109, pp. 14767–14772, Sept. 2012.

[83] J. J. Rice, M. M. Martino, L. De Laporte, F. Tortelli, P. S. Briquez, and J. A. Hubbell, “Engineering the regenerative microenvironment with biomaterials.,” *Advanced healthcare materials*, vol. 2, pp. 57–71, Jan. 2013.